ABDOLMAJID MOHAMMADIAN

CONSERVATIVE CHARACTERISTIC-BASED SCHEMES FOR SHALLOW FLOWS

Thèse présentée
à la Faculté des études supérieures de l'Université Laval
dans le cadre du programme de doctorat en mathématiques
pour l'obtention du grade de Philosophiae Doctor (Ph.D.)

DÉPARTEMENT DE MATHÉMATIQUES ET DE STATISTIQUE
FACULTÉ SCIENCES ET DE GÉNIE
UNIVERSITÉ LAVAL
QUÉBEC

2006

Résumé

Les équations en eaux peu profondes, encore appelées équations de Saint-Venant, sont utilisées dans de nombreux cas importants comme les fleuves, les lacs, les estuaires et les océans. La conservation de certaines quantités est une propriété importante qui est habituellement désirée pour assurer la précision des simulations à long terme et également pour le cas des écoulements complexes avec présence d'ondes de choc. Cette thèse examine tout d'abord la formulation de schémas semi-Lagrangiens, qui sont bien connus pour demeurer stables pour des nombres très élevés de CFL. Cependant, ces schémas perdent leur propriété de stabilité lorsque la conservation totale des quantités, qui est cruciale pour une simulation correcte les ondes de chocs, est imposée. Un schéma semi-Lagrangien entièrement conservatif est développé ici et ce dernier demeure stable pour des nombres élevés de CFL. L'approche proposée est ensuite étendue à la méthode des caractéristiques (MOC) et une version conservative du schéma MOC est développée. Contrairement au schéma MOC original, qui ne peut pas simuler correctement les ondes de choc à cause du manque de conservation, le schéma proposé les simule avec succès. De plus, le nouveau schéma présente des avantages sur le plan numérique, tant pour la diffusion et la dispersion que pour la stabilité. Le cas 2D est ensuite considéré, et la méthode de volume finie est utilisée à cause de son conservation inhérente.

Le cas 2D est ensuite considéré, et la méthode de volumes finis est utilisée à cause de ses qualités inhérentes de conservation. La plupart des méthodes numériques disponibles sont sensibles au problème du déséquilibre entre les termes source et de flux, particulièrement en présence d'un maillage non structuré. D'autre part, la plupart des schémas numériques disponibles (par exemple les schémas HLL et ENO) induisent un niveau élevé de diffusion numérique en simulant des écoulements tourbillonnaires. Trois approches différentes, applicables sur des maillages non structurés sont développées ici. Elles peuvent simuler des conditions complexes d'écoulement comprenant les topographies variables, les écoulements tourbillonnaires, trans-critiques et discontinus.

Finalement plusieurs méthodes de volumes finis upwind sont utilisées, via une analyse de type Fourier, pour évaluer le niveau d`amortissement des modes de Rossby. Contrairement aux bons résultats habituellement obtenus par les méthodes de volumes finis upwind dans

le cas d'écoulements dominés par la convection, on remarque ici que les ondes de Rossby sont amorties de manière excessive.

Abstract

Shallow water equations arise in many important cases such as in rivers, lakes, estuaries and oceans. Conservation is an important property which is usually desired to ensure the accuracy of the long term simulations and also for the case of complex flows with shock-waves. This thesis begins with semi-Lagrangian schemes, which are well known to remain stable for very high CFL numbers. However, they lose their high stability property when the fully conservative property, which is crucial for a correct simulation of shock waves, is imposed. An inherently fully conservative semi-Lagrangian scheme is developed here which remains stable for high CFL numbers. The proposed approach is then extended to the method of characteristics (MOC) and a conservative extension of MOC is developed. Contrary to the original MOC, which is unable to simulate shockwaves due to the lack of conservation, the proposed scheme easily simulates them. Further, the new scheme presents favorable features in terms of numerical diffusion and dispersion. The 2D case is then considered, and the finite volume method is employed due to its inherent conservation properties. Most available numerical methods face the problem of imbalance between the source and flux terms, particularly when unstructured grids are used. On the other hand, most available numerical schemes (such as the HLL and the ENO schemes) induce a high level of numerical diffusion in simulating recirculating flows. Three different approaches using unstructured grids are successfully developed here. The new schemes can simulate complex flow conditions including recirculating, trans-critical and discontinuous flows over variable topographies. Finally, the performance of the upwind finite volume schemes, for Rossby waves, is studied using a Fourier analysis approach. Contrary to the usual good results obtained for those schemes in the case of convection dominated flows, it is observed here that they lead to an excessive damping of the Rossby modes.

Preface

This thesis contains five scientific articles. The authors of each article are specified in the following. The student has carried out the whole research work, all the programming tasks, and the writing of the articles under the supervision of D. Y. Le Roux and helpful comments of other authors. Articles no. 2 and 3 are already published and the articles no. 1 and 4 are in press. The student is the principal author of all the articles. The articles are inserted in the thesis in the following order:

1-Mohamadian A., Le Roux D. (2006) '*Simulation of Shallow Flows over Variable Topography Using Unstructured Grid*', International Journal for Numerical methods in Fluids (in press).

2-Mohamadian A., Le Roux D., Tajrishi M., Mazaheri K. (2005) '*A Mass Conservative Scheme For Simulating Shallow Flows Over Variable Topography Using Unstructured Grid*', Advances in water resources, (Elsevier), Vol. 28, pp. 523-537.

3-Mohamadian A., Le Roux D., (2006) '*A Conservative Semi-Lagrangian Method for the Shallow Water Equations*', Computer Physics Communications (Elsevier), Vol. 174, Issue 2, pp.99-108.

4-Mohamadian A., Le Roux D., Tajrishi M. (2006) '*A Conservative Extension of the Method of Characteristics for 1D shallow flows*', In press in Applied mathematical Modeling, 22 pages (Elsevier).

5-Mohamadian A., Le Roux D., (2006) '*Fourier analysis of upwind schemes in Shallow Water systems for gravity and Rossby waves*', Submitted to International Journal for Numerical methods in Fluids.

To my dear wife and parents

ACKNOWLEDGEMENTS

I would like to thank my supervisor Dr. D. Y. Le Roux, for his constant guidance and encouragement at every stage of the research, for having introduced me to the world of semi-Lagrangian methods and Rossby waves, and for the courses I have passed with him.

The advice of Dr. K. Mazaheri is also gratefully acknowledged. He introduced me to the world of Finite volume methods several years ago.

I would like to thank Drs. J. J. Gervais, R. Guénette and R. Pierre, for being always kindly available to answer my questions during the courses I passed at the Département de mathématiques et de statistique de l'Université Laval.

Financial support was provided by the Institut des sciences mathématiques (ISM), Département de mathématiques et de statistique de l'Université Laval, National Sciences and Engineering Research Council (NSERC), and Fonds Québécois de la Recherche sur la Nature et les Technologies (FQRNT).

Finally, I thank my family whose concern and encouragements were a source of inspiration and strength throughout the thesis. In particular, I wish to extend sincere and deepest gratitude to my wife Lida, whose love, confidence and encouragement made this work possible.

CHAPTER 1

Introduction

Shallow water equations arise in many important cases such as rivers, lakes, estuaries and oceans. Mathematical modeling of these flows is of special importance for many practical applications such as the design of hydraulic structures and prediction of natural events.

Conservation is an important property which is usually desired to ensure the accuracy of numerical simulation. Particularly, in the long term simulations, conservation may be necessary to prevent accumulation of errors in time. Further, some important cases of shallow water flows are supercritical or even a complex combination of super and sub critical regimes. Those include flows produced by sudden opening of control gates in channels, flows over the chute of spillways and the dam-break flows. Such flows usually contain shock waves. Conservation property is then necessary for a correct simulation of shock waves.

On the other hand, most numerical schemes encounter a high level of numerical oscillations in simulating complex flows. Different approaches have been developed in the literature to overcome the instabilities and preventing the oscillations. Characteristics play an essential role in most remedies designed for this purpose. However, most characteristics-based schemes lead to numerical problems such as the lack of conservation (e.g. the method of characteristics and most semi Lagrangian schemes) and imbalance between different terms (e.g. the upwind finite volume methods). The purpose of the present research is therefore the development of conservative, characteristic-based schemes for shallow flows in 1D and 2D, leading to a low level of numerical diffusion and oscillations.

Finally, shallow water equations arise also in the modeling of ocean circulation (see e.g. Vreugdenhil, 1994), where in addition to the convective effects, the Coriolis term plays an important role and the performance of the upwind schemes in this case needs to be studied. In particular, the damping of Rossby wave by a numerical scheme is a very important issue in ocean circulation modeling. This is because most energy-transfer in the ocean scale is due to these waves. An excessive damping of the Rossby modes is therefore unacceptable and leads to erroneous results. The very good performance of the conservative upwind schemes for those flows motivates the following question: How well these schemes perform for large scale flows where the Coriolis parameter plays a key role? This issue is hence studied in the present research.

This thesis is organized as follows:

Chapter 2 deals with the semi-Lagrangian schemes, which are well known to remain stable for very high CFL numbers. Most existing semi-Lagrangian schemes are non-conservative or only mass conservative, while a fully conservation property is crucial for a correct simulation of shock waves. The problem is that, by the imposition of the fully conservative property, the existing semi-Lagrangian schemes lose their high stability property. In this chapter, an inherently fully conservative semi-Lagrangian scheme is developed which remains stable for high CFL numbers.

The proposed approach is then extended to the method of characteristics (MOC) and a conservative extension of MOC is proposed in chapter 3. While the original method of

characteristics is unable to simulate shockwaves due to the lack of conservation, the proposed scheme simulates them very well with a low level of numerical diffusion and dispersion and it is able to simulate complex cases of wave interaction, which is beyond the capability of most existing schemes. This is a considerable improvement which allows for the extension of characteristics schemes to a wide range of real applications.

The 2D shallow water equations are then considered in chapters 4 and 5. Since in most real problems, a complex geometrical boundary is encountered, unstructured grids are usually preferred. They present the desired flexibility for local mesh refinement and complex boundaries. In the past two decades, finite volume methods have become popular due to their inherent conservation property, straightforward formulation for unstructured grids and capability of capturing complex flows by using the characteristic-based schemes for the calculation of the numerical flux. However, in the 2D case, the main difficulty in most existing schemes arises in the treatment of source and flux terms, particularly with unstructured grids. This is due to the imbalance between the source and flux terms. The study of this problem is the main subject of the present research in chapters 3 and 4. It has led in the development of three new well-balanced schemes designed for unstructured grids.

In chapter 4, a new well-balanced mass conservative scheme is introduced. For this scheme, a modification of the Roe scheme is proposed here to obtain the desired balance. Further, the gravity terms are extracted from the flux terms and they are combined with the source terms. The resulting scheme is found to have a good performance not only in the case of flows with variable topography, but also for circulating flows (compared to the experimental data). Moreover, the balance property of this scheme holds for the case of unstructured grids as well. However, this scheme is not fully conservative and may give rise to problems in presence of strong shocks.

In Chapter 5, we introduce two new fully conservative schemes to overcome this problem, and both theoretical and numerical evidences are given to show that the crucial compatibility property holds. The resulting schemes maintain all the satisfactory performances of the previous method (presented in chapter 4) and moreover they simulate satisfactorily very strong shocks. Further, the two new methods proposed in this chapter,

directly deal with the source terms without changing the flux terms. Therefore, contrary to the approach presented in chapter 4, the new methods could be combined with most existing Riemann solvers.

In the previous chapters, the Coriolis parameter has not been considered and the study has been restricted to the small scale flows where convection and gravity effects are dominant. The very good performance of the conservative upwind schemes for those flows motivates the question that how well these schemes perform for large scale flows where the Coriolis parameter plays a key role. This question is the main subject of the last chapter and we employ the Fourier analysis approach to study the behavior of upwind finite volume schemes for both gravity and Rossby waves.

Finally in Chapter 6, the performance of upwind finite volume schemes is examined by a Fourier analysis approach including the study of phase speed, group velocity, damping and dispersion for the gravity waves and most importantly the possible damping of the Rossby waves. In particular, the latter is studied numerically as well and the results are compared with those obtained by using a slope limiter approach. Some concluding remarks complete the study.

CHAPTER 2

Conservative semi-implicit semi-Lagrangian scheme for simulation of shallow flows

In this chapter, we study the semi-Lagrangian method. The feature of this scheme is that it remains stable for high CFL numbers. However, the lack of a full conservation property leads to mass loss and/or an incorrect simulation of shock waves. Here, the SL integrated mass method (SLIM) of Laprise and Plante (1995) is extended to the conservative form of the shallow-water equations and it is combined with a semi-implicit semi-Lagrangian one. The new scheme ensures the full conservation property while preserving the high stability of classical semi-Lagrangian methods.

Une methode conservative semi-Lagrangienne semi implicite pour la simulation de écoulements peu profond.

Résumé

Un schéma semi-Lagrangien (SL) entièrement conservatif est présenté pour résoudre les équations d'écoulements peu profonds. Des schémas SL entièrement conservatifs existent, mais ils assurent seulement la conservation de la masse alors que la quantité de mouvement n'est pas entièrement conservée. Les termes de quantité de mouvement, qui sont principalement responsables de la structure de l'onde dans les écoulements de type ruptures de barrage, sont ensuite discrétisés en employant des schémas non conservatifs traditionnels eulériens. En présence de grandes variations de la surface de l'eau (par exemple les écoulements de type de ruptures de barrage), une telle approche mène à une vitesse de choc incorrecte et a des résultats qui oscillent fortement. En effet, si la conservation de la quantité de mouvement est nécessaire, l'utilisation des schémas existants ne sera possible que pour de petits pas de temps. Dans cet article nous présentons un schéma entièrement conservatif qui peut exactement simuler les écoulements peu profonds avec de grands pas de temps. Dans notre méthode, tous les termes de quantité de mouvement, sont traités de façon conservative, ce qui assure une vitesse précise du choc. La propriété de conservation (totale) améliore considérablement les résultats des schémas SL pour un large éventail d'applications pratiques.

Conservative semi-implicit semi-Lagrangian scheme for simulation of shallow flows

A. MOHAMMADIAN, D. Y. LE ROUX

Abstract.

A fully conservative semi-Lagrangian (SL) scheme is presented to solve for the shallow-water equations. Existing inherently conservative SL schemes only ensure the conservation of mass while momentum is not fully conserved. The gravity terms, which are mainly responsible for the wave structure in dam break flows, are then discretized by using traditional non-conservative Eulerian schemes. In the presence of large variations in water surface (e.g. dam-break type flows), such an approach leads to incorrect shock speed and highly oscillatory results. Indeed, if the conservation of the gravity terms is forced, the use of existing schemes will be restricted to small time steps. In this paper we present a fully conservative scheme which can accurately simulate the shallow flows with a large time step. In our approach, both convective and gravitational terms are treated in a conservative manner, which ensures an accurate shock speed. The fully conservation property improves considerably the performance of common SL schemes for a wide range of practical applications.

Key Words: Conservative, semi-Lagrangian, semi implicit, shallow-water, dam-break

1. Introduction

Hyperbolic systems arise in many cases like shallow flows and gas dynamics. The flow regime changes from subcritical to supercritical in many fluvial flows, and the numerical method should be able to analyze these two types of flows simultaneously. Another difficulty is concerned with flows presenting discontinuous surface like dam break flows.

Extensive research has been performed in this area and different flux vector splitting and flux difference splitting methods have been proposed. Most of these methods have the capability of shock capturing with a high level of accuracy in few computational cells, and in most of them, the flux vector is determined based on the wave propagation structure.

On the other hand, SL schemes have become very popular in CFD to solve for the Navier-Stokes (Xiu and Karniadakis, 2001) and Hamilton Jacobi equations (Falcone and Ferrettiy, 2001), Magneto Hydrodynamics, ocean modeling (Zerroukat, Wood and Staniforth, 2002) and weather simulations (Temperman, Hortal and Simmons, 2001). The SL method greatly enhances computational efficiency because it can usually circumvent the CFL bound associated with traditional Eulerian advection schemes. The time step is then adjusted by the accuracy considerations instead of stability. The possibility of stable integrations with large Courant numbers is not the only virtue of a SL advection scheme. It also gives good phase speeds with little numerical dispersion compared to Eulerian schemes when a high order interpolation is used. For a review of traditional SL schemes and related issues see Staniforth and Coté (1991).

Existing SL schemes cannot be used directly to solve the shallow-water equations, because of the gravity effects, as explained later. One possible approach consists of combining a semi-implicit discretization of the gravity terms with a SL advection scheme (Robert, 1981). This combination has been successfully used in numerical weather prediction (Staniforth and Coté, 1991) and also as a proof-of-concept study in ocean modeling using unstructured meshes by Le Roux, Lin and Staniforth (2000).

Most of existing SL schemes developed to solve shallow-water equations, fail to simulate dam-break type flows. Contrary to Eulerian flux-form method, a common problem encountered with the SL approach is the lack of mass conservation and this is due to the dissipative effect of the interpolation procedure. Exact conservation is crucial to correctly predict the shock speed in dam-break flows and also for long-term simulations.

Many studies have been performed on this issue and a number of conservative SL schemes have been proposed in the literature. Those schemes can be grouped in two categories: corrective, and inherently conservative. The first group was proposed by Priestley (1993), in which a posteriori correction is used to restore the desired quantity whilst minimizing change to the original solution. Such a method has been applied to the shallow-water equations by Gravel and Staniforth (1994). In most schemes of the second type, either a constraint on the interpolating polynomial is applied to exactly satisfy the conservation law, or the SL method is applied directly to the conservative form of the equations. Attention herein is focused on the numerical methods of the second group,

which have been considerably improved in the past few years, and they will be discussed in section 3-2.

Another difficulty arises in the case of strong discontinuities such as the dam-break problem. For a correct simulation of the shock speed, mass conservation is not sufficient, and the gravity source term should be also conserved. Indeed, the shallow-water equations in their *fully conservative* (FC) form (where the gravity effect is considered as a flux term) should be satisfied. Most available conservative SL schemes only ensure mass conservation, and considered the gravity terms in a non-conservative manner (Lin and Rood, 1997). On the other hand, imposing the conservation of the gravity terms leads to a loss of stability when large time steps are used.

Due to the above mentioned problems only few researchers have used the SL methods for the dam-break type flows. Among them, Garcia Navarro and Priestly (1994) (GP) proposed for the first time a fully conservative scheme by employing a corrective (first group) method. They reported that SL methods are attractive for dam-break type flows due to their accuracy and the possibility of using CFL numbers greater than 1. However, the GP scheme may fail to preserve mass, momentum and phase when systems of equations are considered instead of the advection equation alone. This is a consequence of using the corrective approach to overcome the conservation problem of SL methods.

The objective of this paper is to present an inherently and fully conservative SL scheme to solve the shallow-water equations. In terms of computational efficiency, the proposed method, as for the GP scheme, consists of two steps whilst the oscillation suppressing process is done via an artificial viscosity approach rather than a limiter one used in GP scheme. On the other hand due to the inherently conservative approach, the highly expensive linear programming step of the GP method is avoided, and this makes our scheme more efficient. The proposed method is able to simulate dam-break type flows with a high level of accuracy and fluvial flows by using large time steps, without encountering the phase problem as the GP method does. Further, the ideas presented in this paper, may be easily applied to most existing mass conservative SL models to make them fully conservative.

This paper is organized as follows: In section 2 the model equations are presented. In section 3, several methods for solving conservation laws using SL schemes are reviewed

and a new scheme is developed for a scalar conservation law. A suitable integral form of the momentum equation is derived and a new predictor-corrector semi-implicit SL method is proposed. In section 4, the performance of the proposed numerical method is tested for different cases and those are compared with the exact solutions. The ability of the method in performing large time steps is also examined. Some concluding remarks complete the study.

2. The shallow-water equations

The one dimensional depth averaged continuity and momentum equations in a wide channel are written in conservative form (Toro, 2000)

$$\frac{\partial \vec{U}_c}{\partial t} + \frac{\partial \vec{F}}{\partial x} = \vec{S}_c, \tag{1}$$

where $\vec{U}_c$ is the vector of the conserved variables

$$\vec{U}_c = \begin{pmatrix} h \\ p \end{pmatrix}, \tag{2}$$

$\vec{F}$ is the flux vector

$$\vec{F} = \begin{pmatrix} uh \\ up + 0.5gh^2 \end{pmatrix}, \tag{3}$$

and the source term $\vec{S}_c$ including frictional, bed slope, and width variations effects is assumed to be zero. In (2) and (3), t and x are the time and spatial coordinates respectively, h and u are the water depth and the velocity variables respectively, g is the gravitational acceleration and $p = uh$ is the discharge in unit width. In the following, the subscript $_c$ will refer to a conservative variable.

Equation (1) may also be written in non-conservative form (Henderson, 1966)

$$\frac{\partial u}{\partial t} + u\frac{\partial u}{\partial x} = -g\frac{\partial h}{\partial x}, \tag{4}$$

$$\frac{\partial h}{\partial t} + u\frac{\partial h}{\partial x} = -h\frac{\partial u}{\partial x}. \tag{5}$$

3- The SL scheme

3-1-Basic concepts and model equations

In SL schemes, a reference frame is moving with an individual parcel of fluid along a trajectory defined by

$$\frac{dx}{dt} = u(x,t), \tag{6}$$

and the following differential equation is solved

$$\frac{dc}{dt} = S(x,t), \tag{7}$$

where $c(x,t)$ is any physical variable, t is the time, x is the spatial coordinate, u and S are the flow field and the source term respectively, and

$$\frac{d}{dt} = \frac{\partial}{\partial t} + u\frac{\partial}{\partial x}, \tag{8}$$

is the total or Lagrangian derivative. In (7), the total time derivative is simply the rate of change along flow trajectories as

$$\frac{dc}{dt} = \frac{c(x,t) - c(x_d, t-\Delta t)}{\Delta t} = S, \tag{9}$$

where x_d is the departure point of a fluid particle that originates at t-Δt and arrives at x after Δt. In SL schemes an Eulerian computational grid is used and a different set of particles is selected at each time step, and these are required to arrive at mesh nodes at the end of the time step.

As can be seen from (6) and (7), the SL scheme is based on a non-conservative form of the transport equation, and hence, it cannot be used directly to solve conservation laws of the type

$$\frac{\partial c}{\partial t} + \frac{\partial}{\partial x}(uc) = 0. \tag{10}$$

In order to solve (10) using the SL method, the equation is usually rewritten in the non-conservative form

$$\frac{dc}{dt} = -c\frac{\partial u}{\partial x}, \tag{11}$$

where the Lagrangian derivative is approximated along trajectories. Following this approach, (4) and (5) are rewritten as

$$\frac{du}{dt} = -g\frac{\partial h}{\partial x}, \tag{12}$$

$$\frac{dh}{dt} = -h\frac{\partial u}{\partial x}. \tag{13}$$

As shown in Staniforth and Cote (1991), the gravity term in (12) will lead to unstable results if it is discretized using an explicit method. One popular approach for overcoming this problem is the use of an implicit discretization for the gravity term. To this respect, an efficient semi-implicit SL scheme, proposed by Layton and Van de Panne's (2002), is presented in appendix 1, and it will be used later.

3-2-Conservative SL methods

For the sake of simplicity we let S=0 in the remaining of this subsection. Apart from the corrective methods, there are two general approaches for inherently conservative solution of conservation laws when using the SL methods:

(i) Exactly conservative methods written in a non-conservative form (CIP-CSL)

Using this approach, the Lagrangian invariant' c in (7) is constant along the trajectories specified by (6). Hence, equations (6) and (7) lead to

$$c(x,t) = c(x_d, t-\Delta t). \tag{14}$$

An explicit approximation of the Lagrangian derivative leads to the following two step-scheme:

Step1: the SL transport is performed

$$\widetilde{c}(x,t) = c(x_d, t-\Delta t), \tag{15}$$

Step2: the source term is added

$$c(x,t) = \widetilde{c}(x,t) - \Delta t\widetilde{c}(x,t)\frac{\partial u}{\partial t}. \tag{16}$$

Obviously, this approach, which may be considered as a point-wise scheme, is not necessarily conservative. However, Tanaka et al. (2000) and Yabe et al. (2001) showed that

the conservation of the above method can be achieved by using the conservation law (10) as a constraining condition for the interpolation functions. In the Tanaka et al. and Yabe et al. schemes, both *nodal values* and *cell averages* are transported by the SL method (the CIP-CSL type schemes). This approach has been successfully extended to general hyperbolic systems using cubic polynomials by Xiao et al. (2001). Further improvements were also obtained by Xiao (2002) in a more general approach (VSIAM3). However, most existing schemes of type (i) lose their unconditional stability in shallow-water systems due to the presence of gravity source terms.

(ii) SL integrated mass (SLIM) methods

This approach, introduced by Laprise and Plante (1995), is applied directly to the original conservation law (10) and may be considered as a *cell average* scheme. At each step, only average values of variables are transported, and nodal values are calculated using the cell averages. One benefit of this approach is that, no extra source term is present in the formulation, since the conservative form of the equations is used directly. Zerroukat, Wood and Staniforth (2002) recently developed an efficient extension of this scheme for two-dimensional domains.

It this paper, the cell average method (SLIM) is followed, i.e. the nodal values are calculated from the cell averages, and by imposing a monotonicity preserving constraint, the spurious oscillations are avoided. Further, by combining the SLIM method with a semi-implicit point-wise predictor step for evaluating the gravity terms, a fully conservative and stable SLIM scheme for the shallow water equations is constructed. In the following, we first describe the new scheme for scalar conservation laws, and we then extend it to the shallow-water case.

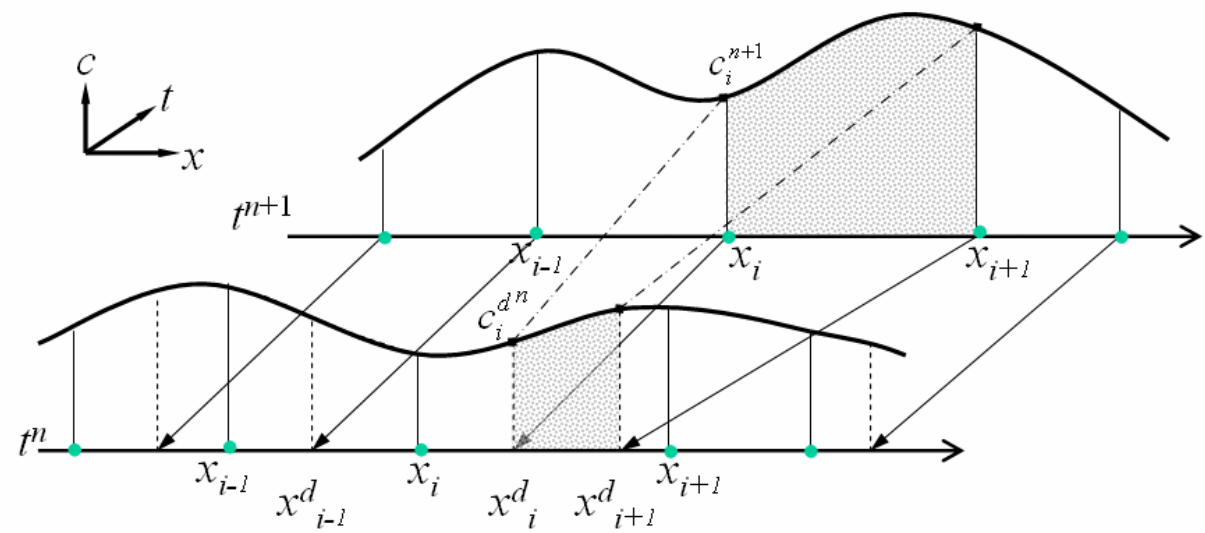

Figure 1. Arrangement of grid points and trajectories. The total derivative is approximated along particle trajectories in non-conservative SL schemes. The mass between two sequential departure points is transported to the corresponding destination cell in conservative SL schemes

Equation (10) is integrated over any moving control volume $[x_1,x_2]$ with $x_1=x_1(x,t)$ and $x_2=x_2(x,t)$. By using the Leibnitz' rule (Laprise & Plante, 1995) we obtain

$$\frac{d}{dt}\int_{x_1(x,t)}^{x_2(x,t)} c(x,t)dx - \left[c(x_2,t)\frac{dx_2}{dt} - c(x_1,t)\frac{dx_1}{dt} \right] + \left[c(x_2,t)u(x_2,t) - c(x_1,t)u(x_2,t) \right] = 0 . \quad (17)$$

If the boundaries $x_1$and x_2 are moving with the fluid we have

$$\frac{dx_1}{dt} = u(x_1,t) , \quad (18)$$

$$\frac{dx_2}{dt} = u(x_2,t) , \quad (19)$$

hence, (17) reduces to

$$\frac{dM(x_1,x_2,t)}{dt} \equiv \frac{d}{dt}\left(\int_{x_1(x,t)}^{x_2(x,t)} c(x,t)dx \right) = 0 . \quad (20)$$

Equation (20) implies the mass $M(x_1, x_2, t)$ contained between any two boundaries x_1 and x_2 (moving with the fluid) is constant, and transported with the flow from the departure point (x_1^n , x_2^n) to the destination points (x_1^{n+1}, x_2^{n+1}).

The domain $\Omega=[x_{min},x_{max}]$ is subdivided into N finite volumes FV_i with unequal spacing $\Delta x_i = x_{i+1}-x_i$, $i=1,2,\ldots,N$, where the grid points x_i and x_{i+1} are respectively the left and right

boundaries of each finite volume i (Figure 1). For each interval (x_i, x_{i+1}) an "initial" condition is defined at time t^n in terms of an interpolation function $\phi_i^n(x)$ as

$$c(x) = \phi_i^n(x) \ , \ x_i < x < x_{i+1} . \tag{21}$$

In SL schemes, $x_1(t)$ and $x_2(t)$ in (20) are chosen such that their position at the new time step $(n+1)$, i.e. $x_1^{n+1}(t)$ and $x_2^{n+1}(t)$, coincide with two sequential grid points, i.e.

$$x_1^{n+1}(t) = x_i \ , \ x_2^{n+1}(t) = x_{i+1} \tag{22}$$

where x_i is the position of i^{th} grid point, and using the fact that these boundaries are moving with fluid, their position at the last time step (n), i.e. $x_1^n(t)$and $x_2^n(t)$ represent the departure points of trajectories of nodes i and $i+1$

$$x_1^{n+1}(t) = x_i^d \ , \ x_2^{n+1}(t) = x_{i+1}^d , \tag{23}$$

where x_i^d is the position of the foot of the trajectory of node i.

Hence, an *inherently* conservative approach is constructed in the following three stages:

(a) Computation of the cell averages

Let x_l and x_m be the grid points such that $x_l < x_i^d < x_{l+1}$ and $x_m < x_{i+1}^d < x_{m+1}$. Then by using (20), the cell average values for each finite volume are calculated as

$$\bar{c}_{i+1/2} = \frac{M(x_i^d, x_{i+1}^d, t^n)}{\Delta x} = \frac{M(x_i, x_{i+1}, t^{n+1})}{\Delta x} , \tag{24}$$

where

$$M(x_i, x_{i+1}, t^{n+1}) = \int_{x_i^d}^{x_{i+1}^d} \phi^n(x) dx$$

$$= \begin{cases} \Delta x_l \int_{\xi_i^d}^{1} \phi_l^n(\xi) d\xi + \sum_{j=l+1}^{m-1} \Delta x_j \bar{\phi}_j^n + \Delta x_m \int_0^{\xi_{i+1}^d} \phi_m^n(\xi) d\xi & , \quad m \geq l+1, \\ \Delta x_l \int_{\xi_i^d}^{\xi_{i+1}^d} \phi_l^n(\xi) d\xi & , \quad m = l. \end{cases} \tag{25}$$

and the local coordinates at the foot of the trajectories read

$$\xi_i^d = (x_i^d - x_l) / \Delta x_l \qquad \text{and} \qquad \xi_{i+1}^d = (x_{i+1}^d - x_m) / \Delta x_m .$$

For the sake of simplicity, a constant grid spacing is assumed in the remainder of the paper.

(b) Computation of the nodal values

The nodal values c_i are calculated by fitting cubic curves on four sequential cells, using the known cell averaged values, and this procedure leads to a fourth order scheme. The resulting interpolation function for calculating the nodal values from the cell-averaged ones leads to

$$c_i = \frac{-\bar{c}_{i-3/2} + 7\bar{c}_{i-1/2} + 7\bar{c}_{i+1/2} - \bar{c}_{i+1/2}}{12\Delta x} . \tag{26}$$

In order to prevent spurious oscillations in (26), we impose

$$\min(\bar{c}_{i-1/2}, \bar{c}_{i+1/2}) \le c_i \le \max(\bar{c}_{i-1/2}, \bar{c}_{i+1/2}) . \tag{27}$$

The monotonicity constraint (27) ensures that the calculated nodal value c_i in (26) will remain bounded.

(c) Construction of the interpolating polynomials

Various polynomial interpolation schemes have been tried in the past, including the piecewise linear method (van Leer, 1977), and the piecewise parabolic method (Woodward and Colella, 1984). Conservative schemes using cubic polynomials have been introduced by Xiao et al. (2001). More recently, higher order non-oscillatory polynomials were proposed in the area of weighted essentially non-oscillatory (WENO) schemes (e.g. Levy et al., 2002).

An efficient alternative is the use of the rational function of Xiao et al. (1996 and 1999) (leading to a monotonic interpolation scheme) which has been recently employed in exactly conservative and oscillation-less SL schemes (Nakamura et al., 2001; Ida, 2002)

$$M(X) = \int_0^X c(\theta) d\theta = \frac{\kappa_i X^3 + \chi_i X^2 + c_i^n X}{1 + \alpha\beta_i X_i} , \tag{28}$$

where X=x-x_i . The coefficients are calculated as

$$\beta_i = \left[(\bar{c}_i - c_i^n) / (c_{i+1}^n - \bar{c}_i) - 1 \right] / \Delta x_i , \tag{29}$$

$$\chi_i = \bar{c}_i \alpha\beta_i + (\bar{c}_i - c_i^n) / \Delta x_i - \kappa_i \Delta x_i , \tag{30}$$

$$\kappa_i = \left[c_i^n - \bar{c}_i + (c_{i+1}^n - \bar{c}_i)(1 + \alpha\beta_i \Delta x_i) \right] / \Delta x_i , \tag{31}$$

$$\alpha = \begin{cases} 1 & for(\bar{c}_i - c_i^n)/(c_{i+1}^n - \bar{c}_i) \geq 0, \\ 0 & otherwise. \end{cases} \tag{32}$$

Finally, differentiating (28) with respect to X, leads to

$$c(X) = \frac{3\kappa_i X^2 + 2\chi_i X + c_i^n}{1+\alpha\beta_i X_i} - \alpha\beta_i \frac{\kappa_i X^3 + \chi_i X^2 + c_i^n X}{(1+\alpha\beta_i X_i)^2}. \tag{33}$$

The rational function defined in (33) coincides with a quadratic one when α=0. The above SL Integrated Mass scheme with the Rational interpolation function (SLIM-R) is summarized as follows

SLIM-R Algorithm:

(i) Draw the trajectories and assign the mass between two sequential departure points to the corresponding destination Eulerian control volume using (24) and (25).

(ii) Calculate the nodal values based on the already calculated cell average values, and impose the constraints (26) and (27).

(iii) Construct the interpolation polynomials based on the cell average values using the rational function (33).

The main difference between the present scheme (SLIM-R) and existing numerical ones (such as the R-CIP-CSL scheme of Nakamura et al., 2001), is the calculation of the nodal values (step ii). Here, the nodal values are directly calculated by the cell average values (already computed). This is an essential step in order to construct fully conservative and stable schemes for shallow-water models. In most existing CIP-CSL type conservative schemes, the nodal values are calculated using the two-step SL procedure (15) and (16). Contrary to most existing schemes, the proposed method can be used to construct fully conservative and stable SL schemes, as shown in section 5.

In order to show the performance of the present method employing the rational function, we compare our results with two other schemes using quadratic polynomials (QUICKEST and R-CIP-CSL2) in a classical advection test. The first scheme is the well-known QUICKEST scheme (Leonard 1979) employing the cell average values of three sequential cells to define the quadratic polynomials. A non-oscillatory version of this scheme is the ULTIMATE QUICKEST scheme (Leonard 1991). The second scheme is the R-CIP-CSL2 method of Nakamura et al. (2001), in which the nodal values are calculated using the two-

step procedure (15) and (16), with the rational function (33). The exact solution is shown in figure 2 after 1500 time steps with a CFL number of 0.2. A low value of the CFL number is used to compare the numerical diffusion of the proposed method (without the constraint (27)) and the QUICKEST scheme. As shown in figure 2, the proposed method gives better results than the QUICKEST scheme in terms of both diffusion and numerical dispersion. In order to investigate the performance of the proposed method using the oscillation suppressing constraint (27), we also compare it with the ULTIMATE QUICKEST and R-CIP-CSL2 schemes and the results are shown in figure 3. Again, the proposed method exhibits a much lower level of numerical diffusion than the ULTIMATE QUICKEST scheme, but the R-CIP-CSL2 method appears to be marginally less diffusive than our scheme. However, contrary to the R-CIP-CSL2 scheme, the proposed method is applicable to the fully conservative form of the shallow water equations as shown in section 3-2-2 and 5.

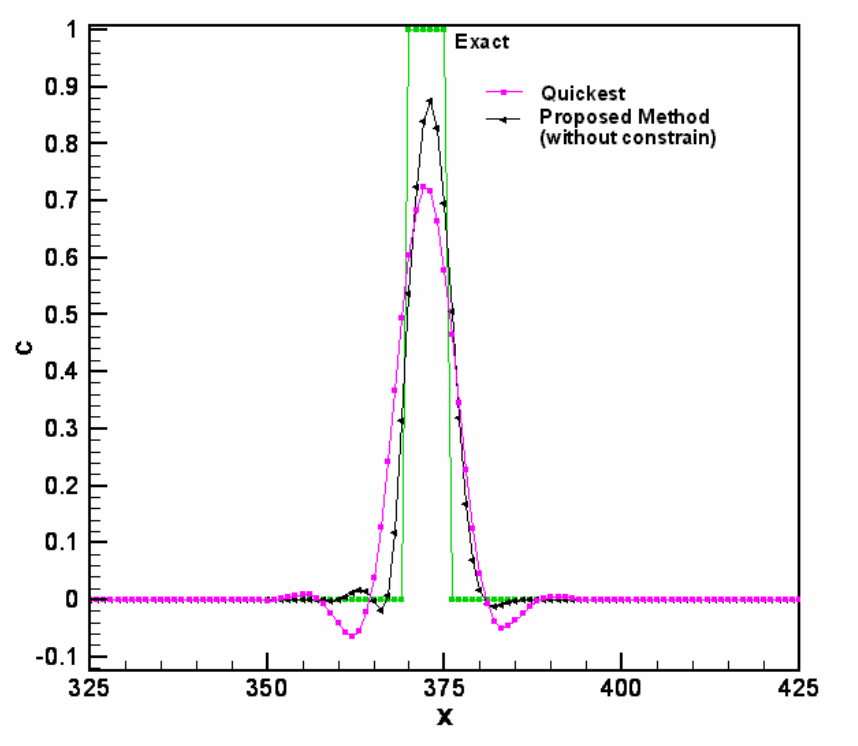

Figure 2. Results of the linear wave after 1500 time step with a CFL number of 0.2

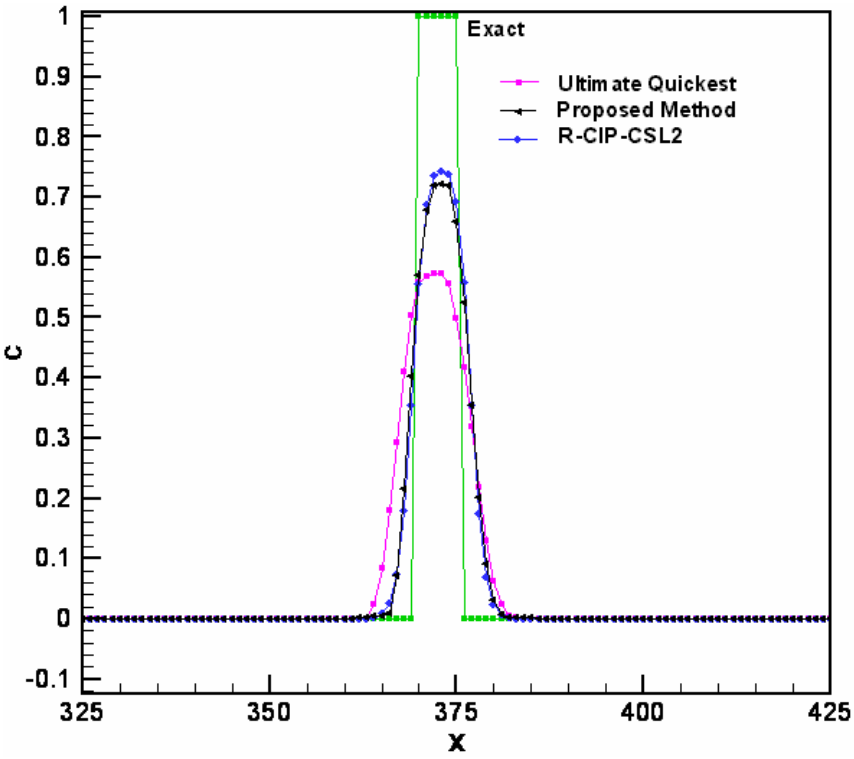

Figure 3. Results of linear wave after 1500 time step with a CFL number of 0.2

3-3- A conservative SL Scheme for shallow-water equations

It is well know that the source terms lead to instabilities when large time steps are employed in the framework of SL schemes. This has led to the development of the semi-implicit SL (SISL) schemes. Here, we intend to show how the SLIM-R scheme could be successfully combined with SISL methods, for constructing a fully conservative scheme.

3-2-1-The continuity equation

The SLIM-R scheme applies directly to (10), and hence no source term is present, contrary to the CIP-CSL schemes case. The continuity equation is the simple scalar conservation law

$$\frac{\partial h}{\partial t}+\frac{\partial (uh)}{\partial x}=0\,,$$

and hence, the SLIM-R scheme can be used directly here.

3-2-2-The momentum equation

The depth averaged momentum equation in (1) is written in the conservative form

$$\frac{\partial p}{\partial t}+\frac{\partial(up+0.5gh^2)}{\partial x}=0, \tag{34}$$

where $p=uh$. Here, we extend the approach of Laprise and Plante (1995) to (34) which is integrated over any control volume $[x_1,x_2]$, moving with the fluid flow. This leads to

$$\frac{d}{dt}\int_{x_1(x,t)}^{x_2(x,t)} p(x,t)dx+0.5g\left[h(x_2,t)^2-h(x_1,t)^2\right]=0. \tag{35}$$

Equation (35) is now integrated over a temporal control volume and we obtain

$$\int_{x_1(x,t^{n+1})}^{x_2(x,t^{n+1})} p(x,t^{n+1})dx=\int_{x_1(x,t^n)}^{x_2(x,t^n)} p(x,t^n)dx-0.5g\left(\int_{t^{n1}}^{t^{n+1}} h(x_2,t)^2dt-\int_{t^{n1}}^{t^{n+1}} h(x_1,t)^2dt\right). \tag{36}$$

By choosing x_1, x_2 as before, (36) is rewritten as

$$\overline{p}_i^{n+1}\Delta x_i=\int_{x_i^d}^{x_{i+1}^d} p(x,t^{n+1})dx-0.5g\left(\int_{t^{n1}}^{t^{n+1}} h(x_2,t)^2dt-\int_{t^{n1}}^{t^{n+1}} h(x_1,t)^2dt\right). \tag{37}$$

We then use a trapezoidal approximation for the pressure integrals

$$\int_{t^{n1}}^{t^{n+1}} h(x_1,t)^2dt=\frac{(h_i^{n+1})^2+(h_i^d)^2}{2}\Delta t, \tag{38}$$

and we obtain

$$\overline{p}_i^{n+1}\Delta x_i=\int_{x_i^d}^{x_{i+1}^d} p(x,t^{n+1})dx-g\Delta t\,\frac{(h_{i+1}^{n+1})^2+(h_{i+1}^d)^2-(h_i^{n+1})^2+(h_i^d)^2}{4}, \tag{39}$$

where the integral $\int_{x_i^d}^{x_{i+1}^d} p(x,t^{n+1})dx$ can be calculated in the same way as in (25). The above approach is conservative, because the second term in right hand side of (39) is in the flux form.

Hence, the nodal values of h^{n+1} are necessary for calculating the right hand side (RHS) of (39). Estimating those nodal values is a crucial step in to preserve the stability of SL schemes, using large time steps, in the case of fully conservative equations.

Here, we use the following SISL scheme to obtain a priori estimation of h^{n+1} when calculating the source term in the RHS of (39)

$$h_i^{n+1} + \Delta t^2 g h_i^n \frac{h_{i+1}^{n+1} - 2h_i^{n+1} + h_{i-1}^{n+1}}{\Delta x^2} = \hat{h}_i^n - \Delta t h_i^n \frac{\hat{u}_{i+1}^n - \hat{u}_{i-1}^n}{2\Delta x}, \qquad (40)$$

where $\hat{h}_i$ and $\hat{u}_i$ are the water depth and velocity calculated at the foot of the trajectory arriving at node *i*. Equation (40) leads to a simple three-diagonal system which can be solved efficiently. The derivation of (40), proposed by Layton and van de Panne (2002) is presented in appendix I, and it has been extended to the 2D case by Layton and van de Panne (2002).

Knowing h^{n+1} from (40), equation (39) can then be solved by using the SLIM-R scheme. The semi-implicit SL scheme with rational function (SI-SLIM-R) is summarized as follows:

SI-SLIM-R Algorithm

(i) Determine the nodal values of h^{n+1} by (40), and use them to calculate the source term in the right hand side of (39)

(ii) Apply the SLIM-R scheme to solve (39)

(iii) Apply the SLIM-R scheme to solve the continuity equation.

As previously mentioned the SLIM-R method, although marginally more diffusive than the R-CIP-CSL2 scheme (Figure 3), is also much more stable. In order to show the performance of the SI-SLIM-R scheme, we now construct the SI-CIP-CSL-R scheme. The latter is obtained by employing the R-CIP-CSL2 scheme at steps (ii) and (iii) in the above SI-SLIM-R algorithm. In the next section we show that, contrary to the SI-SLIM-R scheme, the SI-CIP-CSL-R method is restricted to CFL numbers smaller than 1. Indeed if the calculated cell averaged values are not taken account in the calculation of the nodal values, then the stability region is reduced. This is why the SLIM-R scheme (24)-(33), has been introduced to calculate the nodal values based on the cell averages instead of determining them by the SL transport as for CIP-CSL type schemes.

4- Artificial viscosity

The SL method leads to oscillation-free results in the case of a pure advection equation when a non-oscillatory interpolation function is used. However, this is not the case when the shallow-water equations are considered, and spurious oscillations arise even when a

first order (linear) interpolation scheme is used (Navarro and Priestley, 1994). This is due to the presence of gravitational source term in the momentum equation. Two approaches have been proposed in the past to suppress those oscillations. In the first one (Xiao, 2002), a flux vector splitting method is used to discretize the source terms while in the second approach, the oscillations are suppressed by adding an artificial diffusive term. The latter technique is employed here by following the Tseng et al. (2000) method, where the computed values $\vec{U}_i^{*n+1}$ are corrected by adding a diffusive term as

$$\vec{U}_i^{n+1} = \vec{U}_i^{*n+1} + 0.5\left(R_{i+1/2}\vec{\Phi}_{i+1/2} - R_{i-1/2}\vec{\Phi}_{i-1/2}\right). \tag{41}$$

In (41), $\vec{\Phi}_{i+1/2} = (\Phi^1_{i+1/2}, \Phi^2_{i+1/2})$ is calculated as

$$\Phi^k_{i+1/2} = \psi(\lambda^k_{i+1/2})\left(1-\tau\left|\lambda^k_{i+1/2}\right|\right)\left(1-\varphi\left|r^k_{i+1/2}\right|\right)\alpha^k_{i+1/2}, \tag{42}$$

where k=1 and 2. The entropy correction function ψ in (42) is defined as

$$\psi(w) = \begin{cases} |w| & \text{if } |w| \geq \varepsilon, \\ \varepsilon & \text{if } |w| < \varepsilon. \end{cases} \tag{43}$$

Harten and Hyman (1983) introduced the following formula to calculate ε

$$\varepsilon^k_{i+1/2} = \max\left[0,\quad \lambda^k_{i+1/2} - \lambda^k_i,\quad \lambda^k_{i+1} - \lambda^k_{i+1/2}\right], \tag{44}$$

and characteristic variable in (42) is defined as

$$\alpha_{i+1/2} = L_{i+1/2}(U_{i+1} - U_i). \tag{45}$$

The role of flux limiter function φ in (41) is to supply artificial dissipation when there is a discontinuity or a strong gradient, while adding very little or no dissipation at all in regions of smooth variations. Yee (1989) proposed to calculate φ as

$$\varphi\left(r^k_{i+1/2}\right) = \frac{r^k_{i+1/2} + \left(r^k_{i+1/2}\right)^2}{1 + \left(r^k_{i+1/2}\right)^2}, \tag{46}$$

where

$$r^k_{i+1/2} = \frac{\alpha^k_{i+1/2-\sigma}}{\alpha^k_{i+1/2}}, \tag{47}$$

and

$$\sigma = sign\left(\lambda^k_{i+1/2}\right). \tag{48}$$

In (48), λ^1 and λ^2 are the eigenvalues corresponding to the Jacobian of the flux vector

$$\lambda^1 = u + c, \tag{49}$$

$$\lambda^2 = u - c, \tag{50}$$

where

$$c = \sqrt{gh}. \tag{51}$$

In (41) and (45) R and L are respectively the right and left eigenvector matrices

$$R = \begin{bmatrix} 1 & 1 \\ \lambda^1 & \lambda^2 \end{bmatrix}, \tag{52}$$

and

$$L = \frac{1}{2c}\begin{bmatrix} -\lambda^1 & 1 \\ \lambda^2 & -1 \end{bmatrix}. \tag{53}$$

The mean values of the velocity and water depth can be calculated by using the Roe method

$$u_{i+1/2} = \frac{u_{i+1}\sqrt{h_{i+1}} + u_i\sqrt{h_i}}{\sqrt{h_{i+1}} + \sqrt{h_i}}, \tag{54}$$

$$c_{i+1/2} = \sqrt{g\frac{h_{i+1} + h_i}{2}}. \tag{55}$$

5-Numerical results

In order to study the performance of the numerical method presented here, three test cases have been selected herein. Tests a and b have been chosen to examine the accuracy of the proposed method while test c is used to show the stability of the method. In the Riemann problem tests (a, b), the exact solutions are calculated by using an exact solver, Toro (2000), and the CFL is set to 0.3. In test c, a CFL of 2.0 is used. In all tests a wide horizontal, rectangular and frictionless channel of length 50 m is used.

a –The Dam Break Problem

The dam break problem is the most common test to evaluate the performance of shock capturing schemes in shallow flows. As mentioned by Toro (2000), the ability of a numerical method to correctly resolve shock waves is an important feature of the method in

terms of (i) correct speed of the propagation, (ii) correct strength of the jump, (iii) width of the shock layer and (iv) absence or presence of spurious oscillations in the vicinity of the shock. Here, a dam is located at the channel mid-length. The water depth at the left and right hand sides of the dam are 0.5m and 0.1m, respectively. The dam is instantaneously removed across its entire width and the simulation is performed up to time t=2s. The results obtained for the depth *h* and discharge *p* are presented in figures 4.a and 4.b respectively, and they are compared with the exact solution and the results of the Lyton and van de Panne non-conservative SL scheme (2002). The results consist of a strong right-going shock and a left-going rarefaction. As shown in figures 4.a and 4.b, the non conservative SL scheme leads to large errors in the shock speed and water level right after the shock wave (shock strenght) and it also generates spourious oscillations. These errors are not present in the proposed scheme, which shows a good shock-capturing ability with low oscillations.

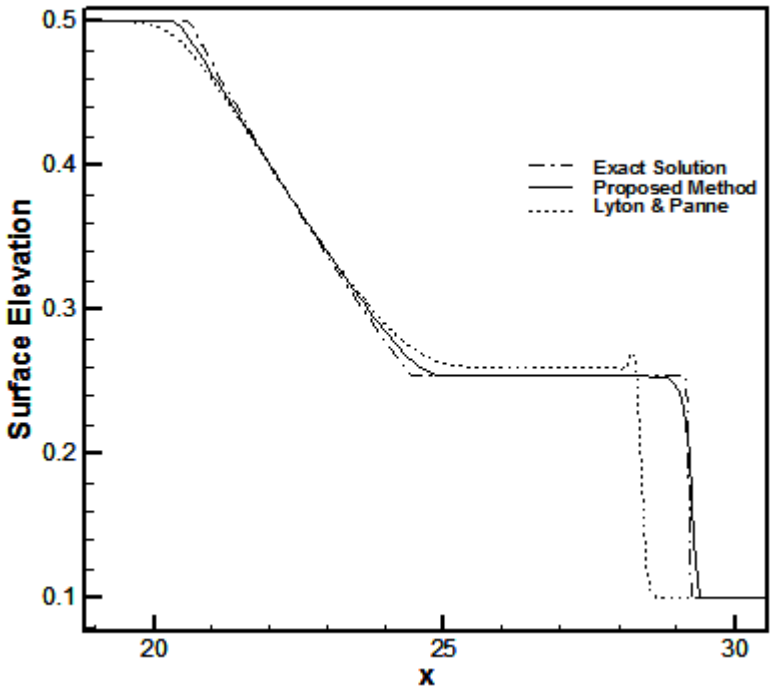

Fig. 4.a. The dam break problem: The water surface elevation at t=2s with non-conservative MOC scheme, the proposed scheme and the exact solution

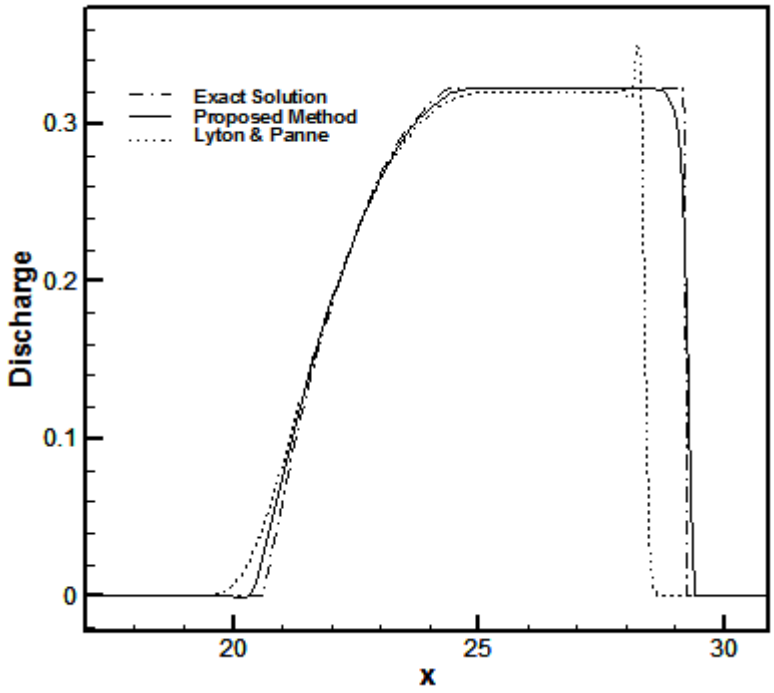

Fig. 4.b. The dam break problem: Water discharge at t=2s with non-conservative MOC scheme, the proposed scheme and the exact solution

b- Left Sonic Rarefaction and Right Shock

In this test, the initial condition has been chosen in order to produce a strong right propagating shock wave and a sonic or trans-critical left propagating rarefaction wave. The important feature here is that the left rarefaction is sonic, i.e. it contains the sonic point where the flow regime changes from super critical to sub critical. Most numerical methods encounter difficulties in simulating sonic rarefactions, and they produce an unphysical jump at the sonic point inside the rarefaction waves. Such schemes are called entropy-violating methods. The water depth is chosen to be 0.5m and 0.05m in left and right sides of the dam, respectively.

Numerical results at t=10s are shown in figure 5 and they are compared with the exact solution and those of the Lyton and van de Panne scheme (2002). The result of the Roe scheme is also shown to illustrate the entropy violating shock inside the rarefaction wave. As shown in figure 5, the proposed scheme is able to correctly simulate the shock speed without exhibiting an unphysical shock.

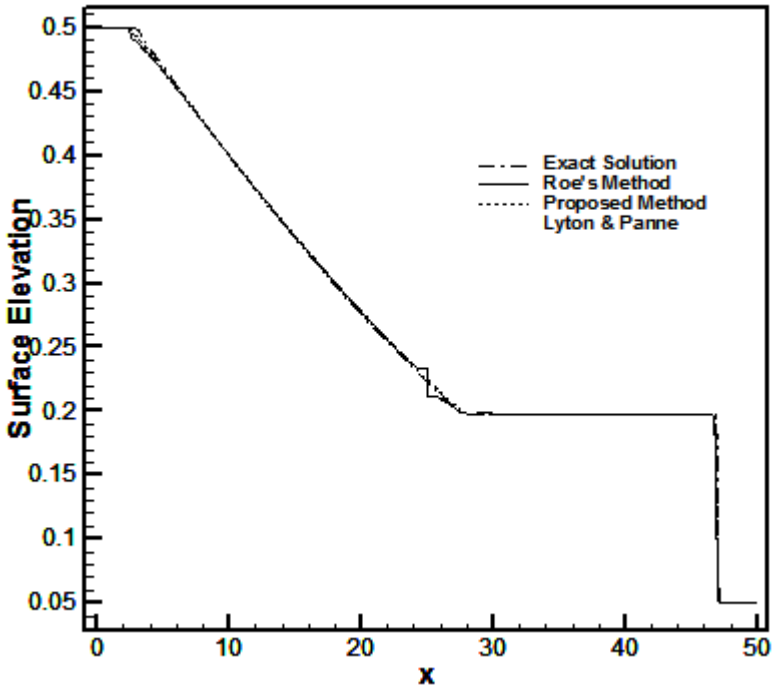

Fig. 5. Left sonic rarefaction and right shock: Water surface elevation at t=10s with proposed method, the Roe scheme and the exact solution.

c- An Stability Test; A small perturbation of stagnant condition

The initial flow velocity is zero in the entire channel with

$$h(x)=\begin{cases}0.5+0.5*\left(\cos\left[\pi\left(1+2\dfrac{x_0-x}{L}\right)\right]+1\right), & for 17.6<x<19.6,\\ 0.5, & otherwise.\end{cases} \qquad (56)$$

where x_0=18.6 m and L=2 m.

Numerical results using CFL=2 are shown in figure 6 and they are compared with those obtained by the Roe method in the case CFL=0.2. Here, the proposed method is stable up to $\mathrm{CFL}\approx 8.0$, while other existing conservative SL methods like R-CIP-CSL2 (Nakamura et al., 2001) fail to simulate it with CFL grater than 1.

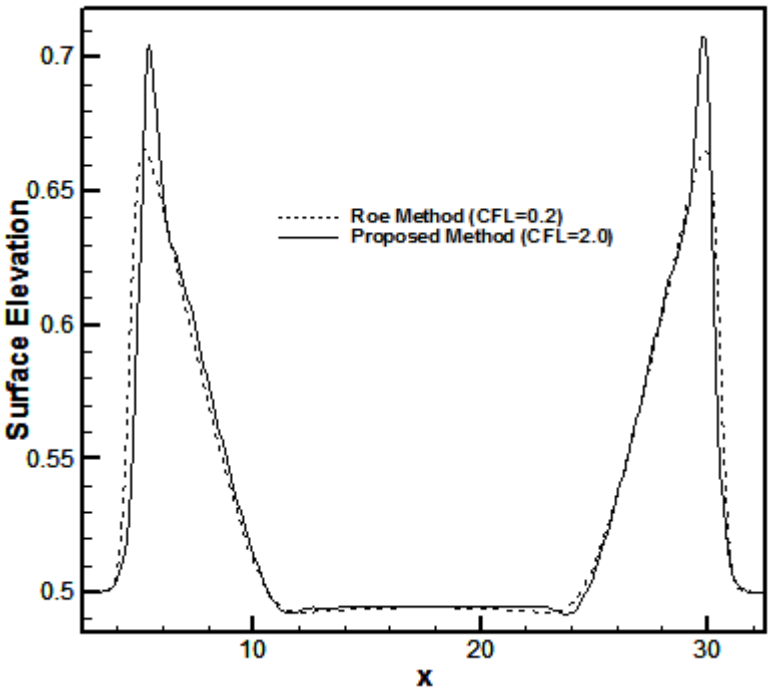

Fig. 6. Cosine hump: The water surface elevation at t=4s with proposed method (CFL=2.0) and Roe scheme (CFL=0.2)

5-Conclusion

SL integrated mass method (SLIM) of Laprise and Plante (1995) has been extended to the conservative form of the shallow-water equations. This method was successfully combined with a semi-implicit SL one, and resulted in a fully conservative SL scheme (SI-SLIM-R).

The most important feature of the proposed scheme is that, not only the mass, but also the gravity source term are conserved during the simulation and the fully conservative form of the shallow-water equations is satisfied. Numerical results showed that contrary to existing CIP-CSL schemes, the proposed algorithm preserves the stability property of SL methods when large time steps are employed. The fully conservation property of the proposed scheme enables it to correctly simulate the shock speed in dam-break type flows.

A number of test cases showed that the proposed method could be used for sub, super and trans-critical flows and also for dam-break type flows. The fully conservation property considerably improves the performance of common SL schemes for a wide range of practical applications.

In terms of computational efficiency, our method, as the G P scheme, consists of two steps but the oscillation suppressing process is done here via an artificial viscosity approach rather than a limiter one used in the GP scheme. Further, the proposed method is free of phase problems which usually arise when corrective methods are employed in solving systems of equations. On the other hand due to the inherently conservative approach, the highly expensive linear programming step of the corrective methods is avoided, and this makes our method more efficient than the GP scheme.

Appendix I -Layton and Van de Panne's SL scheme

In the Layton and van de Panne's scheme (2002), as for most SL schemes, the non-conservative shallow-water equations are written in Lagrangian form

$$\frac{dh}{dt} + h\frac{\partial u}{\partial x} = 0, \tag{I-1}$$

$$\frac{du}{dt} + g\frac{\partial h}{\partial x} = 0\,. \tag{I-2}$$

The Lagrangian derivative is approximated along the trajectories

$$\frac{h^{n+1} - \hat{h}^n}{\Delta t} + h^n \left.\frac{\partial u}{\partial x}\right|^{n+1} = 0, \tag{I-3}$$

$$\frac{u^{n+1} - \hat{u}^n}{\Delta t} + g \left.\frac{\partial h}{\partial x}\right|^{n+1} = 0, \tag{I-4}$$

where $\hat{h}$ and $\hat{u}$ are the water depth and velocity that are calculated at the foot of trajectories. Differentiating the momentum equation with respect to x and substituting in the continuity equation gives

$$h^{n+1} - \Delta t^2 g h^n \left.\frac{\partial^2 h}{\partial x^2}\right|^{n+1} = \hat{h}^n - \Delta t h^n \left.\frac{\partial \hat{u}}{\partial x}\right|^{n}\,. \tag{I-5}$$

Equation (I-5) can be numerically solved by using a centered discretization scheme as

$$h_i^{n+1} - \Delta t^2 g h_i^n \frac{h_{i+1}^{n+1} - 2h_i^{n+1} + h_{i-1}^{n+1}}{\Delta x^2} = \hat{h}_i^n - \Delta t h_i^n \frac{\hat{u}_{i+1}^n - \hat{u}_{i-1}^n}{2\Delta x}\,. \tag{I-6}$$

References

Aureli F., Mignosa P., Tomirotti M. (2000), '*Numerical simulation and experimental verification of dam-breack flows with shocks*', Journal of hydraulic research, 38, 197.

Colella P. and Woodward P. (1984), '*The piecewise parabolic method (PPM) for gas-dynamical simulations*', Journal of computational physics, 54, 174-201.

Falcone M. and Ferrettiy R. (2002), '*semi-Lagrangian schemes for Hamilton–Jacobi equations, discrete representation formulae and Godunov methods*', Journal of computational physics, 175, 559-575.

Garcia Navarro P., Alcrudo F. and Saviron F. (1994), '*1-D open channel flow simulation using TVD MacCormack Scheme*', Journal of Hydraulic engineering, ASCE, 1992; 118(10), 1359-72.

Garcia Navarro P., Priestley A. (1994), '*A Conservative and Shape Preserving semi-Lagrangian Method for Solution of the Shallow-water Equations*', International Journal for Numerical Methods in Fluids, 18, 2.

Gravel S., Staniforth A. (1993), '*A mass-conserving semi-Lagrangian scheme for the shallow-water equations*', Monthly Weather Review, 122, 243.

Ida M., (2002), '*A conservative semi-Lagrangian method for oscillation free computation of advection processes*', Computer phys. communications 116, 121-135.

Laprise J. and Plante A. (1995), '*A class of semi-Lagrangian integrated mass (SLIM)numerical transport algorithms*' , Monthly Weather Review, 123, 2551-2566.

Leonard B. P. (1979), '*A stable accurate convective modeling procedure based on quadratic upstream interpolation*', Comp. Methods in Appl. Mech. and Eng. 19, 59-98.

Leonard B. P. (1991), '*The ultimate conservative difference scheme applied to unsteady one-dimensional advection*', Comp. Methods in Appl. Mech. and Eng. 88, 17-74.

Le Roux D. Y., Lin C. A. and Staniforth A. (2000), '*A semi-implicit semi-Lagrangian finite-element shallow-water ocean model*', Monthly Weather Review, 128, 1384.

Levy D., Puppo G. and Russo G. (2002), '*A fourth order central WENO scheme for multi-dimensional hyperbolic systems of conservation Laws*', SIAM Journal on scientific computing, 24, 2002, pp. 480-506.

Lin S. J. and Rood R. B., (1997), '*An explicit flux-form semi-Lagrangian shallow-water model on the sphere*', Q. J. R. Meterol. Soc. 123, 2477-2498.

Lyton A. T. and van de Panne M. (2002), '*A numerically efficient and stable algorithm for animating water wave*', Visual computer, 18, 41-53.

Nakamura T., Tanaka R., Yabe T. and Takizawa K. (2001), '*Exactly conservative semi-Lagrangian scheme for multi-dimensional hyperbolic equations with directional splitting technique*', Journal of computational physics, 174, 171-207.

Priestly A. (1993), '*A quasi-conservative version of the semi-Lagrangian advection scheme*', Monthly Weather Review, 121, 621-629.

Staniforth A. and Cote J. (1991), '*Semi-Lagrangian integration scheme for atmospheric models- a review*', Monthly Weather Review, 119, 2206-2223.

Tanaka R., Nakamura T., and Yabe T. (2000), '*Constructing exactly conservative scheme in a non-conservative form*', Computer physics communications, 126, 232-243.

Temperman C., Hortal M. and Simmons A. (2001), '*A two-time-level semi-Lagrangian global spectral model*', Q. J. R. Meteorol. Soc, 127, 111-127.

Tseng M. H. and Chu C. R. (2000), '*The simulation of dam-break type flows by an improved predictor-corrector TVD scheme*', Advances in water resources, 23,637-643.

van Leer B. (1977), '*Towards the ultimate conservative difference scheme IV: A new approach to numerical convection*', Journal of computational physics, 23, 276-299.

Xiao F., Yabe T., Ito T. (1996), '*constructing oscillation preventing scheme for advection equation by rational function*', Computer physics communications, 93, 1.

Xiao F., Yabe T., Ebisuzaki T. (1999), '*An oscillation suppressing semi-Lagrangian solver for advection equation*', Computer physics communications 116, 121-135.

Xiao F. and Yabe T. (2001), '*Completely conservative and oscillation-less semi-Lagrangian schemes for advection transportation*', Journal of computational physics, 170, 498-522.

Xiao F. (2002), '*Profile modifiable conservative transport schemes and a simple multi-integrated moment formulation for hydrodynamics*', "Computational Fluid Dynamics 2002", (Proceedings of the 2nd international conference on CFD, Sydney, Australia), Springer, 2003, ISBN 3-540-00739-3.

Xiu D. and Karniadakis G. (2001),'*A semi-Lagrangian High-Order Method for Navier–Stokes Equations*', Journal of computational physics, 172, 658-684.

Yabe T., Tanaka R., Nakamura T. and Xiao F. (2001), '*Exactly conservative semi-Lagrangian methods (CIP-CSL) in one dimension*', Monthly Weather Review, 126, 232.

Zerroukat M., Wood N., and Staniforth A. (2002), '*Slice: A semi-Lagrangian inherently conserving and efficient scheme for transport problems*', Q. J. R. Meterol. Soc. 128, 2801-2820.

Yee H. (1989), '*A class of high-resolution explicit and implicit shock-capturing methods*', NASA TM-101088.

Harten A. and Hyman P. (1983), '*Self adjusting grid methods for one-dimensional hyperbolic conservation laws*', Journal of computational physics, 50, 235-269.

CHAPTER 3

A conservative extension of the method of characteristics for 1-d shallow flows

In the second chapter, a fully conservative semi-Lagrangian scheme was developed by ensuring the conservation of mass and momentum in the polynomial fitting step. In this chapter, this approach is extended to the method of characteristics and a fully conservative MOC method is proposed where the fully conservation property is imposed in the

interpolation step. The resulting scheme is shown to produce a low level of numerical diffusion and dispersion.

Une prolongation conservative de la méthode des caractéristiques pour les écoulements peu profonds 1-d.

Résumé

La méthode des caractéristiques (MOC) a été employée pendant longtemps dans les canaux ouverts. Elle est basée sur une formulation non conservative des équations, et par conséquent elle ne peut pas être employée directement pour résoudre des écoulements peu profonds discontinus.Dans cet article nous développons une version conservative du schéma MOC pour les écoulements peu profonds 1-D en imposant la loi de conservation à l'étape d'interpolation. La propriété de conservation du schéma permet de modéliser précisément un choc et permet au schéma MOC de simuler des écoulements de type ruptures de barrage. En employant une fonction appropriée d'interpolation, la méthode proposée peut également produire des résultats présentant peu d'oscillations et tout à fait précis. Un certain nombre de cas tests difficiles montre que le schéma proposé se compare avantageusement a la méthode MOC traditionnelle (non conservatrice) dans le cas de type ruptures de barrage et de simulations d'écoulements trans-critiques.

A conservative extension of the method of characteristics for 1-d shallow flows

A. MOHAMMADIAN, D. Y. LE ROUX , M. TAJRISHI

Abstract. *The method of characteristics (MOC) has been used for a long time in open channels and pipes flows. It is based on non-conservative equations, and hence it cannot be used directly for solving discontinuous shallow flows. In this paper we develop a conservative version of the MOC scheme for 1-D shallow flows by imposing the conservation law at the interpolation step. The conservation property of the scheme ensures the production of an accurate shock modeling and enables the MOC scheme to simulate dam-break type flows. By using a proper interpolation function, the proposed method can also produce quite accurate low-oscillatory results. A number of challenging test cases show considerable improvement compared to the traditional non-conservative MOC scheme in the case of dam break type and trans-critical flow simulations.*

Key Words: Conservative, method of characteristics, shallow-water, dam-break.

1. Introduction

The flow regime changes from subcritical to supercritical in many fluvial flows, and the numerical method should be able to analyze these two types of flows simultaneously. Another difficulty encountered by the numerical method deals with flows which result from the sudden opening and closing of control gates and dam break flows.

Extensive research has been performed in this area during the last two decades and different numerical schemes have been developed in the context of finite difference (FDM), finite element (FEM), finite volume (FVM), Lagrangian (LM), and semi-Lagrangian (SLM) methods. The characteristics play an essential role in most of existing numerical schemes, especially in those which are designed to simulate both sub and super critical flows. The use of characteristics and wave propagation structure stabilizes the numerical methods and prevents spurious oscillations (Leveque, 2002).

Attention has been focused almost exclusively on the FVM, which is inherently conservative, and several shock capturing schemes have been proposed using flux vector and flux difference splitting methods, e.g. Roe (1981), Van Leer (1982), Harten and Osher (1987). The FVM has also been considered to solve the shallow-water equations, e.g. Glaister (1988), Alcrudo and Navarro (1993), Nujic (1995), Zhao (1996) and Wang (2000). Most of these FVM have the capability of capturing shocks quite accurately in few computational cells, and for most of them, the flux vector is determined based on the characteristics and wave propagation structure. The use of the characteristics has not been restricted to FVM. For example, Fennema and Chaudry (1987) presented some characteristics-based finite difference schemes for dam break flows, and Hicks and Steffler (1992) used a characteristic-dissipative Galerkin FEM to solve the shallow water equations.

The conservation of mass and momentum is an important issue for all numerical schemes. Although the governing equations can be written in a non-conservative form for smooth flows, they are originally derived from the conservation laws, and numerical schemes may have to satisfy the conservation property. The exact conservation is crucial in some cases including long term simulations, where mass errors may accumulate in time and discontinuous flows. In the presence of nonlinear fluxes, conservation laws may lead to singularities, and consequently weak solutions derived from the underlying integral conservative relations, have to be introduced. Many studies have been performed in this area and a number of conservative schemes have been published in the literature. Those may be grouped in two categories: corrective and inherently conservative schemes (such as flux form schemes). Among the algorithms of the first group (corrective schemes), Garcia Navarro and Priestley (1994) used a posteriori correction to restore the desired quantity whilst minimizing change to the original solution. Their approach is based on an averaging between high and low order schemes, where the averaging factors at all grid points and for each time-step are adjusted somehow to minimize the mass misbalance by a linear programming type approach, which is computationally expensive. Moreover, this method only guarantees the phase conservation when a single scalar equation is considered. For most of the second type schemes (inherently conservative), mass conservation is obtained by imposing a constraint at the polynomial interpolation step. Attention herein is focused on the second group.

Another important issue of numerical schemes deals with the ability of the method in properly simulating transcritical flows. Indeed, solutions of the integral conservative equations are not unique, and a number of numerical schemes produce nonphysical results, e.g. the Roe scheme may lead a shock inside a rarefaction wave in the case of transcritical flows.

Methods of characteristics have been used for a long time by hydraulic engineers in open channels and pipe flows, and their popularity is largely due to their simple implementation. Those methods are based on non-conservative equations, hence they do not ensure the conservation properties and they cannot be used directly to solve discontinuous flows. The objective of this paper is to develop an inherently conservative characteristics based scheme with a high level of accuracy to simulate dam-break type flows. To this end, we impose the conservation law at the interpolation step level. We show that by using a uniformly non-oscillatory (UNO) scheme and a conservative interpolation function, the MOC scheme can produce high accurate low-oscillatory results in simulating complex discontinuous 1-D shallow flows.

Challenging test cases performed in the paper (including strong sonic shocks and dry bed problems) show that the proposed scheme is potentially a competing method for high resolution schemes. Moreover, the computational effort of the proposed method is comparable to the cost of a typical high resolution scheme (the Roe approximate solver with a standard second order interpolation scheme using the minmod slope limiter).

The proposed method may also be extended to the 2D case by considering either the cone of characteristics, or 1D characteristics schemes in the direction orthogonal to the cell interfaces.

The paper is organized as follows: In section 2 the model equations are presented and in section 3 and 4 the MOC scheme is described and discretized, respectively. In section 5, a new conservative interpolation method is developed, and the method for calculating the slope of the characteristics is presented in section 6. The performance of the proposed numerical method is tested for different cases, and those are compared with exact solutions in section 7. Some concluding remarks complete the study.

2- The one dimensional shallow-water equations

The one dimensional depth averaged continuity and momentum equations in a wide channel are written in conservative form (Toro, 2000)

$$\frac{\partial \vec{U}_c}{\partial t} + \frac{\partial \vec{F}}{\partial x} = \vec{S}_c, \tag{1}$$

where $\vec{U}_c$ is the vector of the conserved variables

$$\vec{U}_c = \begin{pmatrix} h \\ p \end{pmatrix}, \tag{2}$$

$\vec{F}$ is the flux vector

$$\vec{F} = \begin{pmatrix} uh \\ up + 0.5gh^2 \end{pmatrix}, \tag{3}$$

and the source term $\vec{S}_c$ (including frictional, bed slope, and width variations effects) is assumed to be zero. In (2) and (3), *t* and *x* are the time and spatial coordinates respectively, *h* and *u* are the water depth and the velocity variables respectively, *g* is the gravitational acceleration and $p = uh$ is the discharge in unit width. In the following the subscript $_c$ will refer to a conservative variable.

Equation (1) may also be written in non-conservative form (Henderson, 1966)

$$\frac{\partial u}{\partial t} + u\frac{\partial u}{\partial x} = -g\frac{\partial h}{\partial x}, \tag{4}$$

$$\frac{\partial h}{\partial t} + u\frac{\partial h}{\partial x} = -h\frac{\partial u}{\partial x}. \tag{5}$$

3- Review of the MOC scheme

Consider the one dimensional advection equation

$$\frac{\partial f}{\partial t} + \lambda\frac{\partial f}{\partial x} = 0, \tag{6}$$

where *f(x,t)* is any physical variable to be transported and λ is the phase speed. In the MOC scheme, the reference frame is moving at the speed $\lambda = dx/dt$, and thus the total derivative of *f* reads

$$\frac{df}{dt} = \frac{\partial f}{\partial t} + \frac{\partial f}{\partial x}\left(\frac{dx}{dt}\right) = \frac{\partial f}{\partial t} + \lambda \frac{\partial f}{\partial x}. \tag{7}$$

Hence, (6) is reduced to

$$\frac{df}{dt} = 0, \tag{8}$$

which implies that the value of f is constant in such frames. The trace of the moving frame in the global x-t coordinate system is called the characteristic. Thus, (6) implies that the value of f is constant along the characteristic (defined by $dx/dt = \lambda$) in the global x-t frame, and this leads to the following solution

$$f(x,t) = f(x_d, t - \Delta t), \tag{9}$$

where x_d is the departure point of a characteristic that originates at time $t - \Delta t$ and arrives at position x at time t. In (6)-(9), the MOC scheme is based on a non-conservative form of the transport equation, and hence, it cannot be used directly when conservation laws have to be satisfied.

In the following, we assume the initial condition is known at time t^n on the arbitrary interval $[x_{\min}, x_{\max}]$, subdivided into N segments with unequal spacing $\Delta x_i = x_{i+1} - x_i$, $i = 1,2,...,N$, where x_i represents the position of the grid point i. In the original MOC scheme, the characteristics are drawn in the time-space coordinate system to specify the profile of f at each time step. Hence, the original MOC scheme is grid free and the grid point positions change in time. Similarly, in the grid based numerical MOC schemes, the values of the variables at grid points are obtained at the next time step by drawing the characteristics using one of the following methods:

(i) *Departure-based*: The characteristics are drawn such that the departure points, at the previous time step (t^n) coincide with the grid points. An interpolation procedure is thus necessary to find the grid point values at the new time step (t^{n+1})

(ii) *Destination-based*: The characteristics are drawn such that their arrival points, at the next time step (t^{n+1}) coincide with the grid points as shown in Figure 1. An interpolation procedure is hence needed at the old time step (t^n), to find the values of f at the departure points, say x_i^d.

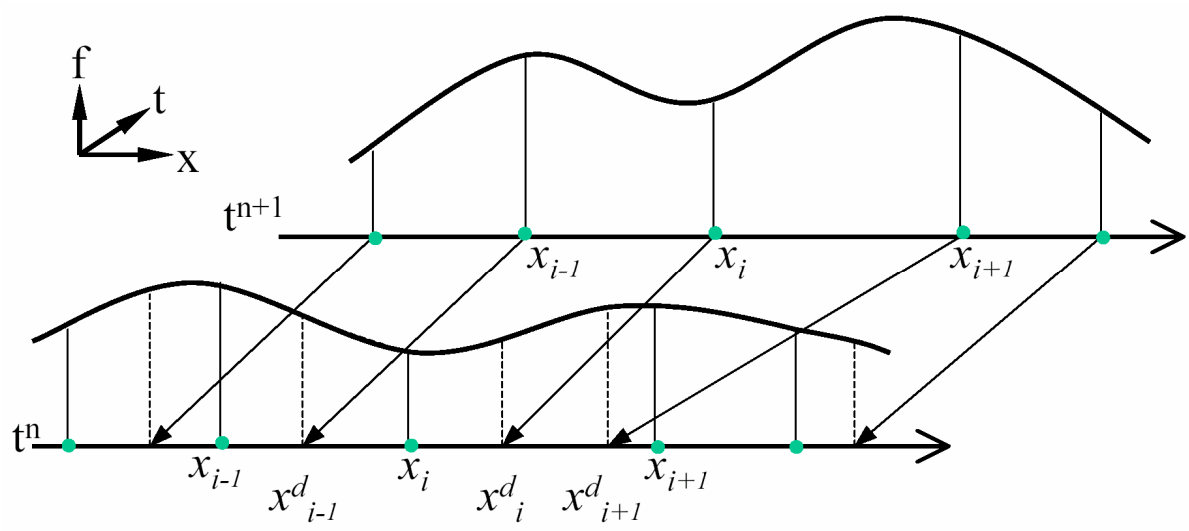

Figure 1. Arrangement of grid points and characteristics in the case of the destination-based method.

In this paper a destination-based method is followed, and the procedure to solve for (6) consists of the following two stages:

(i) Drawing the characteristics from the destination points (x_i, t^{n+1}) to find the departure points (x_i^d, t^n), i.e. the foots of the characteristics, in the space-time coordinate system,

(ii) Calculating the value of f at the foots of the characteristics at time t^{n+1}, i.e. f_i^{n+1}.

When the particle paths are used instead of the characteristics (i.e. when the frame moves with the fluid particle speed and not the characteristic speed), the method is named the semi-Lagrangian (SL) method. Usually the characteristics are not coinciding with the particle paths, except in the case of a pure (linear) advection equation. In existing SL methods, the left hand sides of (4) and (5) are considered as total derivatives along the particle path (i.e. the frame moves with the fluid particle speed u). Such an approach leads to oscillatory results, even when a first order interpolation is used (Garcia Navarro and Priestley, 1994). This is due to the effect of the gravity term, which is considered as a source term in SL schemes. In order to overcome this difficulty, we have chosen to use the method of characteristics in the present paper, and not the semi-Lagrangian one. A destination-based method is applied to the characteristic form of the shallow water

equations, and the source terms in the right hand sides of (4) and (5) are included in the advection terms, as it is shown in the next section.

4- Destination-based moc for the shallow-water equations

The shallow-water equations expressed in characteristic form (Henderson, 1966) are written as

$$\frac{\partial R_1}{\partial t} + \lambda_1 \frac{\partial R_1}{\partial x} = 0, \tag{10}$$

$$\frac{\partial R_2}{\partial t} + \lambda_2 \frac{\partial R_2}{\partial x} = 0, \tag{11}$$

where $R_1 = u + 2c$, $R_2 = u - 2c$, $\lambda_1 = u + c$, $\lambda_2 = u - c$ and $c = \sqrt{gh}$.

As for the advection equation, (10) and (11) can be solved using the characteristic approach, and this leads to the Riemann invariants

$$R_1(x,t) = R_1(x - \tilde{\lambda}_1 \Delta t, t - \Delta t), \tag{12}$$

$$R_2(x,t) = R_2(x - \tilde{\lambda}_2 \Delta t, t - \Delta t), \tag{13}$$

where $\tilde{\lambda}_1$ and $\tilde{\lambda}_2$ represent the nonlinear terms that have to be computed. The procedure to evaluate $\tilde{\lambda}_1$ and $\tilde{\lambda}_2$ will be discussed in details in section 5.

When solving for (12) and (13) using the original grid free MOC scheme, two characteristics are drawn from each node (x_i, t^n) and the intersection of the characteristics specifies the new computational nodes. Hence, in the destination-based MOC scheme, as described above for the scalar advection case, the characteristics are drawn back from (x_i, t^{n+1}) and R_1 and R_2 are calculated at the foot of the characteristics, leading to

$$R_{1i}^d = \frac{p_{1i}^d}{h_{1i}^d} + 2\sqrt{g h_{1i}^d}, \tag{14}$$

$$R_{2i}^d = \frac{p_{2i}^d}{h_{2i}^d} - 2\sqrt{g h_{2i}^d}, \tag{15}$$

where h_{ji}^d and p_{ji}^d are the values of h and p at the foot of the characteristic corresponding to λ_j, j=1,2. The method for calculating the slope of the characteristics and the interpolation

procedure are discussed in sections 5 and 6. Once the Riemann invariants are known, the nodal values of the conserved variables are computed from (14) and (15). This leads to

$$h_i^{n+1} = \frac{\left(R_{1i}^d - R_{2i}^d\right)^2}{4g}, \tag{16}$$

$$p_i^{n+1} = \frac{\left(R_{1i}^d + R_{2i}^d\right)}{2} h_i^{n+1}. \tag{17}$$

For the case of a dry bed, an appropriate choice is obtained based on the exact solution (see e.g. Toro, 2000). For example for the case of right dry bed, we obtain

$$u_i^{n+1} = \frac{R_{1i}^d}{3} \quad , \quad h_i^{n+1} = \frac{\left(R_{1i}^d\right)^2}{9g}. \tag{18}$$

5- Conservative interpolation

As mentioned in the previous section, the MOC scheme employs the non-conservative form of the equations, and therefore the procedure is not conservative. In order to impose the conservation property, the interpolation functions are defined in terms of the conserved variables *h* and *p* as

$$\phi_{hi}(x) = h(x) \quad , \quad x_i < x < x_{i+1} \quad , \tag{19}$$

$$\phi_{pi}(x) = p(x) \quad , \quad x_i < x < x_{i+1} \quad . \tag{20}$$

We then use a control volume approach and consider each cell $[x_i, x_{i+1}]$ as a finite volume FV_i. Following Xiao and Yabe (2001) the interpolation functions are chosen to be cubic polynomials. The use of higher order polynomials is possible, but it has a negligible impact on the accuracy of the results and it considerably increases the computational cost of numerical scheme.

In order to construct a cubic polynomial for *h* in each cell, we need four conditions. Three conditions result from imposing the mass conservation at the cell level

$$\int_{x_{i-1}}^{x_i} \phi_{hi}^n(x)dx = \overline{h}_{i-1/2}^{\,n} \Delta x, \tag{21}$$

$$\int_{x_i}^{x_{i+1}} \phi_{hi}^n(x)dx = \overline{h}_{i+1/2}^{\,n} \Delta x, \tag{22}$$

$$\int_{x_{i+1}}^{x_{i+2}} \phi_{hi}^{n}(x)dx = \bar{h}_{i+3/2}^{n}\Delta x\,, \tag{23}$$

where $\bar{h}_{i+1/2}^{n}$ is defined as the averaged depth over FV_i and it is calculated here by using the following α-scheme

$$\bar{h}_{i+1/2}^{n} = \bar{h}_{i+1/2}^{n-1} + \frac{\Delta t}{\Delta x}\left[\alpha\left(p_{i+1}^{n} - p_{i}^{n}\right) + (1-\alpha)\left(p_{i+1}^{n-1} - p_{i}^{n-1}\right)\right], \tag{24}$$

where α is a weighting factor with $0 \le \alpha \le 1$. Similarly,

$$\bar{p}_{i+1/2}^{n} = \bar{p}_{i+1/2}^{n-1} + \frac{\Delta t}{\Delta x}\left[\alpha\left(M_{i+1}^{n} - M_{i}^{n}\right) + (1-\alpha)\left(M_{i+1}^{n-1} - M_{i}^{n-1}\right)\right], \tag{25}$$

where

$$M_{i}^{n} = u_{i}^{n} p_{i}^{n} + 0.5g\left(h_{i}^{n}\right)^{2}. \tag{26}$$

The above approach is conservative since it is written in the flux form. Equations (24) and (25) are solved without recourse to solve a linear system, because the values of p_i^n and h_i^n have already been determined by the MOC scheme, hence the right hand sides of (24) and (25) are known.

Finally, the last condition is imposed on the slope of the interpolation function at the cell mid-points

$$\left.\frac{\partial \phi_{hi}^{n}}{\partial x}\right|_{x=x_{i+1/2}} = d_{i+1/2}^{n}\,, \tag{27}$$

where $d_{i+1/2}^{n}$ represents the slope of $\phi_{hi}^{n}(x)$ at $x_{i+1/2}$ and it may be calculated by a curve fitting scheme. Any high order interpolation scheme may be employed to calculate $d_{i+1/2}^{n}$. On the other hand, a number of oscillation free schemes are available in the literature such as Essentially Non-Oscillatory schemes (ENO) e.g. Shu and Osher (1988), Weighted Essentially Non-Oscillatory (WENO) schemes e.g. Levy et al. (2002) and Uniformly Non-Oscillatory schemes e.g. Harten and Osher (1987). The performance of the above methods depends on the employed numerical discretization schemes and the physical problems which are considered. A detailed discussion of the above different approaches may be found in Leveque (2002).

Xiao and Yabe (2001) have successfully employed Harten and Osher's UNO reconstruction and obtained accurate results in solving advection equations. The UNO

method is free of oscillations at the vicinity of discontinuous regions when an appropriate slope limiter is used. Slope limiters usually prevent the oscillations in high order accurate schemes by reducing the order of accuracy only in the vicinity of shocks and steep changes. In such regions, increasing the order of accuracy will increase the level of oscillations, and in fact, a first order scheme usually gives more accurate results. In the UNO scheme a minmod-type slope limiter was employed by Harten and Osher (1987) and adopted here. This leads to

$$\left(d^n_{i+1/2}\right)_{UNO} = \min \operatorname{mod}(S^+_{i+1/2}, S^-_{i+1/2}), \tag{28}$$

where the minmod function is defined as

$$\min \operatorname{mod}(a,b) = \begin{cases} m(a,b) \ , \text{ if } a \text{ and } b \text{ have same sign,} \\ 0 \quad\ , \text{ if } a \text{ and } b \text{ have opposite signs,} \end{cases} \tag{29}$$

with

$$m(a,b) = \begin{cases} a \ , \text{ if } |a| < |b|, \\ b \ , \text{ otherwise.} \end{cases} \tag{30}$$

The piecewise-quadratic reconstruction functions in the Harten and Osher (1987) scheme are defined as

$$S^+_{i-1/2} = h[x_{i-1/2}, x_{i+1/2}] - \Delta x \min \operatorname{mod}(h[x_{i-3/2}, x_{i-1/2}, x_{i+1/2}], h[x_{i-1/2}, x_{i+1/2}, x_{i+3/2}]) \tag{31}$$

and

$$S^-_{i-1/2} = h[x_{i-3/2}, x_{i-1/2}] - \Delta x \ \min \operatorname{mod}(h[x_{i-5/2}, x_{i-3/2}, x_{i-1/2}], h[x_{i-3/2}, x_{i-1/2}, x_{i+1/2}]) \tag{32}$$

where the first and second Newton-divided differences are respectively

$$h[x_{i-1/2}, x_{i+1/2}] = \frac{h^n_{i+1/2} - h^n_{i-1/2}}{\Delta x} \tag{33}$$

and

$$h[x_{i-1/2}, x_{i+1/2}, x_{i+3/2}] = \frac{h^n_{i+3/2} - 2h^n_{i+1/2} + h^n_{i-1/2}}{\Delta x}. \tag{34}$$

Another simple but interesting choice is the Collela and Woodward (1984) method where

$$\left(d^n_{i+1/2}\right)_{CW} = \begin{cases} \min\left(\left|\delta h^n_{i+\frac{1}{2}}\right|, 2\left|h^n_{i+\frac{3}{2}} - h^n_{i+\frac{1}{2}}\right|, 2\left|h^n_{i+\frac{1}{2}} - h^n_{i-\frac{1}{2}}\right|\right)\dfrac{\mathrm{sgn}\left(\delta h^n_{i+\frac{1}{2}}\right)}{\Delta x}, if\left(h^n_{i+\frac{1}{2}} - h^n_{i-\frac{1}{2}}\right)\left(h^n_{i+\frac{3}{2}} - h^n_{i+\frac{1}{2}}\right) > 0 \\ 0, \text{otherwise.} \end{cases} \tag{35}$$

with

$$\delta h^n_{i+1/2} = \left(h^n_{i+3/2} - h^n_{i-1/2}\right)/2 \tag{36}$$

It was observed in the numerical experiments in the present study that the UNO scheme tends to produce numerical diffusion with the proposed method while the CW scheme produces numerical oscillations. A reasonable choice is therefore an average value as

$$d^n_{i+1/2} = \beta\left(d^n_{i+1/2}\right)_{UNO} + (1-\beta)\left(d^n_{i+1/2}\right)_{CW} \tag{37}$$

with $0 \le \beta \le 1$. The weighting factor β was set to 0.5 in all test cases in this paper. Imposing the above-mentioned four conditions, the piecewise cubic polynomial function for a constant grid spacing is written as

$$\phi^n_{hi}(x) = a_{0i} + a_{1i}(x - x_i) + a_{2i}(x - x_i)^2 + a_{3i}(x - x_i)^3, \quad for \quad x \in [x_i, x_{i+1}], \tag{38}$$

where

$$a_{0i} = -\frac{2\Delta x d^n_{i+1/2}}{5} + \frac{2\bar{h}^n_{i-1/2}}{15} + \frac{5\bar{h}^n_{i+1/2}}{6} + \frac{\bar{h}^n_{i+3/2}}{30} \tag{39}$$

$$a_{1i} = \frac{2d^n_{i+1/2}}{5} - \frac{4\bar{h}^n_{i-1/2}}{5\Delta x} + \frac{\bar{h}^n_{i+1/2}}{\Delta x} - \frac{\bar{h}^n_{i+3/2}}{5\Delta x} \tag{40}$$

$$a_{2i} = \frac{6d^n_{i+1/2}}{5\Delta x} + \frac{11\bar{h}^n_{i-1/2}}{10\Delta x^2} - \frac{\bar{h}^n_{i+1/2}}{\Delta x^2} - \frac{\bar{h}^n_{i+3/2}}{10\Delta x^2} \tag{41}$$

$$a_{3i} = -\frac{4d^n_{i+1/2}}{5\Delta x^2} - \frac{2\bar{h}^n_{i-1/2}}{5\Delta x^3} + \frac{2\bar{h}^n_{i+3/2}}{5\Delta x^3} \tag{42}$$

The interpolation function for *p*, i.e. $\phi^n_{pi}(x)$, is constructed in a similar manner.

6-Calculation of the slope of the characteristics

When using the MOC scheme, it is necessary to compute the values of *u* and *c* at the midpoints of the characteristics in order to draw the characteristics. Those values are

calculated as average values between the departure and the arrival points of the characteristics. For most MOC schemes the calculation of the slopes is done through an iterative procedure, i.e. once the nodal values of *u* and *c* are obtained at a new time step, they are averaged at the characteristics midpoints in order to recalculate the slopes and this process is repeated until it converges (usually within two iterations). However, such an iterative procedure is usually not necessary with the current method and the characteristics speeds $\widetilde{\lambda}_1$ and $\widetilde{\lambda}_2$ at a given time step are calculated using the Roe approximation as

$$\widetilde{u}_i = \frac{\overline{u}^n_{i-1/2}\sqrt{\overline{h}^n_{i-1/2}} + \overline{u}^n_{i+1/2}\sqrt{\overline{h}^n_{i+1/2}}}{\sqrt{\overline{h}^n_{i-1/2}} + \sqrt{\overline{h}^n_{i+1/2}}} \quad , \quad \widetilde{c}_i = \sqrt{g(\overline{h}^n_{i-1/2} + \overline{h}^n_{i+1/2})/2} \tag{43}$$

All numerical tests presented in this paper are performed without recourse to an iterative procedure. The stability condition of the proposed scheme is the usual CFL condition (smaller than 1) since we have used a control volume approach. It should be mentioned that in the case of discontinuous flows, the length of the time step is usually chosen on the basis of accuracy considerations rather than stability.

7-Numerical results

In order to study the performance of the proposed numerical method, seven test cases have been selected herein. The numerical results have been compared to a high-resolution MUSCL-type finite volume scheme where the Roe approximate solver with entropy fix has been employed with a minmod slope limiter at the reconstruction step (see e.g. Toro 2000 for details).

For the Riemann problem tests (a, b, c, d, e and f), the exact solutions have been calculated by using an exact Riemann solver, Toro (2000). The location of the initial discontinuity is x=25 m in the cases a to f. In order to validate the proposed scheme, the results of the non-conservative MOC scheme are also presented using a cubic Lagrange polynomial (Appendix 1), except for test a and c, where the cubic non-conservative MOC leads to instabilities and hence a linear non-conservative MOC is preferred. For all tests a wide horizontal, rectangular and frictionless channel is used. The length of the channel is chosen to be 50m for tests a,b,c and d. The weighting factor α was set to 0.84 in all test cases, based on numerical experiments. A number of 600 computational cells have been used in all tests. A typical CFL of 0.6 has been used in all test cases except for test e where

the CFL has been set to 0.81 and 0.66 for cases (*i*) and (*ii*) respectively, to compare with the MUSCL scheme, and in the accuracy test (g) where a CFL of 0.2 was selected in order to compare the numerical diffusion of the proposed method with that of the MUSCL scheme in a numerical-diffusion-dominant case. The numerical results are presented for typical time steps where the error of other schemes becomes significant compared to the proposed approach.

a –The Dam Break Problem with a Sonic Rarefaction

The dam break problem is the most common test to evaluate the performnce of shock capturing schemes in shallow flows. Here, a dam is located at the channel mid-length. The water depth at the left and right hand sides of the dam is 1m and 0.01 m, respectively. The dam is instantaneously removed across its entire width and the simulation is performed up to time t=4s. The important feature here is that the left rarefaction is sonic, i.e. it contains the sonic point where the flow regime changes from super critical to sub critical. Most numerical methods encounter difficulties in simulating sonic rarefactions, and they produce an unphysical jump at the sonic point inside the rarefaction waves. Such schemes are called entropy-violating methods. The results obtained for the depth h and the discharge p are presented in figures 2.a and 2.b respectively, and they are compared with the results of the non-conservative MOC scheme, the exact solution and the MUSCL scheme. As shown in figures 2.a and 2.b, the non- conservative MOC scheme leads to large errors in the shock speed and the water depth right after the shock wave (shock strength). These errors are not present in the proposed method and the MUSCL scheme. It is also seen that the proposed method does not lead to entropy violating solutions.

The proposed scheme and the MUSCL method lead to comparable CPU time (roughly 0.1 s) on a Pentium IV processor and a Microsoft Fortran Power Station Software (release mode). However, the duration of the experiment is not long enough to precisely compare the computational cost of the two methods. This is why, we have rerun the experiment by using 4200 computational cells and found 4.6 s and 4.2 s for the proposed method and the MUSCL scheme, respectively. Therefore, the proposed method is about 10% more expensive, which is expected since in the selected MUSCL scheme, only linear

reconstruction is used while here we use cubic reconstruction. This ratio is the same for all the experiments conducted in the remaining sections.

In order to see the effect of the number of numerical cells on the results and to verify the grid independency, the value of the water depth in the intermediate state (upstream the shock) is shown in Figure 2c for different cell numbers. As it is observed, the modified method can easily give the exact value with a few grid points, which is a consequence of the conservation property. On the other hand, the non-conservative MOC scheme exhibits large errors and cannot simulate the exact result.

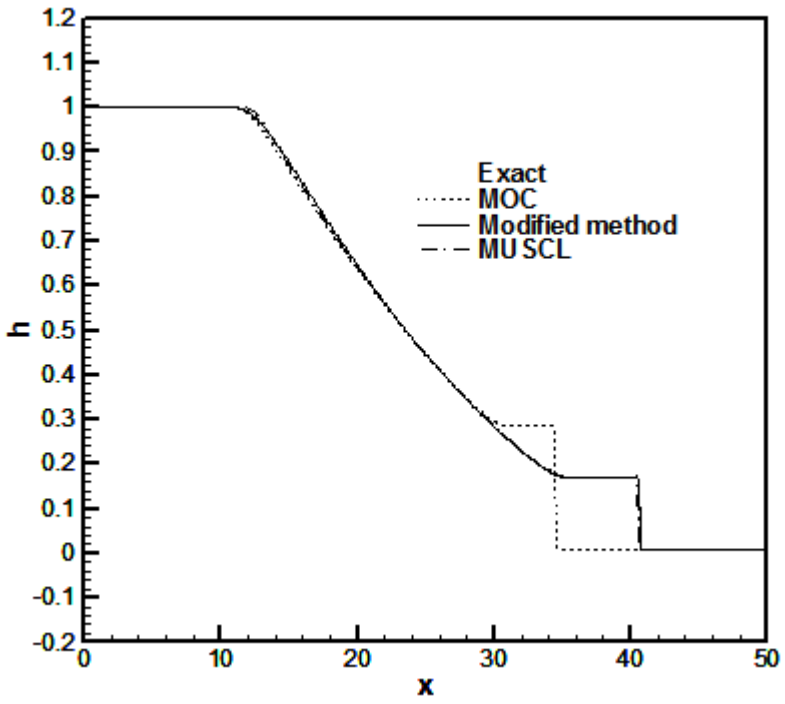

Fig. 2.a. The dam break problem: The water surface elevation at t=4 using non-conservative MOC scheme, the proposed method and the exact solution.

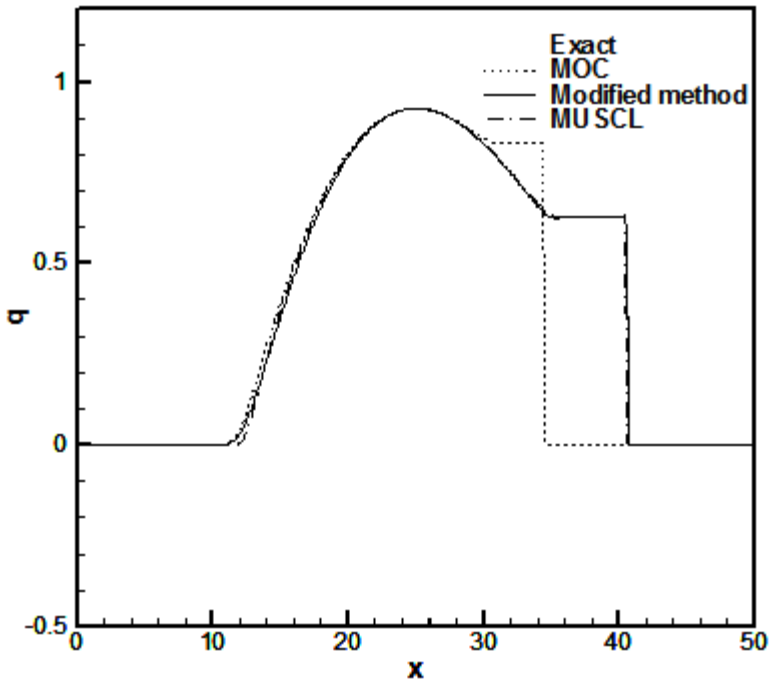

Fig. 2.b. The dam break problem: Water discharge at t=4 using non-conservative MOC scheme, the proposed method and the exact solution.

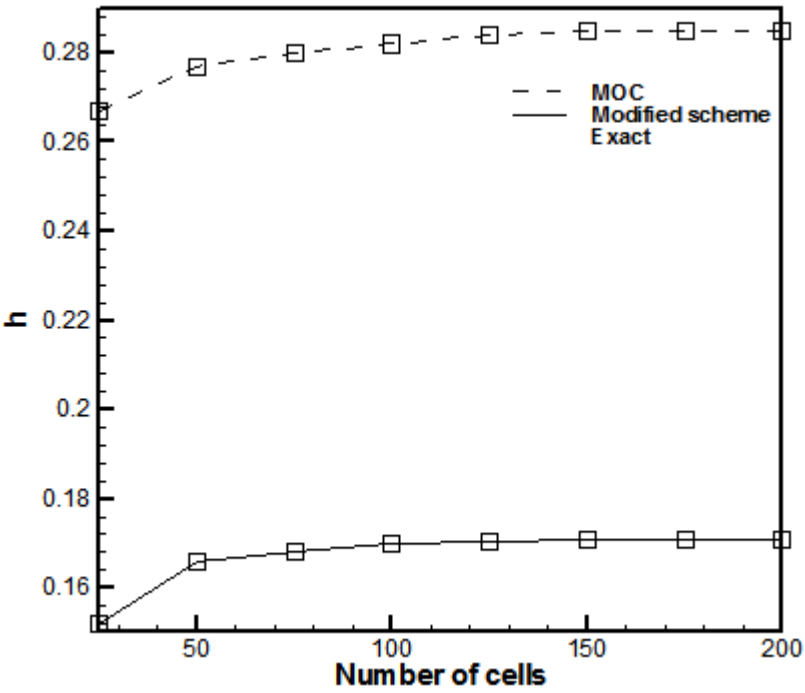

Fig. 2.c. The effect of the number of numerical cells on the results; the water depth in intermediate state for different cell numbers using the non-conservative MOC scheme, the *proposed method and the exact solution.*

b– Generation of a Dry Bed

In this test, the initial condition has been chosen in order to obtain two rarefaction waves separated by a dry bed. As shown in Toro (2000), some numerical methods face serious difficulties in solving such a test case, particularly due to the presence of the dry bed. The water depth is 0.1m and the initial velocity is 3 and –3 m/s at the left and right hand sides of the discontinuity, respectively. The latter is located at the channel mid-legnth. The numerical results at t = 5 s (as propsed by Toro, 2000) are presented in figure 3 and they are compared with those of the non-conservative MOC scheme and the exact solution. As shown in figure 3, both the non-conservative and conservative MOC schemes solve this problem successfully. The non-conservative approach exhibits however better results than the conservative one for the rarefaction wave. Indeed, the good performance of non-conservative schemes in mild flows has already been observed and those schemes have been used to develop adaptive conservative/non-nonservative schemes (Toro, 2000). However, the proposed scheme has a reasonable capability of simulating the mild flow region and it can simulate the dry bed flow as well (see also the test f; the dambreak test on dry bed).

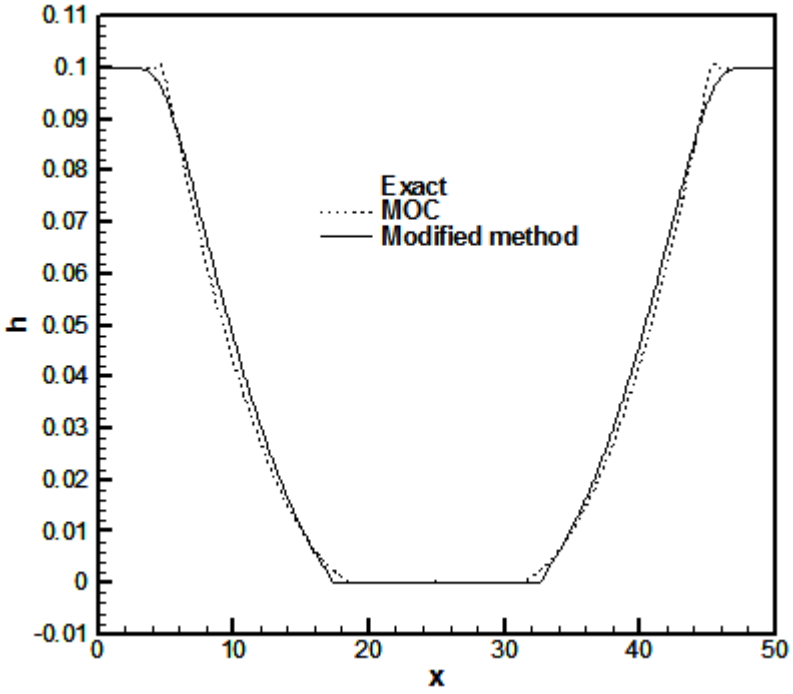

Fig. 3. Generation of a dry bed: The water surface elevation at t=5 using the non-conservative MOC scheme, the proposed method and the exact solution.

c– The Dam Break Problem with a Depth ratio of 1000

In the dam break tests, an appropriate numerical method should give good results for arbitrary h_L and h_R. In this test case we show that the proposed method, can simulate the problems of high depth ratio better than the MUSCL scheme.

In this test, the initial condition has been chosen in order to produce a right propagating shock wave and a sonic or trans-critical left rarefaction wave. The water depth is chosen to be 1m and .001m in left and right sides of the dam, respectively.

Simulation results at time t=4s are presented in figures 4.a and 4.b and they are compared with the results of the non-conservative MOC scheme and the exact solution. The MUSCL scheme leads to instability and cannot be used to simulate this test case with a CFL of 0.6. As can be seen in figure 4, both non-conservative and conservative MOC approachs could solve this problem without exhibiting an unphysical shock. However, the non-conservative approach leads to large errors in the numerical solution, contrary to those obtained with the

modified scheme. Recall that for the non-conservative MOC scheme, linear polynomials have been used instead of cubic ones to avoid unstable spurious oscillations.

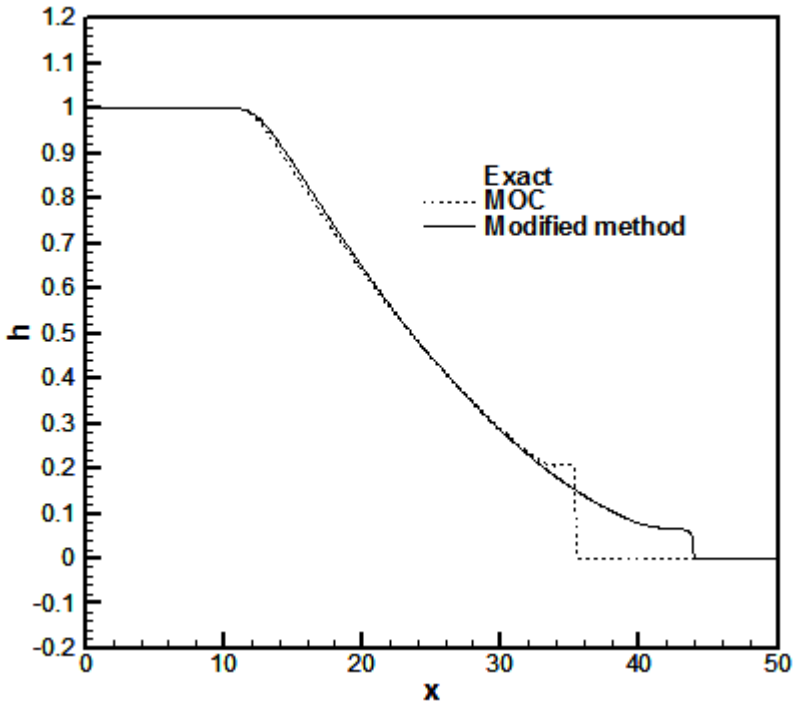

Fig. 4.a- Left sonic rarefaction and right shock: The water surface elevation at t=4s using the non-conservative MOC scheme, the proposed method, and the exact solution.

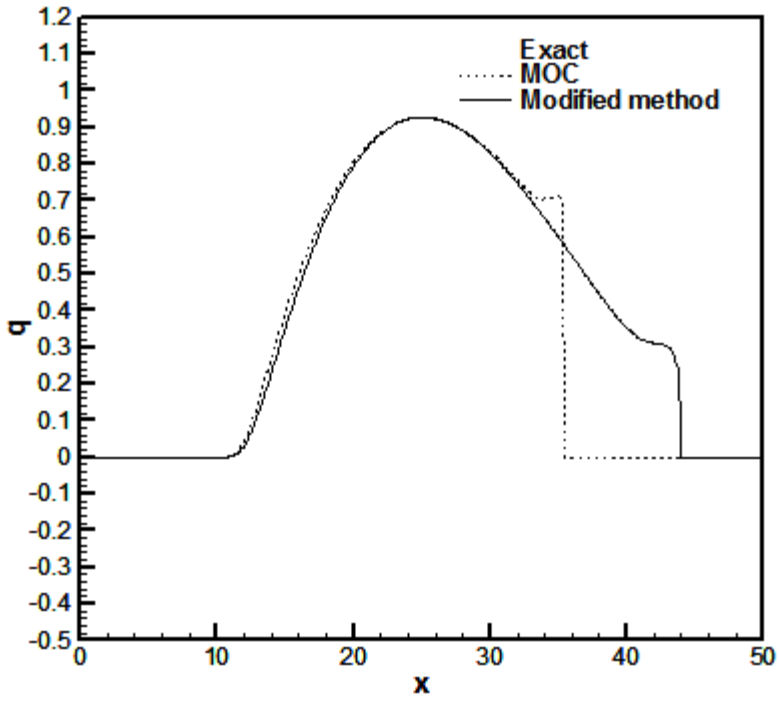

Fig 4.b. As for fig.4.a but for the water discharge.

d –Initial Converging Flow

The initial condition has been chosen here as to produce two shock waves propagating in opposite direction. Herein, the water depth is chosen to be 1m and the initial velocity is set to 3m/s and –3m/s in left and right hand sides of the discontinuity, respectively. The numerical results at t = 5s are presented in figure 5 and they are compared with those of the non-conservative MOC scheme, the MUSCL scheme and exact solution. As it can be seen in figure 5, the non-conservative approach leads to large errors and produces a high level of spurious oscillations, while the proposed method and the MUSCL scheme simulate the water level and the shock speed accurately and coincide quite well with the exact solution. The level of the numerical oscillations of the proposed method are slightly higher than those of the MUSCL scheme in this test. However, this is not always the case as shown in the next test.

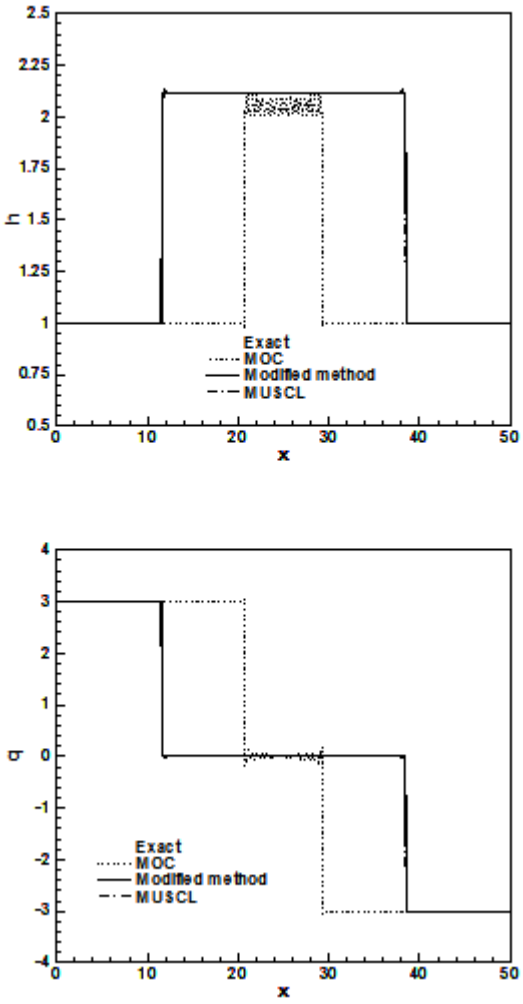

Fig. 5. Initial converging flow at t=5 using the non-conservative MOC scheme, the proposed method and the exact solution; water surface elevation (left) and velocity (right).

e– Interaction of waves

In this test, initially used by Wang (2000), two dams are located at positions 100m and 900m respectively, in a channel of length 1000m. The water is initially stagnant in the channel, and it is subdivided in three parts by the dams. In order to show the characteristics of the interaction two cases are considered: (1) h_{01}=100m, h_{02}=2m, h_{03}=100m and (2) h_{01}=200m, h_{02}=2m, h_{03}=80m, where h_{0i} represents the initial water depth in the part i of the channel, i=1,2,3, as shown in figure 6.1. In both cases $h_{01} > h_{02}$ and $h_{02} < h_{03}$ hence the

two shocks are moving toward each other. Reflecting boundary conditions are assumed here. The “exact” solutions here are obtained using a high resolution scheme on a grid of 6000 computational cells.

The numerical results of the proposed method are shown at different times in figures 6.2.a (depth) and 6.2.b (velocity). After the interaction, two shocks are traveling back in opposite directions and complex combinations of shock waves and rarefactions are produced. Contrary to the proposed method, non-conservative MOC and the MUSCL schemes fail to simulate this problem with a CFL of 0.8. This again shows the good stability properties of the proposed method in complex problems.

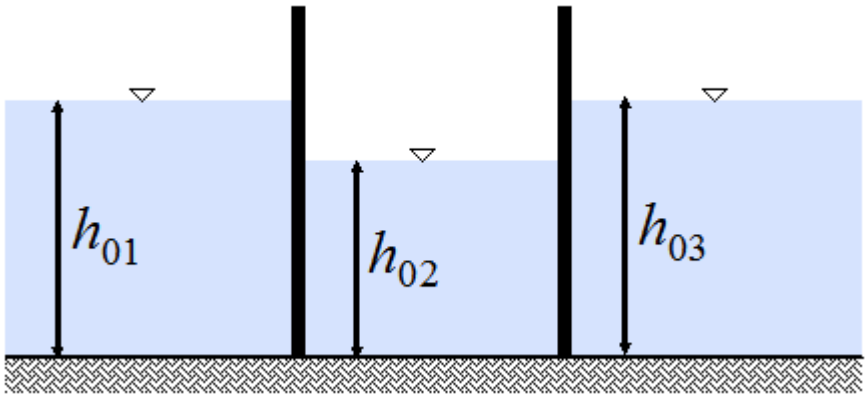

Fig. 6.1. A schematic view of test e (correspond to case 1). Two dams are located in a channel.

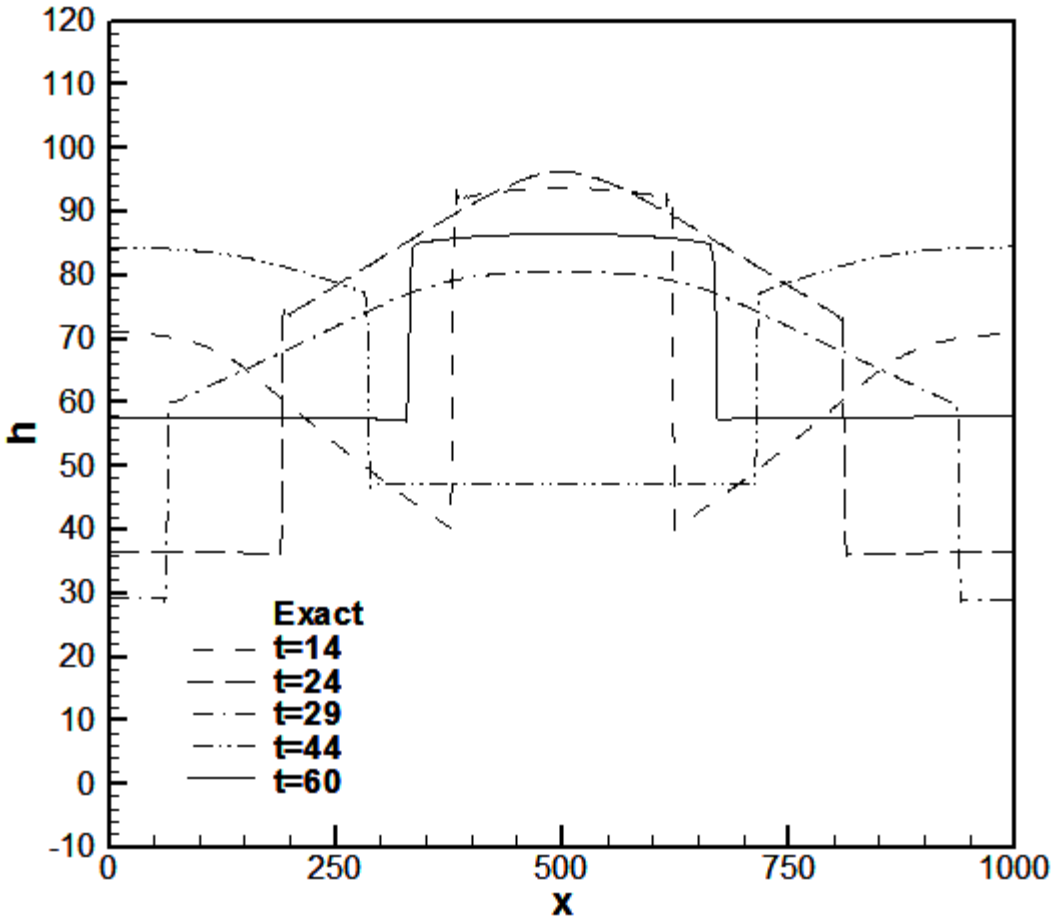

Fig 6.2.a. The interaction of waves, case (1): The water surface elevation at different times using the proposed method and the “exact” solution.

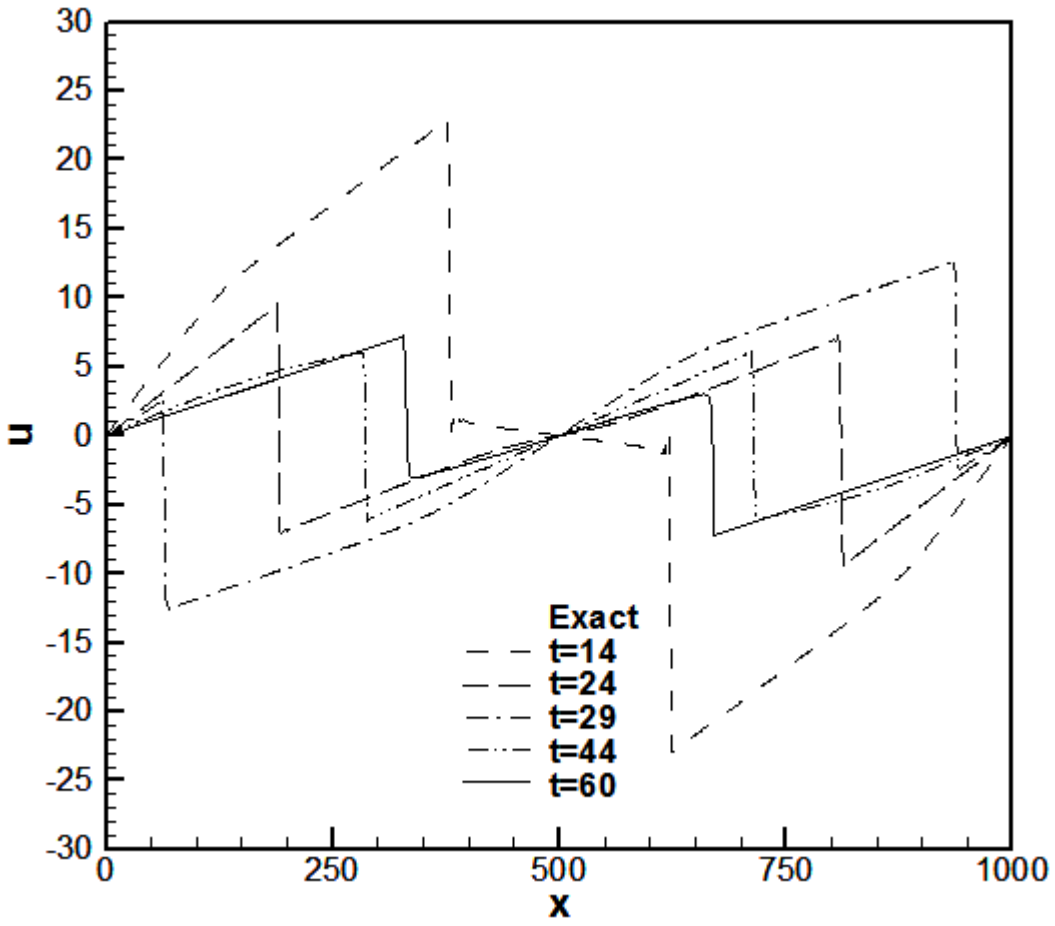

Fig 6.2.b. As for fig. 6.2.a but for the water velocity.

For the second set of data, corresponding to a non case $h_{01} > h_{02} > h_{03}$, two separate dambreak flows occur at the beginning of the simulation, and this leads to a pair of very strong inward moving shock waves. After these waves combine completely, a complex right moving combination of rarefactions and shocks appear in the domain. The numerical results of the water surface are shown at different times in figures 6.3.a and 6.3.b for the proposed and MUSCL schemes, respectively. Similar results for water velocity are shown in figures 6.3.c and 6.3.d. As shown in those figures, the modified scheme is able to produce accurate shock speeds and water surface elevations with low numerical oscillations and the level of numerical oscillations are less than those of the MUSCL scheme.

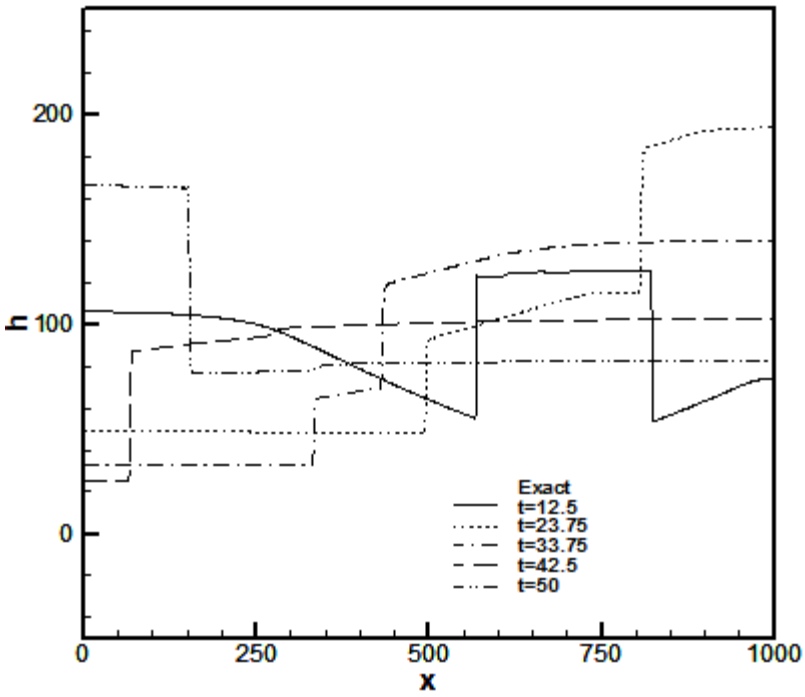

Fig 6.3.a. The interaction of waves, case (2): the water surface elevation at different times using the proposed method.

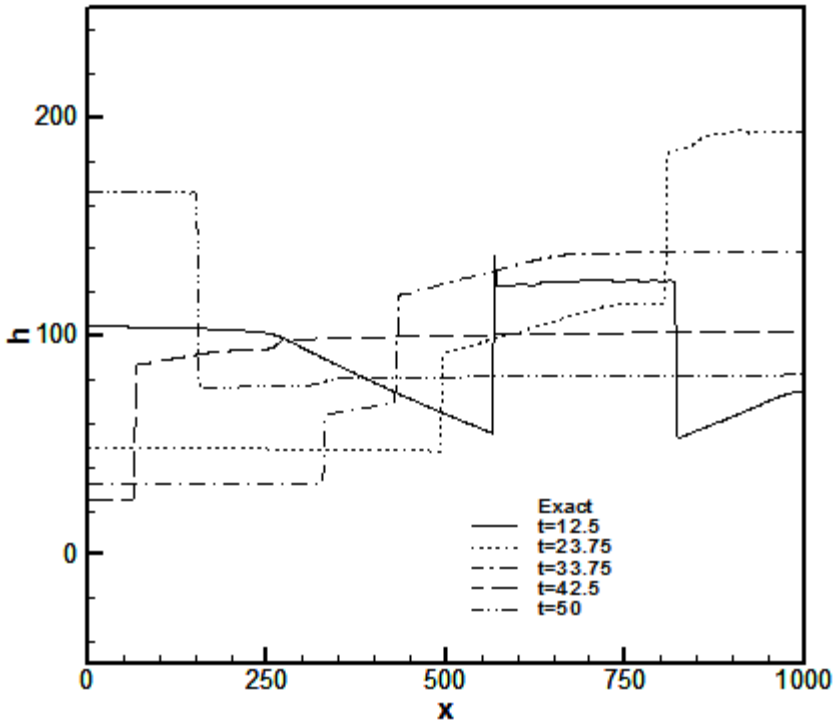

Fig 6.3.b. As for fig. 6.3.a but for the MUSCL scheme.

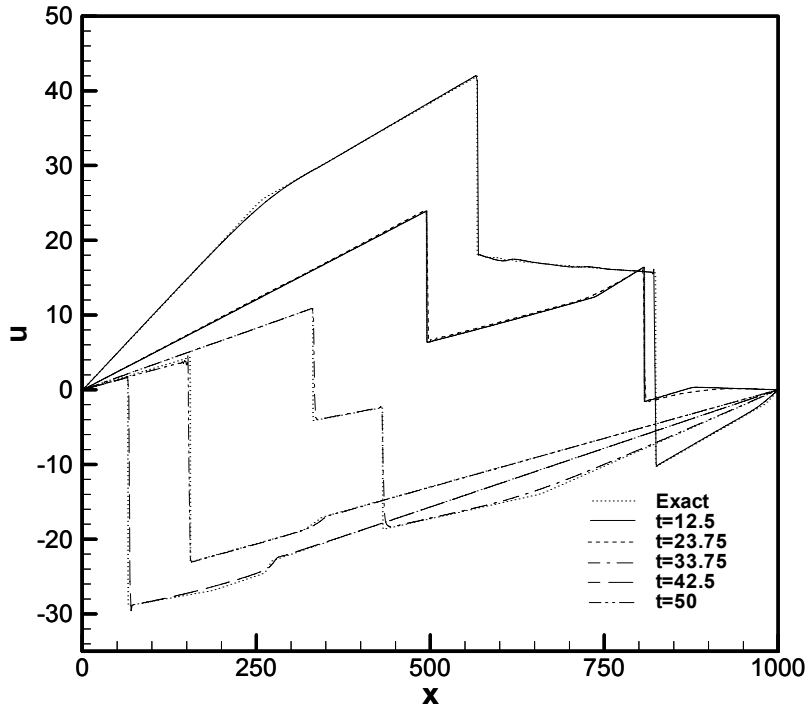

Fig 6.3.c. As for fig. 6.3.a but for the water velocity**.**

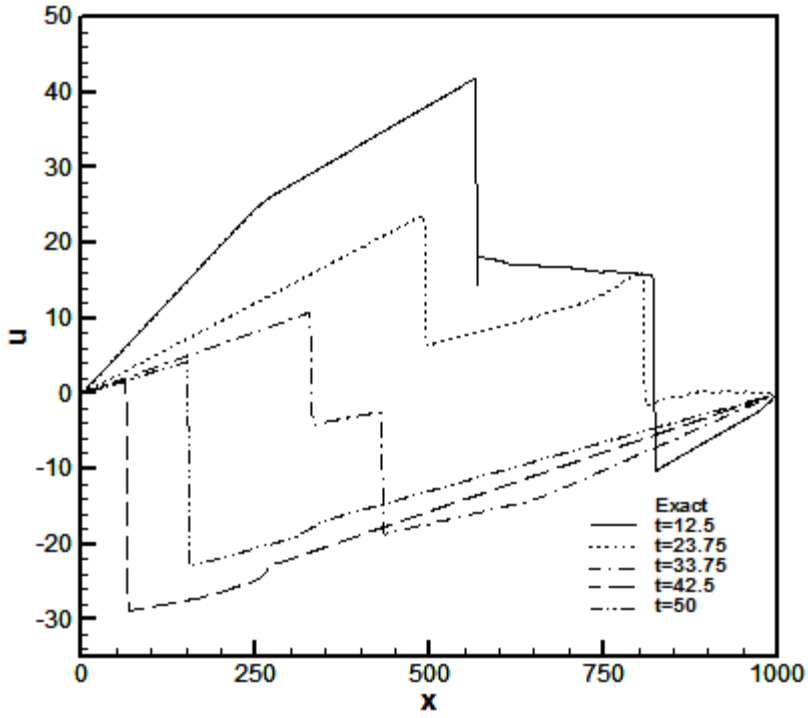

Fig 6.3.d. As for fig. 6.3.c but for the MUSCL scheme.

f- Dam break on dry bed

The numerical simulation of the dam break test over a dry bed is a challenging one, since even small numerical oscillations may lead to negative depths and hence to instabilities. The numerical results of the proposed method are shown in figures 7 and they compare well with the exact solution and the MUSCL scheme. This test also shows that the proposed scheme is able to simulate dam break type flows with any depth ratios (h_L/h_R).

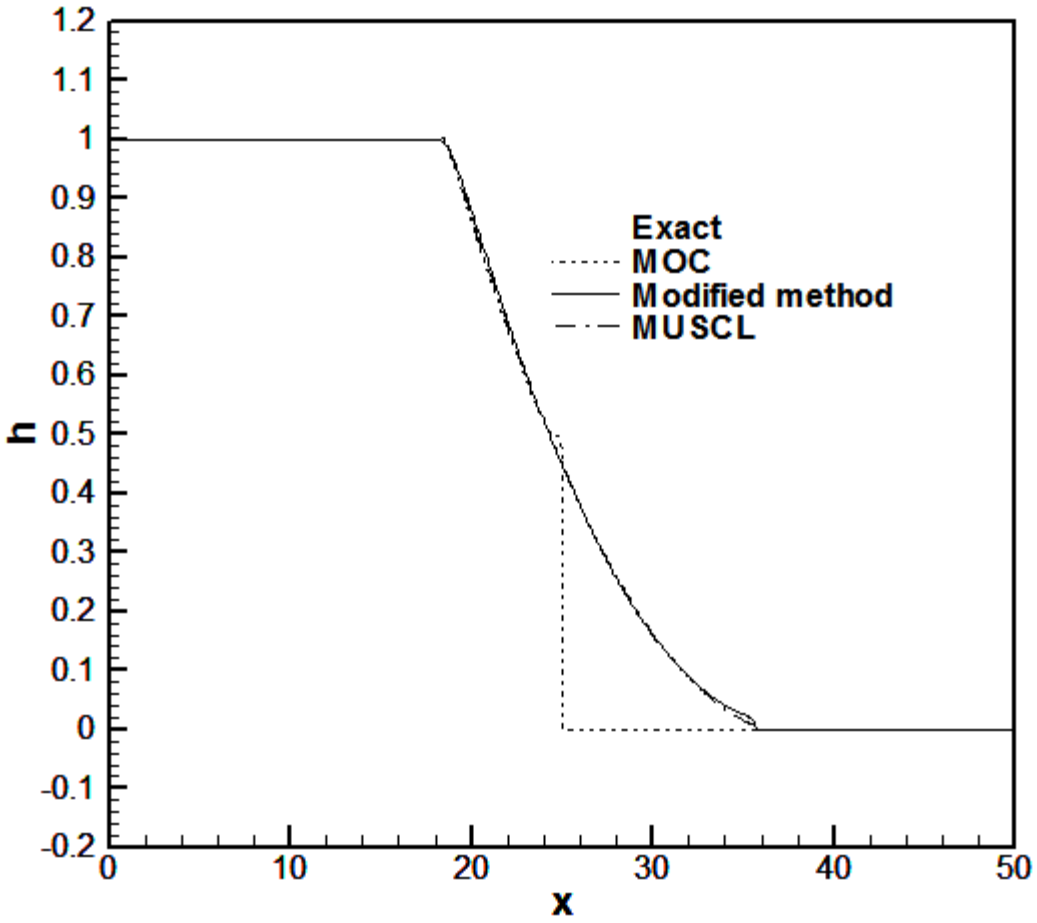

Fig. 7. Dam break on dry bed: The water discharge at t=2 s, obtained by using the proposed method, is compared to the exact solution.

g- An accuracy test; A small perturbation of stagnant condition

The initial flow velocity is zero in the entire channel with

$$h(x)=\begin{cases}1.0+0.05*\left(\cos\left[\pi\left(1+2\dfrac{x_0-x}{L}\right)\right]+1\right), & for 17.6<x<19.6,\\ 1.0, & otherwise,\end{cases} \tag{44}$$

where x_0=18.6 m and L=2 m.

The numerical results obtained at t = 3 s with the weighting factors $\alpha=0.84$ and $\alpha=0.5$ in (23) and (24) are shown in figure 8 and they are compared with the results of the MUSCL scheme. The proposed method is clearly much less diffusive than the MUSCL scheme, especially when a centered scheme ($\alpha=0.5$) is employed, as expected.

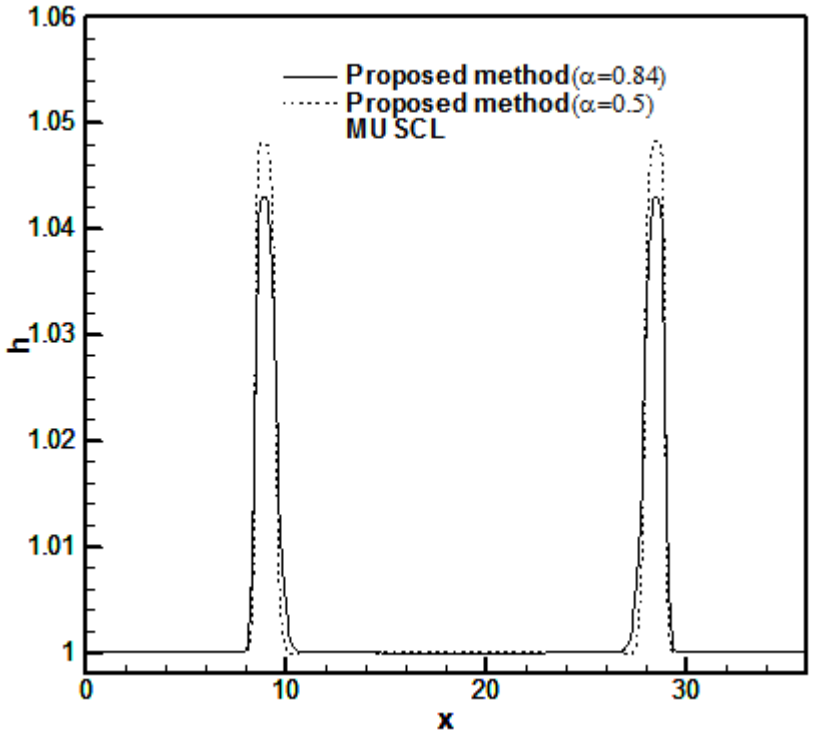

Fig. 8. Small perturbation of stagnant condition, left and right-going waves resulted from an initial cosine-type hump of water surface at t=3s.

8-Conclusion

A conservative MOC scheme has been introduced to simulate dam break type flows. The proposed method can simulate sub, super and trans critical flows very accurately. By using an appropriate interpolation function, the scheme also produces high accurate low-oscillatory solutions. The conservation property of the scheme ensures a high accuracy of the shock speed and it considerably improves the performance of the original MOC scheme. Hence, the modified method extends the classical MOC schemes for a wide range of complex flows, as shown in a number of challenging test cases e.g. interaction of waves and dry-bed problems.

The computational effort of the proposed method is comparable to the cost of a muscl-type high resolution scheme (the Roe approximate solver with a minmod slope limiter at the reconstruction step). Finally, the proposed method may be extended to the 2D case by considering either the cone of characteristics, or 1D characteristics schemes in the direction orthogonal to the cell interfaces. The latter is currently under development and promising preliminary results have already been obtained.

Appendix-1-Cubic Lagrange interpolation

A fourth order accurate interpolation scheme results from the use of the cubic Lagrange polynomials $\phi_{hi}(x\ )$ defined over the interval $[x_{i-1}, x_{i+2}]$ and expressed as

$$\phi_h(x) = \sum_{i=1}^{4} C_i(x) h_i \,, \tag{37}$$

where the coefficients $C_i(x)$ are computed as

$$C_i(x) = \frac{\prod_{k \neq i}^{4} (x - x_k)}{\prod_{k \neq i}^{4} (x_i - x_k)} \,. \tag{38}$$

The cubic Lagrange polynomials satisfy the condition of $\phi_h(x_j) = h_j$ for j= *i*-1, *i*, *i*+1 and *i*+2.

References

F. Alcrudo and P. Garcia-Navarro (1993), '*A High Resolution Godunov-Type Scheme in Finite Volumes for the 2D Shallow Water Equations*'. Int.J. Numer. Methods in Fluids, 16, pp. 489.

Colella P. and Woodward P. (1984), '*The piecewise parabolic method (PPM) for gas-dynamical simulations*', Journal of computational physics, 54, 174-201.

R. J. Fennema and M. H. Chaudhry (1987), '*Simulation of one-dimensional dam-break flows*', Journal of Hydraulic Research, Vol. 25, No. 1, 41-51.

P. Garcia Navarro, A. Priestley (1994), '*A Conservative and Shape Preserving SL Method for Solution of the Shallow-water Equations*', International Journal for Numerical Methods in Fluids, 18, 2.

P. Glaister (1988), '*Approximate Riemann Solutions of the Shallow Water Equations*'. Journal of Hyd. Research, 26, No. 3, 293-306.

A. Harten and S. Osher (1987), '*Uniformly high-order accurate non-oscillatory schemes, I*', SIAM Journal of numerical analysis, 24, 279.
F. M. Henderson (1966), '*Open channel flow*', Collier MacMillan, London.
E. F. Hicks and P. M. Steffler (1992), '*Characteristics dissipative Galerkin scheme for open channel flow*', Journal of Hydraulic Engineering, ASCE, Vol. 118, No. 2, 337-352.
R. J. LeVeque (2002), '*Finite Volume Methods for Hyperbolic Problems*', Cambridge university press, UK.
Levy D., Puppo G. and Russo G. (2002), '*A fourth order central WENO scheme for multi-dimensional hyperbolic systems of conservation Laws*', SIAM Journal on scientific computing, 24, 2002, pp. 480-506.
M. Nujic (1995), '*Efficient Implementation of Non-Oscillatory Schemes of Free Surface Flows*', J. Hyd. Res. , vol. 33, No. 1, pp. 101.
P. L. Roe (1981), '*Approximate Riemann solvers, parameter vectors and difference schemes*', Journal of computational physics, 43, 357-372.
H. H. G. Savenije (1992), '*Lagrangian solution of St. Venant's equations for alluvial estuary*', Journal of Hydraulic engineering, ASCE, Vol. 118, No. 8, 1153-1163.
C. W. Shu , S. Osher (1988), '*Efficient implementation of essentially non-oscillatory shock-capturing schemes*', Journal of Computational Physics, v.77 n.2, p.439-471,
E. F. Toro (2000), '*Shock Capturing Methods for Free Surface Shallow Flows*', John Wiley and sons.
Van Leer, B. (1982), '*Flux Vector Splitting of the Euler Equations*', Lecture Notes in Physics, Vol. 170, pp. 507-512.
J. S. Wang (2000), '*Finite Difference TVD Scheme for Computation of Dam-Break Flows*', J. Hydr. ASCE, No. 4, pp. 253.
F. Xiao and T. Yabe (2001), '*Completely conservative and oscillation-less SL schemes for advection transportation*', Journal of computational physics, 170, 498-522.
D. Zhao, H. Shen, G. Tabios, J. Lai and W. Tan (1996), '*Approximate Reimann Solver in FVM for 2d Hydraulic Shock Wave Modeling*', J. Hydr. ASCE, No. 12, pp. 692.

CHAPTER 4

A mass conservative scheme for simulating shallow flows over variable topographies using unstructured grid

In chapter 4, the 2-D shallow water equations are numerically solved using a characteristic-based finite volume method over unstructured grids, which are of great interest for real applications. In the 2D case, the main difficulty in most existing schemes arises in the treatment of source and flux terms, particularly with unstructured grids. This is due to the

imbalance between the source and flux terms. Here, a new scheme is introduced, based on a modification to the Roe method, which satisfies the balance property.

Un schéma conservatif pour la masse permettant de simuler les écoulements peu profonds avec des topographies variables et des maillages non structurés.

Résumé

La plupart des méthodes numériques disponibles sont inadéquates en présence de topographies variables à cause du non équilibre des termes source et de flux. Les améliorations apportés à ces difficultés fonctionnent généralement bien pour des maillages structurés, mais ne sont pas directement applicables pour des maillages non structurés. D'autre part, malgré leur bonne performance pour des écoulements discontinus, la plupart des schémas numériques disponibles (par exemple les méthodes HLL et ENO) induisent un niveau élevé de diffusion numérique en simulant des écoulements tourbillonnaires. Une méthode numérique pour simuler des écoulements tourbillonnaires peu profonds en présence d'une topographie variable et des maillages non structurés est présentée. Cette approche, conservant la masse, peut simuler différentes conditions d'écoulement comprenant les topographies variables, les écoulements tourbillonnaires, transcritiques et discontinus, sans recourir à la technique d'upwinding pour les termes de source et avec peu de diffusion numérique. Différents tests numériques sont présentés pour montrer la performance du schéma dans le cas de problèmes difficiles.

A Mass Conservative Scheme For Simulating Shallow Flows Over Variable Topographies Using Unstructured Grids

A. MOHAMMADIAN, D. Y. LE ROUX, M. TAJRISHI, K. MAZAHERI

Abstract. *Most available numerical methods face problems, in the presence of variable topographies, due to the imbalance between the source and flux terms. Treatments for this problem generally work well for structured grids, but most of them are not directly applicable for unstructured grids. On the other hand, despite of their good performance for discontinuous flows, most available numerical schemes (such as HLL flux and ENO schemes) induce a high level of numerical diffusion in simulating recirculating flows. A numerical method for simulating shallow recirculating flows over a variable topography on unstructured grids is presented. This mass conservative approach can simulate different flow conditions including recirculating, transcritical and discontinuous flows over variable topographies without upwinding of source terms and with a low level of numerical diffusion. Different numerical tests cases are presented to show the performance of the scheme for some challenging problems.*

Key Words: Shallow-water, variable topography, unstructured grid, recirculating flow, finite volume method, mass conservative approach

1- Introduction

Shallow recirculating flows cover a wide category of fluvial flows. They occur in many hydraulic situations such as breakwaters, bridge piers, embayment and channel junctions. Modeling these flows is important for engineering applications and optimum design of hydraulic structures. On the other hand, for many fluvial flows, the flow regime changes from subcritical to supercritical and the employed numerical method should be able to solve sub, super and trans-critical flows. In this paper our primary interest is the simulation of the above-mentioned flows using unstructured grids. Unstructured grids are attractive

because of their flexibility for representing irregular boundaries and for local mesh refinement.

Extensive research has been performed in the area of shallow-water equations, and several upwind methods originally designed to solve the Euler equations have been extended to the shallow-water system. Those are for example, the Roe method (Glaister, 1988), the Beam-Warming scheme (Fenemma and Chaudry, 1987), the Monotonic Upstream Schemes for Conservation Laws (MUSCL) using curve-linear coordinate (Alcrudo and Navarro, 1993), the Osher and Salmon scheme (Zhao et. al., 1994), the Essentially Non-Oscillatory (ENO) schemes (Nujic, 1995) and the Harten, Lax and van Leer (HLL) solver (Minhgam and Causon, 1998). Most of these methods have the capability of shock capturing with a high level of accuracy in few computational cells, and the flux vector is determined based on the wave propagation structure.

Some of these methods perform well for particular types of flow like discontinuous or transcritical flows over flat topographies, but in the case of flows over variable topography and recirculating flows around structures, there is room for considerable improvement. Some modifications have been brought to the above mentioned methods in the case of variable topographies and structured grids. Bermudez and Vazquez-Cendon (1994) extended the van Leer's Q-scheme for variable topographies by using an *upwind discretization of the source terms* and they introduced the C property, which states that the scheme should preserve the stagnant conditions. Their work has been extended in the case of a general 1-D channel with breath variation by Vazquez-Cendon (1999). Hubbard and Navarro (2001) then extended the Vasquez-Cendon approach to flux difference splitting schemes. However, upwinding of source terms is computationally expensive for practical applications because the source terms have to be projected on a basis of eigenvectors. LeVeque (1998), introduced *a Riemann problem inside a cell* for balancing the source terms and the flux gradients, and the resulting method was found to preserve both *stagnant* and *quasi steady state* conditions. However, the LeVeque's scheme is not directly transportable to unstructured grids. Kurganov and Levy (2002) extended their *Central-Upwind* scheme for the shallow-water equations and by using the water surface elevation instead of the depth, they proposed an adaptive algorithm for variable topographies. They also proved that their scheme preserves the steady state condition with a positive depth,

without resorting to any artificial drying and wetting strategy. Unfortunately, their scheme poorly performs in the case of circulating flows, as shown in the following. Alcrudo and Benkhaldon (2001) defined the topography such that a sudden change in the topography occurs at the interface of two cells. They also developed a Riemann solver at the interface with a sudden change in the bed elevation. However, their approach leads to several cases of Riemann fan and it is numerically too expensive. Vukovic and Sopta (2002) extended the ENO and Weighted ENO (WENO) schemes to shallow-water equations with the source terms in 1-D channels. Jin (2002) developed the *interface method*, which preserves the steady state condition up to second order accuracy on structured grid, but his approach is not directly usable on unstructured grids. Xu (2002) proposed a second order gas kinetic scheme for shallow-water flows over variable topographies. The gas kinetic schemes are basically different from characteristics based schemes and they should be tested for challenging test cases such as recirculating flows. Nujic (1995) used the water level variable instead of the depth and he extracted the gravitational terms from flux functions. Then, using the Shu and Osher (SO) scheme (1988), he computed the flux vector and obtained accurate results for dam break problems over variable topographies. Unfortunately, the SO scheme (1988) generates a high level of numerical diffusion in the case of recirculating flows, as shown in the following.

Zhou et. al. (2001) introduced the *surface gradient method* and showed that interpolating the depth without considering the bed variations may lead to erroneous results. They used the interpolated water surface elevation to calculate the depth at the interface and they showed that this approach combined with the HLL flux function (Harten, 1983) satisfies the C property. Their scheme performs very well for variable topographies without any extra efforts for balancing the source terms and the flux gradients. However, the C property does not hold for unstructured grids and moreover, the HLL flux induces a high level of numerical viscosity in recirculating flows, as shown in the following.

The objective of this paper is to present an efficient numerical method for *recirculating* flows over variable topographies on unstructured grids. In order to fulfill this goal, the Nujic method (1995) is combined with the Roe scheme, and the surface gradient method (Zhou et. al., 2001) is used for calculating the water depth at the interface. The resulting scheme is *mass* conservative, i.e. the convection terms are conserved but the gravity source

term is discretized using a non-conservative method. Hence, it can simulate flows over variable topographies without upwinding of source terms. Several numerical tests are presented to show that the non-conservative discretization of the source terms induces a minor effect on the ability of the proposed scheme in simulating discontinuous flows. On the other hand, the mass conservation property ensures that the errors will not accumulate in time, which is crucial for the long-term simulations.

This paper is organized as follows. The model equations and the numerical schemes are presented in sections 2 and 3, respectively. In section 4, some test case problems are numerically simulated, and they show the accuracy of the proposed method. Some concluding remarks complete the study.

2- Governing equations

The shallow water equations (SW) in a conservative form are written as

$$\frac{\partial \vec{U}}{\partial t} + \nabla \cdot \vec{F} = \vec{S} + \nabla \cdot \vec{F}^{d}, \tag{2.1}$$

$\vec{U}^{t} = (h, uh, vh)$ with, $\vec{F} = (\vec{E}, \vec{G})$ and

$$\vec{E} = \begin{pmatrix} uh \\ u^2 h + 0.5gh^2 \\ uvh \end{pmatrix}, \quad \vec{G} = \begin{pmatrix} vh \\ uvh \\ v^2 h + 0.5gh^2 \end{pmatrix}, \tag{2.2}$$

where h is the water depth, u and v are the velocity components (Figure 2-1) and g is the gravitational acceleration.

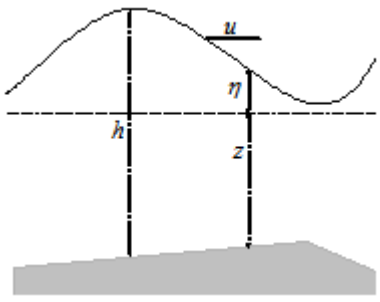

Fig. 2-1. Schematic diagram of an unsteady 1-D flow over an irregular bottom and the corresponding notation.

The superscript ^{d} refers to the diffusion and the diffusive flux has the following form

$$\vec{F}^{d} = (\vec{E}^{d}, \vec{G}^{d}), \tag{2.3}$$

where

$$\vec{E}^{d} = \begin{pmatrix} 0 \\ (\nu + \nu_t)h\partial u/\partial x \\ (\nu + \nu_t)h\partial v/\partial x \end{pmatrix} \quad , \quad \vec{G}^{d} = \begin{pmatrix} 0 \\ (\nu + \nu_t)h\partial u/\partial y \\ (\nu + \nu_t)h\partial v/\partial y \end{pmatrix} \tag{2.4}$$

and ν and ν_t are water and eddy viscosity coefficients respectively.

The source term $\vec{S}$ is written as

$$\vec{S} = \begin{pmatrix} 0 \\ c_f u\sqrt{u^2 + v^2} + gh\partial z/\partial x \\ c_f \nu\sqrt{u^2 + v^2} + gh\partial z/\partial y \end{pmatrix}, \tag{2.5}$$

where z_b is the distance between the bed surface and the reference level (Figure 2-1) and c_f is the friction coefficient. The SW equations may also be written in a non-conservative form

$$\frac{\partial \vec{U}}{\partial t} + A\frac{\partial \vec{U}}{\partial x} + B\frac{\partial \vec{U}}{\partial y} = \vec{S} + \nabla \cdot \vec{F}^{d}, \tag{2.6}$$

where A and B are the Jacobian matrices

$$A = \frac{\partial \vec{E}}{\partial \vec{U}} = \begin{pmatrix} 0 & 1 & 0 \\ -u^2 + c^2 & 2u & 0 \\ -uv & v & u \end{pmatrix} \quad , \quad B = \frac{\partial \vec{G}}{\partial \vec{U}} = \begin{pmatrix} 0 & 0 & 1 \\ -uv & v & u \\ -v^2 + c^2 & 0 & 2v \end{pmatrix}, \tag{2.7}$$

and $c = \sqrt{gh}$ is the wave velocity.

The eigenvalues a^i and b^i, (i=1,2,3) corresponding to the matrices A and B respectively are

$a^1 = u + c, a^2 = u, a^3 = u - c$ and $b^1 = v + c, \quad b^2 = v, \quad b^3 = v - c$, respectively.

3- Numerical scheme

3-1-Finite volume methods on unstructured grids

In this paper, the variables are located at the geometric centers of the cells, and each triangle represents a control volume. Let $\mathcal{A}$ be the area of a triangle with boundary *s*. The SW equations are integrated over every control volume

$$\int_t \int_{\mathcal{A}} \left(\frac{\partial \vec{U}}{\partial t} + \nabla \cdot \vec{F} - \vec{S} - \nabla \cdot \vec{F}^d \right) d\mathcal{A} dt = 0. \tag{3.1}$$

The time integration is performed by using the first order forward (explicit) Euler time-stepping scheme, which leads to

$$\int_{\mathcal{A}} \left(\frac{\vec{U}^{n+1} - \vec{U}^n}{\Delta t} + \left(\nabla \cdot \vec{F} - \vec{S} - \nabla \cdot \vec{F}^d \right)^n \right) d\mathcal{A} = 0. \tag{3.2}$$

In (3.2) the accuracy of the time stepping scheme may be increased to second order by employing the Lax-Wendroff scheme as described in section 3.5. By using the divergence theorem, the diffusive and convective flux integrals are transformed into boundary integrals

$$\int_{\mathcal{A}} \left(\nabla \cdot \vec{F} - \nabla \cdot \vec{F} \right) d\mathcal{A} = \oint_s \left(\vec{F} \cdot \vec{n} - \vec{F}^d \cdot \vec{n} \right) ds \,, \tag{3.3}$$

and the boundary integral is approximated by a summation over the triangle edges

$$\oint_s \left(\vec{F} \cdot \vec{n} - \vec{F}^d \cdot \vec{n} \right) ds - = \sum_{k=1}^{3} \left(\vec{F}_k \cdot \vec{n}_k - \vec{F}_k^d \cdot \vec{n}_k \right) ds_k \,. \tag{3.4}$$

The diffusive fluxes on the cell interfaces are usually approximated by a centered scheme

$$\vec{F}^d = 0.5 \left(\vec{F}_R^d + \vec{F}_L^d \right) \tag{3.5}$$

and the convective fluxes $\vec{F}$ in the Godunov type methods are calculated based on an exact or approximate Riemann solver. Most approximate Riemann solvers are written as

$$\vec{F} = 0.5 \left(\vec{F}_R + \vec{F}_L - \Delta \vec{F}^* \right), \tag{3.6}$$

where $\vec{F}_L = \vec{F}\left(\vec{U}_L\right)$ and $\vec{F}_R = \vec{F}\left(\vec{U}_R\right)$ are the left and right flux vectors. The subscripts $\cdot_R$ and $\cdot_L$ represent the evaluation of the right and left sides of the interface, respectively, and $\Delta \vec{F}^*$ is the flux difference. When $\Delta \vec{F}^* = 0$ in (3.6), the scheme is equivalent to a standard centered scheme. Hence, $\Delta \vec{F}^*$ may be considered as an “artificial diffusive flux”.

The maximum possible (stable) artificial diffusive flux is employed in the Lax–Fredrichs scheme, which in the 1-D case is written as

$$\Delta\vec{F}^{*} = \frac{\Delta x}{\Delta t}\Delta\vec{U}\,, \tag{3.7}$$

where $\Delta\vec{U} = \left(\vec{U}_R - \vec{U}_L\right)$.

A less diffusive approximation for the artificial diffusive flux is that of the Rusanov scheme

$$\Delta\vec{F}^{*} = -|\,a_{\max}\,|(\vec{U}_R - \vec{U}_L)\,, \tag{3.8}$$

where a_{max} is the greatest eigenvalue of the Jacobian matrices corresponding to the left and right flux vectors in (3. 6). The Rusanov scheme is the base of many central schemes, and it provides good results in the case of shock wave problems (see Leveque, 2002 for more details). However, $\Delta\vec{F}^{*}$ in (3.8) excessively damps the solutions for recirculating flows.

Another approach, which works well for both recirculating flows and shock wave problems, is the Roe method, for which an approximate Riemann solver is obtained by solving a linearized system. Here, $\Delta\vec{F}^{*}$ is calculated as

$$\Delta\vec{F}^{*} = \left|A\right|\Delta\vec{U} \cong \left|\widetilde{A}\right|\sum_{k=1}^{3}\widetilde{\alpha}^{k}\widetilde{\vec{e}}^{\,k} = \sum_{k=1}^{3}\widetilde{\alpha}^{k}\left|\widetilde{a}^{k}\right|\widetilde{\vec{e}}^{\,k}\,, \tag{3.9}$$

where $A = \partial(\vec{F}.\vec{n})/\partial\vec{U}$ is the Jacobian matrix of the flux projection in the normal direction, $\widetilde{A}$ is Roe average Jacobian matrix, which satisfies $\Delta\vec{F} = \widetilde{A}\Delta\vec{U}$ with

$$\widetilde{A} = \frac{\partial\left(\vec{F}.\vec{n}\right)}{\partial\vec{u}} = \begin{pmatrix} 0 & n_x & n_y \\ \left(\widetilde{c}^{\,2} - \widetilde{u}^{\,2}\right)n_x - \widetilde{u}\widetilde{v}n_y & 2\widetilde{u}n + \widetilde{v}n_y & \widetilde{u}n_y \\ -\widetilde{u}\widetilde{v}n_x + \left(\widetilde{c}^{\,2} - \widetilde{v}^{\,2}\right)n_y & \widetilde{v}n_x & \widetilde{u}n_x + 2\widetilde{v}n_y \end{pmatrix}, \tag{3.10}$$

where

$$\widetilde{u} = \frac{u_R\sqrt{h_R} + u_L\sqrt{h_L}}{\sqrt{h_R} + \sqrt{h_L}} \quad , \quad \widetilde{v} = \frac{v_R\sqrt{h_R} + v_L\sqrt{h_L}}{\sqrt{h_R} + \sqrt{h_L}} \quad , \quad \widetilde{c} = \sqrt{g(h_R + h_L)/2}\,. \tag{3.11}$$

and the eigenvalues of $\widetilde{A}$ are simply

$$\widetilde{a}^{1} = \widetilde{u}n_x + \widetilde{v}n_y + \widetilde{c} \quad , \quad \widetilde{a}^{2} = \widetilde{u}n_x + \widetilde{v}n_y \quad , \quad \widetilde{a}^{3} = \widetilde{u}n_x + \widetilde{v}n_y - \widetilde{c}\,, \tag{3.12}$$

with the corresponding eigenvectors

$$\tilde{\vec{e}}^1 = \begin{pmatrix} 1 \\ \tilde{u} + \tilde{c} n_x \\ \tilde{v} + \tilde{c} n_y \end{pmatrix} , \quad \tilde{\vec{e}}^2 = \begin{pmatrix} 0 \\ -\tilde{c} n_y \\ \tilde{c} n_x \end{pmatrix} , \quad \tilde{\vec{e}}^3 = \begin{pmatrix} 1 \\ \tilde{u} - \tilde{c} n_x \\ \tilde{v} - \tilde{c} n_y \end{pmatrix}, \tag{3.13}$$

respectively. The $\tilde{\alpha}^k$ coefficients in (3.9) arise from the decomposition of $\Delta\vec{U}$ in the basis $(\vec{e}_1, \vec{e}_2, \vec{e}_3)$, and they depend on the jumps $\Delta = (\ )_R - (\ )_L$ with

$$\tilde{\alpha}^{1,3} = \frac{\Delta h}{2} \pm \frac{1}{2\tilde{c}} \left[\Delta(hu) n_x + \Delta(hv) n_y - (\tilde{u} n_x + \tilde{v} n_y) \Delta h \right], \tag{3.14}$$

$$\tilde{\alpha}^2 = \frac{1}{\tilde{c}} \left(\left[\Delta(hv) - \tilde{v} \Delta h \right] n_x - \left[\Delta(hu) - \tilde{u} \Delta h \right] n_y \right). \tag{3.15}$$

Shu and Osher (1988) showed that instead of using the Roe approximate solver with $\Delta\vec{U}$ expressed in the eigenvector basis, the ENO schemes can be efficiently implemented using a simpler Rusanov-type approximate solver with artificial diffusive flux

$$\Delta\vec{F}^* = -|\alpha| (\vec{U}_R - \vec{U}_L), \tag{3.16}$$

where $\alpha = \lambda |a_{\max}|$ (with $\lambda \le 1$), and a TVD Runge-Kutta time marching method.

3-2- The surface gradient method

In order to calculate the numerical fluxes in (3.5) and (3.6), the values of the variables at the left and right sides of the interface must be calculated. Zhou et. al. (2001) proposed the surface gradient method, in which the water surface elevation η is interpolated at the cell faces instead of the water depth. The water depth at the cell face is then calculated using the water surface elevation and the bed topography. For example, once η_L is calculated, the water depth can be obtained as

$$h_L = \eta_L + z_e, \tag{3.17}$$

where z_e is the distance between the bed surface and the reference level (Fig. 2-1) at triangle edge midpoints. The surface gradient method leads to $\Delta h = 0$ at the cell faces in the case of stagnant water conditions.

The velocities at cell interfaces are also calculated from the depth integrated velocities uh and vh at cell faces as

$$u_L = \frac{(uh)_L}{h_L}. \tag{3.18}$$

3-3- Calculation of derivatives

The derivatives of a scalar variable c on unstructured grids are calculated using the divergence theorem, and we obtain

$$\left(\frac{\partial c}{\partial x}\right)_i = \frac{1}{\mathcal{A}_i}\int_{\mathcal{A}} \frac{\partial c}{\partial x} d\mathcal{A} \approx \frac{c_1 \Delta y_1 + c_2 \Delta y_2 + c_3 \Delta y_3}{\mathcal{A}_i}, \tag{3.19}$$

$$\left(\frac{\partial c}{\partial y}\right)_i = \frac{1}{\mathcal{A}_i}\int_{\mathcal{A}} \frac{\partial c}{\partial y} d\mathcal{A} \approx -\frac{c_1 \Delta x_1 + c_2 \Delta x_2 + c_3 \Delta x_3}{\mathcal{A}_i}, \tag{3.20}$$

where (see figure 3-1)

$$\Delta y_1 = y_3 - y_2 \quad , \quad \Delta x_1 = x_3 - x_2 \quad , \quad c_1 = (c_1^L + c_1^R)/2\,, \tag{3.21}$$

$$\Delta y_2 = y_1 - y_3 \quad , \quad \Delta x_2 = x_1 - x_3 \quad , \quad c_2 = (c_2^L + c_2^R)/2\,, \tag{3.22}$$

$$\Delta y_3 = y_2 - y_1 \quad , \quad \Delta x_3 = x_2 - x_1 \quad , \quad c_3 = (c_3^L + c_3^R)/2\,. \tag{3.23}$$

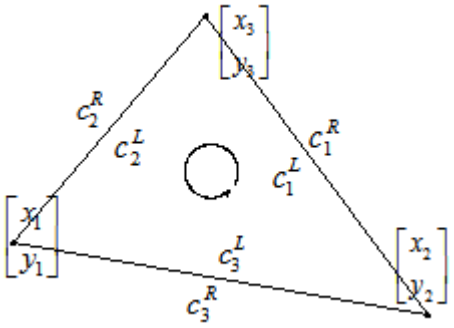

Fig. 3-1. The triangular cell i with the quantities c_j^R and c_j^L computed at the right (R) and left (L) sides respectively at a given face j, j=1,2,3. The coordinates (x_j, y_j), j=1,2,3, are located at the three vertices of cell i.

This approach may be used for calculating the $gh(\partial z/\partial x)$ and $gh(\partial z/\partial y)$ terms and also the viscous terms, i.e.

$$\left(\nu h\frac{\partial u}{\partial x}\right)_i \approx \nu h_i \frac{u_1 \Delta y_1 + u_2 \Delta y_2 + u_3 \Delta y_3}{A_i}. \qquad (3.24)$$

The treatment of variable topographies now follows.

3-4- Variable topographies

As mentioned in the previous sections, the bed slope (BS) term $gh\partial z/\partial x$ is included in the source term, and it is usually discretized using a centered scheme. This leads to an imbalance between the depth gradient (DG) term $0.5g\partial h^2/\partial x$ and the BS term and hence to an artificial source term in the numerical solution. In order to overcome this problem, the Nujic method (1995) is adopted and modified here in the following manner.

In the Nujic method, the DG term is extracted from the flux functions and it is discretized using a central scheme. However, the eigenvalues of the original system are used to calculate the fluxes using the SO scheme. The BS term is then dicretized in the Nujic method such that the compatibility between the DG and BS terms is guaranteed. On structured grids, as was shown by Nujic (1995), this is easily possible, but on unstructured grids a compatible discretization of the BS term is not as straightforward as on structured grids.

Nujic used the Shu and Osher (1988) method (SO) with $\lambda \simeq 0.4$ and mentioned that the SO scheme is attractive for solving dam break problems. However, as shown in the following, the SO scheme produces significant numerical diffusion in the case of recirculating flows. In order to reduce it, we use here the Roe approximate solver (3.9) instead of the SO scheme, employed in the Nujic method, as follows.

The discretized SW equations using the Roe method lead to

$$\vec{U}^{n+1} = \vec{U}^n - 0.5\Delta t/\Delta x\left(\left(\vec{F}_L + \vec{F}_R - \Delta\vec{F}^*\right)^n_{i+1/2} - \left(\vec{F}_L + \vec{F}_R - \Delta\vec{F}^*\right)^n_{i-1/2}\right) + \Delta t\vec{S}, \qquad (3.25)$$

or, by rearranging the terms

$$\vec{U}^{n+1} = \vec{U}^n + \vec{L} + \vec{K}, \qquad (3.26)$$

where

$$\vec{K} = \begin{pmatrix} k_1 \\ k_2 \end{pmatrix} = \begin{pmatrix} 0 \\ g\Delta t/\Delta x h_i (z_{i+1/2} - z_{i-1/2}) - 0.5g\Delta t/\Delta x\left(\left(h_L^2 + h_R^2\right)_{i+1/2} - \left(h_L^2 + h_R^2\right)_{i-1/2}\right) \end{pmatrix}, \qquad (3.27)$$

and $\vec{L}$ includes all the remaining terms of the right hand side of (3.25). In the case of stagnant conditions η is constant, and Δh is thus zero at the cell faces using the surface gradient method. Because the stagnant conditions, we also have $uh = 0$ and $\Delta(uh) = 0$. Therefore, the $\tilde{\alpha}^k$ coefficients calculated using (3.14) and (3.15) vanish and hence, $\Delta\vec{F}^* = 0$. All other terms in $\vec{L}$ also vanish in the case of stagnant conditions. In order to satisfy the C property $\vec{K}$ must also vanish, which is not the case when using k_2 as defined in (3.27). By rewriting k_2 in (3.27) as

$$k_2 = g\Delta t/\Delta x h_i (z_{i+1/2} - z_{i-1/2}) - 0.5 g\Delta t/\Delta x \left[\left((h_L)_{i+1/2} + (h_L)_{i-1/2}\right)\left((h_L)_{i+1/2} - (h_L)_{i-1/2}\right) + \left((h_R)_{i+1/2} + (h_R)_{i-1/2}\right)\left((h_R)_{i+1/2} - (h_R)_{i-1/2}\right)\right], \tag{3.28}$$

using the following approximations

$$h_i = 0.5\left((h_R)_{i+1/2} + (h_R)_{i-1/2}\right) + O(\Delta x^2), \tag{3.29}$$

$$h_i = 0.5\left((h_L)_{i+1/2} + (h_L)_{i-1/2}\right) + O(\Delta x^2), \tag{3.30}$$

and neglecting the second order terms, equation (3.28) leads to

$$k_2 = -g\Delta t h_i \frac{\left(\eta_L + \eta_R\right)_{i+1/2} - \left(\eta_L + \eta_R\right)_{i-1/2}}{2\Delta x}. \tag{3.31}$$

The k_2 component in (3.31) obviously vanishes because of stagnant conditions and hence the C property is now satisfied. In the tests presented below, it is shown that neglecting the second order terms in (3.29) and (3.30) has a minor effect on the TVD property of the Roe method, while considerably improves its performance in the case of variable topographies.

This approach may be viewed as a mass-conservative approach. Although the discretization of the gradient term is not conservative, the convection terms are treated in a conservative manner, hence the mass is conserved, which is crucial for the long term simulations.

A similar approach is used for the 2-D case. The bed slope term in a triangular control volume *i* may be discretized using the central scheme (3.19) as

$$\left(gh\frac{\partial z}{\partial x}\right)_i \approx gh_i\left(\frac{\partial z}{\partial x}\right)_i \approx gh_i\left(\frac{z_1\Delta y_1 + z_2\Delta y_2 + z_3\Delta y_3}{A_i}\right), \tag{3.32}$$

and $\vec{K} = (k_1, k_2, k_3)$ in (3.26), with $k_1 = 0$ and

$$k_2 = g\Delta t / \mathcal{A}_i \left[h_i (z_1 \Delta y_1 + z_2 \Delta y_2 + z_3 \Delta y_3) - 0.5 \left(\left(h_L^2 + h_R^2 \right)_1 \Delta y_1 + \left(h_L^2 + h_R^2 \right)_2 \Delta y_2 + \left(h_L^2 + h_R^2 \right)_3 \Delta y_3 \right) \right], \tag{3.33}$$

$$k_3 = -g\Delta t / \mathcal{A}_i \left[h_i (z_1 \Delta x_1 + z_2 \Delta x_2 + z_3 \Delta x_3) - 0.5 \left(\left(h_L^2 + h_R^2 \right)_1 \Delta x_1 + \left(h_L^2 + h_R^2 \right)_2 \Delta x_2 + \left(h_L^2 + h_R^2 \right)_3 \Delta x_3 \right) \right]. \tag{3.34}$$

Then, Δy_3 is replaced in (3.33) by $\Delta y_3 = -(\Delta y_1 + \Delta y_2)$ and using

$$h_i \approx \frac{(h_R)_1 + (h_R)_3}{2} \approx \frac{(h_L)_1 + (h_L)_3}{2} \approx \frac{(h_R)_2 + (h_R)_3}{2} \approx \frac{(h_L)_2 + (h_L)_3}{2}, \tag{3.35}$$

we obtain

$$k_2 = -0.5 g (\Delta t / \mathcal{A}_i) h_i \left(\left(\eta_L + \eta_R \right)_1 \Delta y_1 + \left(\eta_L + \eta_R \right)_2 \Delta y_2 + \left(\eta_L + \eta_R \right)_3 \Delta y_3 \right). \tag{3.36}$$

Similarly, the same procedure leads to

$$k_3 = 0.5 g (\Delta t / \mathcal{A}_i) h_i \left(\left(\eta_L + \eta_R \right)_1 \Delta x_1 + \left(\eta_L + \eta_R \right)_2 \Delta x_2 + \left(\eta_L + \eta_R \right)_3 \Delta x_3 \right). \tag{3.37}$$

The components k_2 and k_3 in (3.36) and (3.37), are obviously zero in the case of stagnant conditions and hence, the C property is satisfied. Note (3.36) and (3.37) reduce to (3.31) in the 1-D case.

3-5- Entropy and high resolution corrections

The Roe method violates the entropy condition in the case of sonic rarefaction (transcritical flow), and produces a shock inside a sonic rarefaction, which is obviously incorrect for the SW equations. Many methods have been proposed to overcome this problem. Here, we use the approach proposed by Harten and Hyman (1983) with

$$\Delta \vec{F}^* = \sum_{k=1}^{3} \tilde{\alpha}^k \, \psi(\tilde{a}^k) \tilde{\vec{e}}^k, \tag{3.38}$$

instead of (3.9). Here, the entropy correction function ψ is defined as

$$\psi(w) = \begin{cases} |w| & \text{if } |w| \geq \varepsilon, \\ \varepsilon & \text{if } |w| < \varepsilon. \end{cases} \tag{3.39}$$

Harten and Hyman (1983) proposed to calculate ε as

$$\varepsilon^k = \max\left[0, \quad \tilde{a}^k - a_L^k, \quad a_R^k - \tilde{a}^k\right]. \tag{3.40}$$

The first order Roe scheme can be extended to a high resolution method by adding a correction term (based on the Lax-Wendroff scheme) to $\Delta\vec{F}^*$ in the first order flux (3.5). The resulting $\Delta\vec{F}^*$ is written in the following form

$$\Delta\vec{F}^* = \sum_{k=1}^{3}\left[1-\left(1-\lambda\frac{\Delta t}{\Delta x}\left|\tilde{a}^k\right|\right)\varphi^k\right]\tilde{\alpha}^k\psi\left(\tilde{a}^k\right)\tilde{\vec{e}}^k, \tag{3.41}$$

where φ^k is the flux limiter associated with the kth component of the decomposition. Here, $\Delta\vec{F}^*$ vanishes in the case of stagnant conditions (since $\tilde{\alpha}^k$ vanishes) and hence, the C property still holds with the high resolution scheme.

The flux limiter approach (3.41) has also been employed by Hubbard and Navarro (2000) on a triangular grid with an upwind discretization of the source terms and led to good results. The implementation of (3.41) for 2-D cases has been described in Leveque (2002). All the computations presented below are performed by using the minmod flux limiter as described in Leveque (2002).

3-6- Stability and boundary conditions

Due to the explicit discretization of the convective terms, a CFL number less than 1 is an upper limit for stability. This is the case when the non-linear effects are not dominant, like in the Leveque's 1-D test case presented below using a CFL value of 0.99. However, for most existing schemes, the stability considerations are more restrictive when nonlinear effects are dominant, and this is also the case for the present scheme. Based on numerical experiments, there is no significant difference between the stability condition of the original Roe scheme and the modified one proposed here, in the case of smooth flows.

On the other hand, the proposed corrections in (3.29) and (3.30) induce a minor effect on the non-oscillatory feature of the Roe scheme in simulating discontinuous flows with a high CFL number. However, by choosing a slightly smaller time step (usually 10-20% less than the original Roe scheme), the oscillations disappear. For example, in the dambreak test case 4-1 presented below, using a first order scheme, the oscillations are not seen when the CFL number is less than 0.83, and the scheme is stable up to a CFL of 0.93. When using high

resolution scheme, the oscillations are not observed when the CFL number is less than 0.75 and the scheme is stable up to a CFL of 0.9. In 2D, the CFL condition is defined as

$$CFL = \min\left[\frac{\left(\sqrt{u_i^2 + v_i^2} + c_i\right)\Delta t}{d_{ij}}\right] \tag{3.42}$$

where d_{ij} is the distance between the centroid of each cell i and its neighbors j.

The numerical treatment of the boundary conditions is performed by setting the variables at the boundary edges based on the theory of characteristics (Alcrudo and Navarro, 1993). For subcritical flows, two external conditions must be specified at inflow boundaries, whereas only one is required at the outflow one. However, two-dimensional supercritical flows require the imposition of three inflow boundary conditions and none at the downstream side.

In the particular case of solid wall, both velocity components are set equal to zero. The depth variables are calculated by using the information carried out by the outgoing bi-charachteristics (the Riemann invariants). However, in most practical cases those may be simply set to the corresponding values of the adjacent inner cells.

4- Numerical results

In order to study the performance of the numerical scheme, some tests have been performed herein. Tests 4-1 and 4-2 show the ability of the model for simulating dam-break type flows. The remaining tests show the performance of the proposed scheme for variable topographies and recirculating flows. In tests 4-1 to 4-4 and 4-9-1 we examine 1-D problems and the other tests are performed using the two dimensional model. In all tests the CFL number ranges between 0.35 and 1.0. In all figures and tables, the SI system has been used, i.e. the water depth and the water surface elevation are in *m* and the water discharge is in m^3/s. In all tests a high resolution scheme is employed except otherwise mentioned.

4-1 –The dam break problem

The dam break problem is a common test for evaluating shock capturing schemes in shallow flows. Here, a dam is located at the mid point of a channel of length 50 m. The

water depth at left and right hand side of the dam is 0.5m and 0.25 m respectively. The dam is instantaneously removed across its entire width and the flow conditions are computed up to time t = 8 s. A CFL number of 0.65 was chosen in order to compare the first and second order schemes introduced in (3-38) and (3-41), respectively. The results consist of a right shock and a left rarefaction. The results for the depth (*h*) and discharge (*uh*) are presented in figures 4-1-a and 4-1-b respectively. As it can be seen, both first and second order schemes are able to provide good results without numerical oscillations. Further, the second order scheme requires less grid points than the first order one, to capture the shock wave. In the dam break tests, the maximum value of h_L/h_R is a measure of the performance of the numerical scheme. In the next section we show that the proposed method can simulate the dambreak problem with all depth ratios (even on a dry bed).

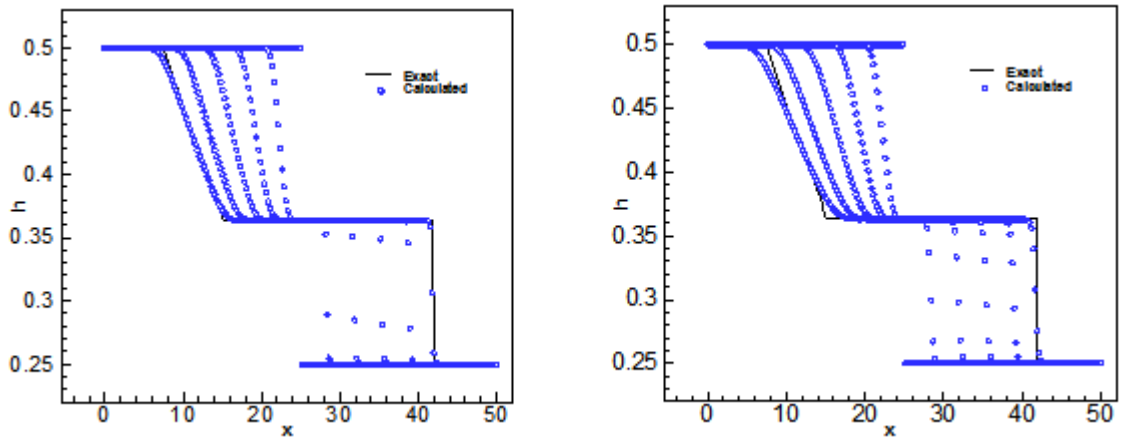

Fig. 4-1-a. Calculated depth at t=1.6, 3.2, 4.8, 6.4 and 8s with the proposed method; second order (left) and first order (right).

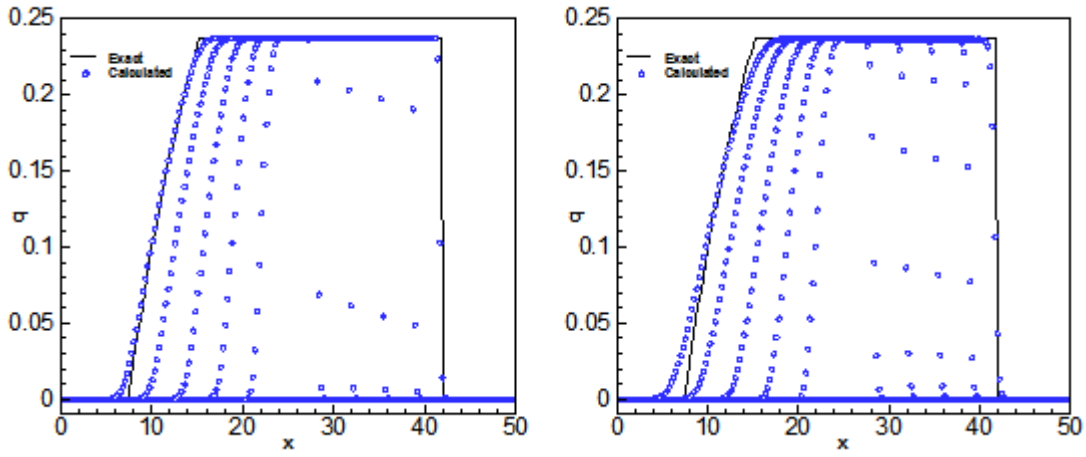

Fig. 4-1-b. Calculated discharge at t=1.6, 3.2, 4.8, 6.4 and 8s with the proposed method; second order (left) and first order (right).

4-2- Toro's Riemann problems

We now investigate the ability of the proposed scheme in performing several challenging test cases designed by Toro (2000). A summary of the initial conditions used in these test cases is presented in table 1, where h_L, u_L, h_R, u_R, denote the initial depth and velocity in the left and right hand side of the discontinuity, x_0 is the position of the discontinuity and t_{out} is the output time. In all tests a wide horizontal, rectangular and frictionless channel of length 50 m is used. In all tests a second order scheme is used and the results are compared with those of the Roe scheme (second order) and the analytical solutions.

Table 1. Data for Toro's test problems.

Test	h_L(m)	u_L(m)	h_R(m)	u_R(m)	x_0(m)	t_{out}(s)
4-2-1	1.0	2.5	0.1	0.0	10.0	7.0
4-2-2	1.0	-5.0	1.0	5.0	25.0	2.5
4-3-3	1.0	0.0	0.0	0.0	20.0	4.0
4-2-4	0. 1	-3.0	0.1	3.0	25.0	5.0

4-2-1– Left sonic rarefaction and right shock

The initial condition has been chosen as to produce a strong shock wave and a sonic or transcritical left rarefaction wave. The results of this test are presented in figure 4-2-1, and they are compared with those of the original Roe scheme. As it can be seen, both the Roe scheme and the proposed method give good results.

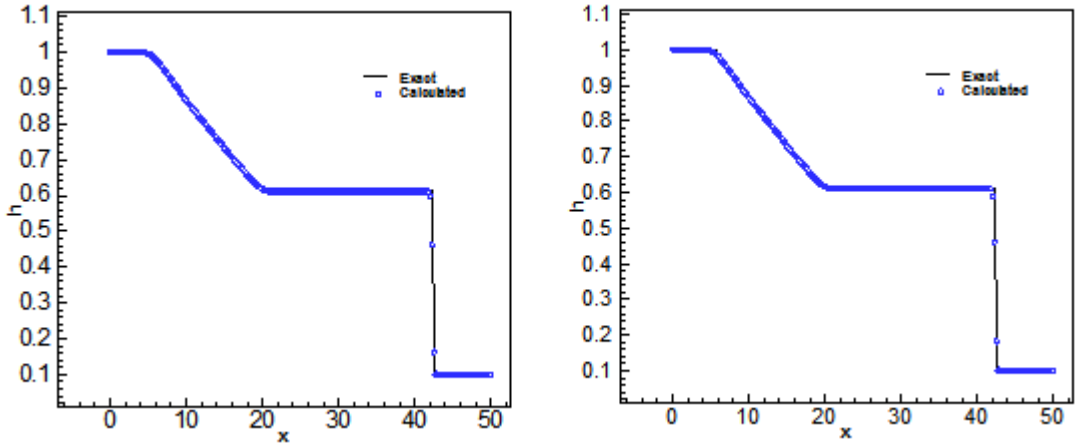

Fig. 4-2-1. Left sonic rarefaction and right shock test case. Calculated water depth with the proposed method (left) and the Roe scheme (right)

4-2-2 – Two rarefactions and nearly dry bed

In this test, the initial conditions have been chosen in order to produce two rarefacrtion waves and a nearly dry bed. The results are shown in figure 4-2-2 for the original Roe scheme and the proposed method. They confirm that the proposed modifications do not change the performance of the Roe method for this problem.

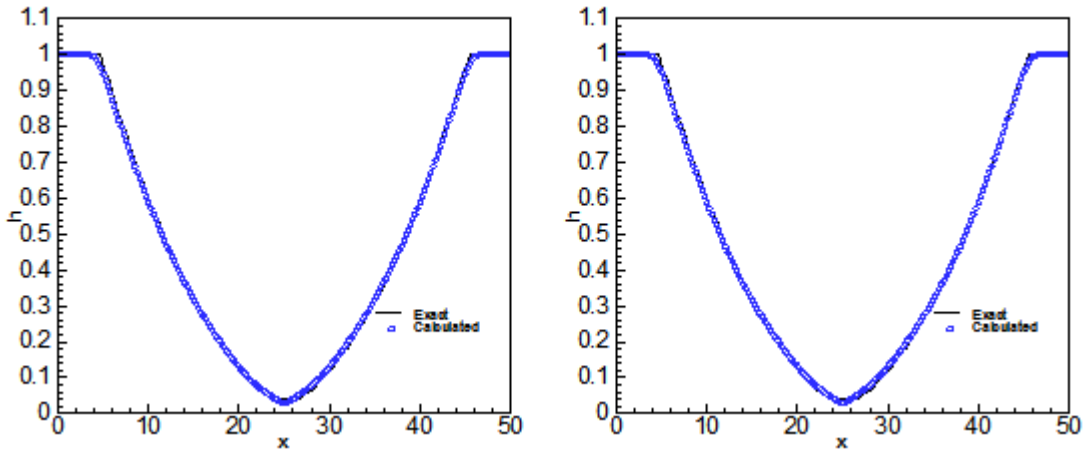

Fig. 4-2-2. Two rarefactions and nearly dry bed test case. Calculated water depth with the proposed method (left) and the Roe scheme (right)

4-2-3-Dambreak on dry bed

Jha et. al. (1996) reported that the Roe method using the second order accurate correction fails to simulate the dambreak problem when $h_L/h_R<0.002$. In order to overcome this problem, the flux limiter function is also set here to zero when $h<10^{-5}$, i.e. the model is second order accurate everywhere except close to the shock region and the wet/dry border. The results are presented in figure 4-2-3, and they are again compared with those of the original Roe scheme (with the modified flux limiter function). They show that the proposed method is able to simulate the dambreak type flows whatever the choice of depth ratio h_L/h_R.

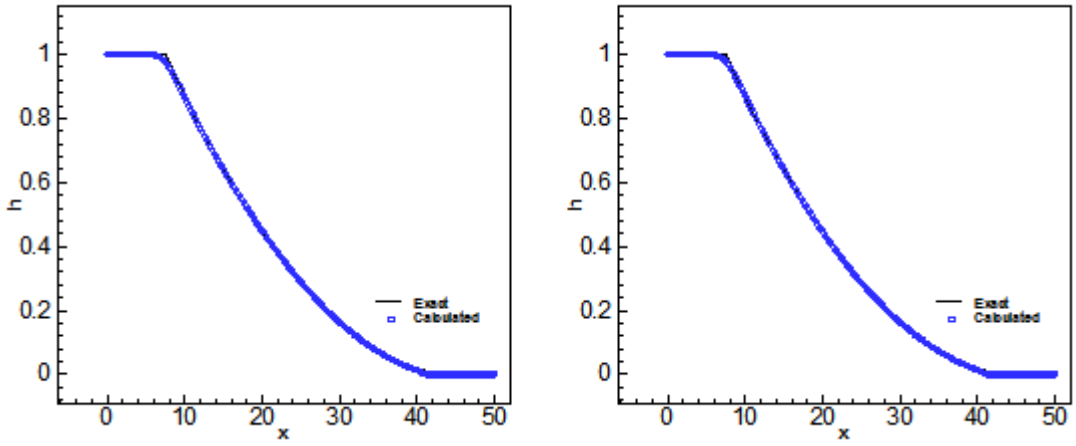

Fig. 4-2-3. Dambreak on dry bed. Calculated water depth with the proposed method (left) and the Roe scheme (right).

4-2-4-Generation of a dry bed

The initial condition has been chosen in order to produce a solution consisting of two rarefaction waves with a portion of a dry bed between them. The results of this test are presented in figure 4-2-4, and they are again compared with those of the Roe scheme. As it can bee seen, both schemes produce similar results, i.e. the proposed modification does not change the quality of the results of the Roe scheme for this test. Hence, tests 4-2-3 and 4-2-4 show the ability of the proposed scheme in simulating dry bed problems.

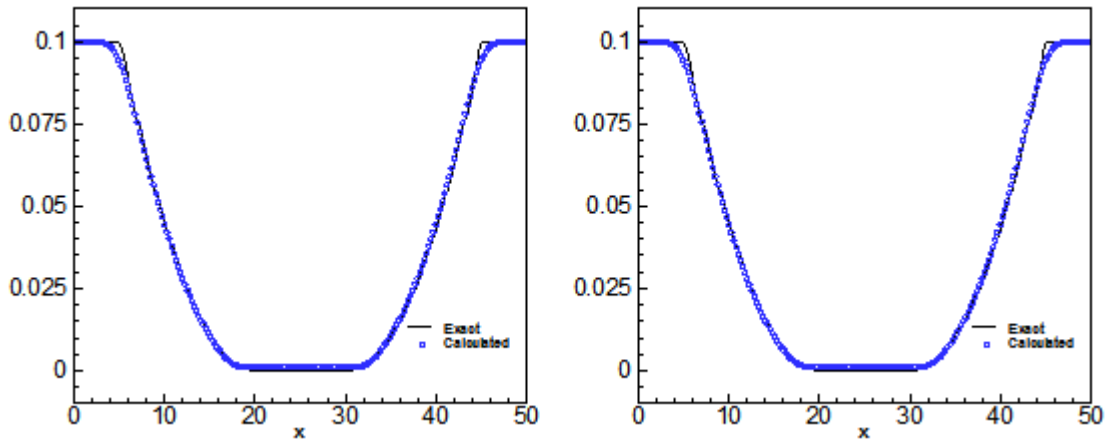

Fig. 4-2-4. Generation of a dry bed. Calculated water depth with the proposed method (left) and the Roe scheme (right).

4-3-Tidal wave flow

4-3-1-Tidal wave flow over regular topography

This one dimensional test was proposed by Bermudez and Vazquez (1994). The topography is defined as

$$z(x) = -50.5 + \frac{40x}{L} - 10\sin\left[\pi\left(\frac{4x}{L} - \frac{1}{2}\right)\right], \tag{4.1}$$

where L=14000m is the channel length. By defining $H(x)$=-$z(x)$, the initial conditions write

$$h(x,0) = H(x), \tag{4.2}$$

$$u(x,0) = 0 \tag{4.3}$$

with the boundary conditions

$$h(0,t) = H(0) + 4 - 4\sin\left[\pi\left(\frac{4t}{86400} + \frac{1}{2}\right)\right], \tag{4.4}$$

$$u(L,t) = 0. \tag{4.5}$$

For this test, Bermudez and Vazquez (1994) derived the following analytical solution

$$h(x,t) = H(x) + 4 - 4\sin\left[\pi\left(\frac{4t}{86400} + \frac{1}{2}\right)\right], \tag{4.6}$$

$$u(x,t) = \frac{(x-L)\pi}{5400h(x,t)}\cos\left[\pi\left(\frac{4t}{86400}+\frac{1}{2}\right)\right]. \qquad (4.7)$$

At time t = 7552.13, the results are shown in figure 4-3-1, and are in a good agreement with the exact solution.

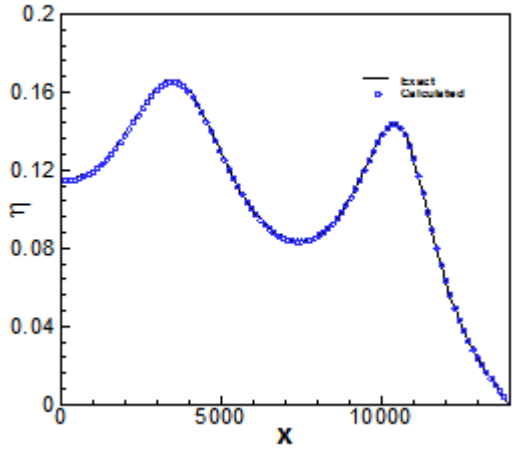

Figure 4-3-1. Tidal wave flow in a channel with variable topography.

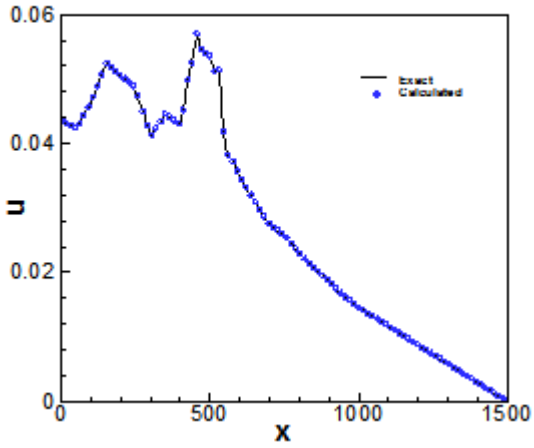

Figure 4-3-2. Tidal wave flow over an irregular bed.

4-3-2- Tidal wave flow over an irregular bed

Here, the topography is defined in table 2. This irregular bed was proposed at a workshop on dambreak wave simulations (Goutal and Maurel, 1997).

The initial and boundary conditions are identical to those used in test 4-3-1, with

L=1500 m, $H(x)= H(0)-z(x)$, $H(0)=16m$.

The analytical solution is given by (4.6) and (4.7). At time t = 10800 s the results, shown in figure 4-3-2, indicate the ability of the scheme in simulating irregular topographies.

Table 2. Topography for Irregular Bed.

X(m)	0	50	100	150	250	300	350	400	425	435	450	475	500	505
Z(m)	0	20	2.5	5	5	3	5	5	7.5	8	9	9	9.1	9
X(m)	530	550	565	575	600	650	700	750	800	820	900	950	1000	1500
Z(m)	9	6	5.5	5.5	5	4	3	3	2.3	2	1.2	0.4	0	0

4-4- Steady flow over a bump

This problem was also proposed at the workshop on dam-break simulations (Goutal and Maurel, 1997). The topography is defined as

$$z(x) = \begin{cases} 0.2 - 0.05(x-10)^2 & \text{if } 8 < x < 12, \\ 0 & \text{otherwise.} \end{cases} \quad (4.8)$$

Depending on the initial and boundary conditions, the flow may be subcritical, transcritical (with or without a steady shock), or supercritical. The analytical solution of this problem is given in Goutal (1997). The global relative error R is defined as

$$R = \sqrt{\sum_i \left(\frac{h_i^n - h_i^{n-1}}{h_i^n} \right)^2}, \quad (4.9)$$

where h_i^n and h_i^{n-1} are the local water depths at the current and previous time levels. A mesh of 150 nodes was used in all computations.

Three different cases are considered:

(i) *Transcritical flow without a shock*

The boundary conditions are defined as

Downstream: The water level h=0.66m is imposed only when the flow is subcritical.

Upstream: The discharge *uh*=1.53 m^3/h is imposed.

The surface profile is plotted in Figure 4-4-1, and it shows a good agreement with the analytical solution. The computed discharge is also compared with the theoretical one in Figure 4-4-1. The numerical oscillations observed in figure 4-4-1 (right) are also present in most existing schemes. This behavior is related to the fact that the C property, although it is widely accepted in the literature as a good-enough measure to test the ability of the numerical schemes in the presence of real topographies, does not guarantee that the steady state condition with non-zero discharge is well captured.

(ii) *Transcritical flow with a shock*

The boundary conditions are defined as

Downstream: The water level h=0.33m is imposed.

Upstream: The discharge *uh*=0.18 m^3/h is imposed.

Figure 4-4-2 (left) shows that a good agreement is obtained between the analytical solution and the computed water surface elevation. A comparison of the computed discharge with the theoretical results is shown in figure 4-4-2 (right). The oscillations have the same origin as previously mentioned in (i).

(iii) *Subcritical flow*

The boundary conditions are now defined as

Downstream: The water level h=2.m is imposed.

Upstream: The discharge *uh*=4.42 m^3/h is imposed.

The numerical results are depicted in figure 4-4-3 (left), and again they show an excellent agreement between the analytical solution and the computed water surface elevation. A comparison of the computed discharge with the analytical results is shown in figure 4-4-3 (right). Again, the oscillations have the same origin than previously mentioned in (i).

The convergence history performed for the tests (i), (ii), (iii) is shown in figure 4-4-4, which shows that for all problems, the convergence is obtained in a reasonable number of iterations.

In order to examine the 2-D model in different flow regimes over variable topographies, the present test case is also performed with the 2-D model. The unstructured grid used here is shown in figure 4-4-5. The corner triangles do not complete a rectangle but this does not have any effect on the results. The results corresponding to the boundary conditions (i), (ii), (iii) are compared with the analytical solution in figure 4-4-6, and they show that the current method can simulate all cases accurately.

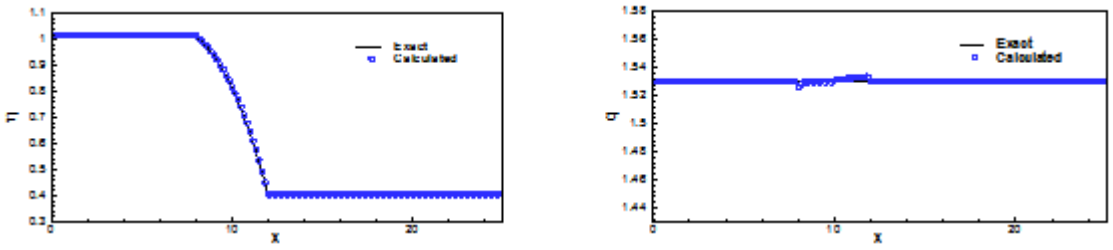

Figure 4-4-1. Steady transcritical flow over a bump without a shock: Water surface elevation (left) and discharge (right).

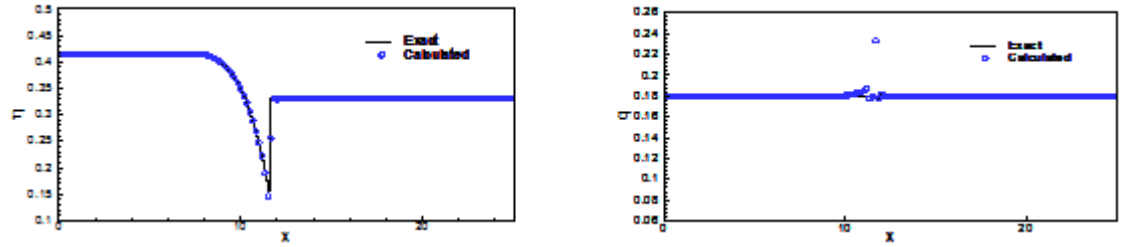

Figure 4-4-2. As for fig. 4-4-1 but for the steady transcritical flow over a bump with a shock.

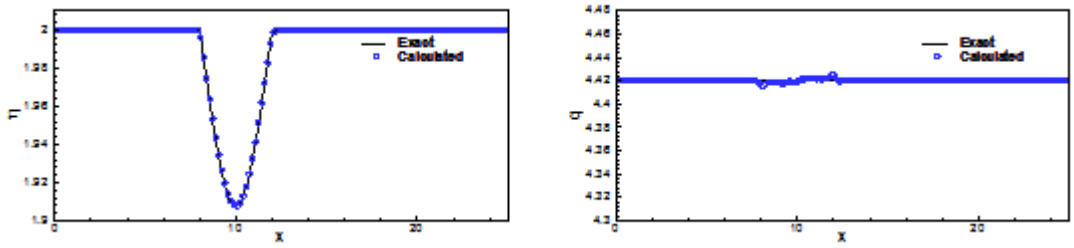

Figure 4-4-3. As for fig. 4-4-1 but for the steady subcritical flow over a bump.

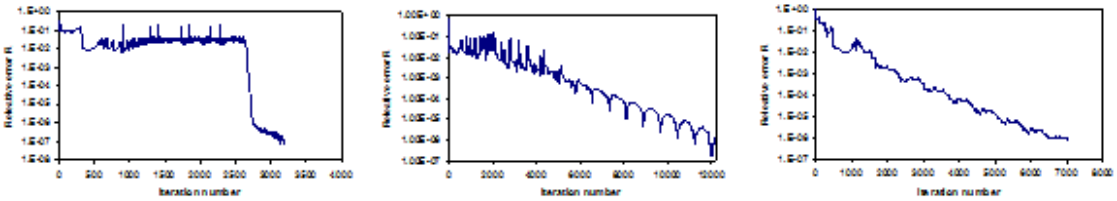

Figure 4-4-4. Convergence history for tests (i), (ii), (iii), from left to right respectively.

Figure 4-4-5. Unstructured triangular grid used for the steady flow over a bump.

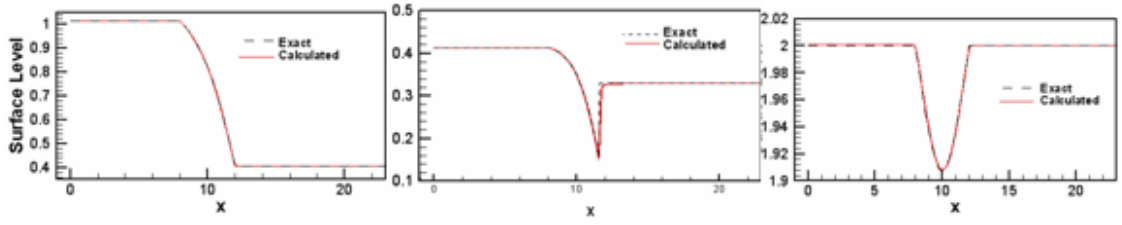

Figure 4-4-6. Different cases of flow over a bump (the 2D model): Water surface elevation.

4-5-Bore Reflection

4-5-1- Alcrudo and Navarro's oblique wave problem

An oblique wave is generated by the interaction between a supercritical flow and a converging wall, with an angle of $\theta = 8.95^{o}$ between the wall and the stream-wise direction. The upstream condition is a uniform supercritical flow with a depth of 1 m, and the flow velocity is such that u=8.57 m/s and v = 0.0 m/s. The analytical solution for this problem is h_d=1.5m and $\sqrt{u^2+v^2} = 7.9525$ m/s, respectively, and the numerical results are shown in figure 4-5-1-a and 4-5-1-b. The calculated depth and flow velocity are h_d=1.4995 m and $\sqrt{u^2+v^2} = 7.9556$ m/s. Hence, it appears that the model is able to simulate this test case accurately, without exhibiting numerical oscillations.

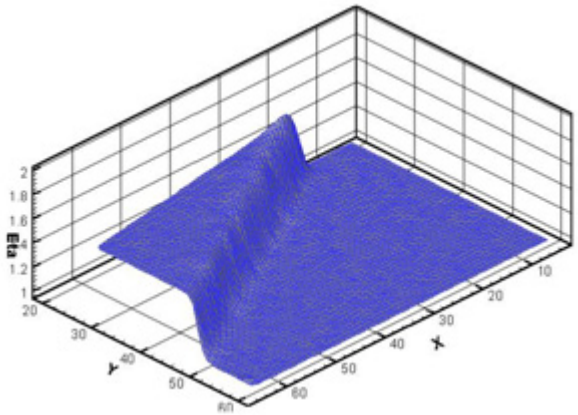

Fig 4-5-1-a. Oblique wave problem: 3D view of calculated water level.

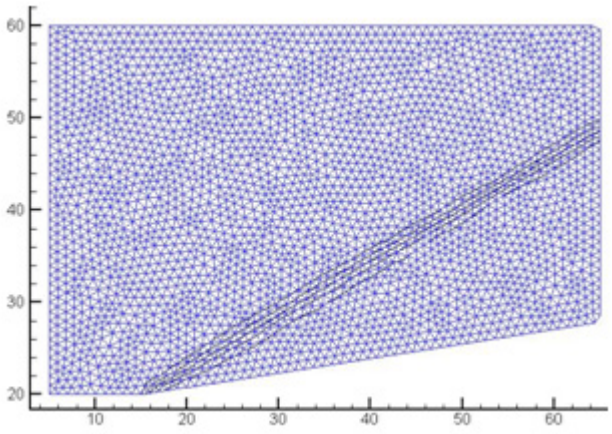

Fig 4-5-1-b. Oblique wave problem: Grid and contours of water level.

4-5-2- Shock-on-shock interaction

This test, including an exact solution, was proposed by Causon et. al. (1999). A schematic representing the problem and the unstructured grid used in the simulation, are presented in figure 4-5-2-a. Based on the interaction of the shock-waves, four regions (1), (2), (3) and (4) are formed, where β_A is the angle between the shock wave and the original flow direction and β_D represents the angle between the shock wave and the side wall.

The numerical simulation has been performed by using an averaged value of 0.65 for the CFL number. The water depth is 1 m in the undisturbed region, the upstream Froude number is 2.7 and the wall deflection angle is 12^o. The simulation was pursued until a steady state solution was obtained using the high-resolution scheme. A two dimensional view of the water level is shown in figure 4-5-2-b. A comparison between the computed and the exact solution is presented in Table 3. As it can be seen, the numerical model can accurately simulate the water surface and the shock-on-shock interaction.

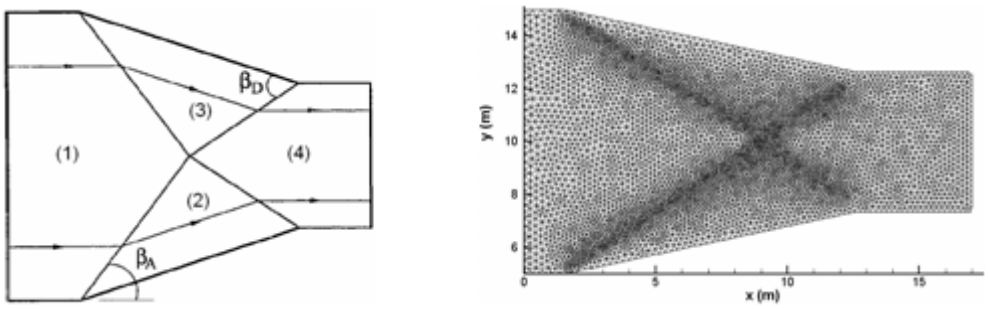

Figure 4-5-2-a- A schema of the shock-on-shock interaction problem (Left) and the triangular grid used in the simulation of the shock-on-shock interaction problem (right).

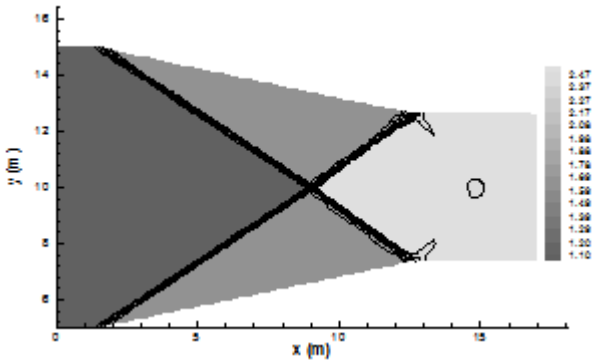

Fig 4-5-2-b- Shock on Shock interaction: Contours of calculated water surface elevation.

Table 3- comparison between calculated results and exact solution.

State 2			State 4		
Variable	**Theory**	**Computed**	**Variable**	**Theory**	**Computed**
Fr	1.868	1.87	Fr	1.249	1.249
Depth (m)	1.676	1.674	Depth (m)	2.562	2.560
Velocity(m/s)	7.571	7.58	Velocity(m/s)	6.258	6.26
β_A (°)	33.688	33.69	β_D (°)	48.102	48.764

4-6- Circular dam break

To test again the performance of the proposed method, we now consider the breaking of a cylindrical dam and the time evolution of the subsequent waves (Alcrudo and Navarro, 1993). Two regions of still water are separated by a cylindrical wall of radius r = 11 *m*, such that the water depth is 10 *m* on the inner side and is 1 *m* outside the dam. The computed water surface profile using 6328 cells at time t = 0.69 *s* is shown in figure 4-6 (left) and it is compared with the HLL scheme results (figure 4-6, right). As it can be seen, the method performs well and smooth results are obtained. Further, the radial symmetry of the computed solution numerical method is respected.

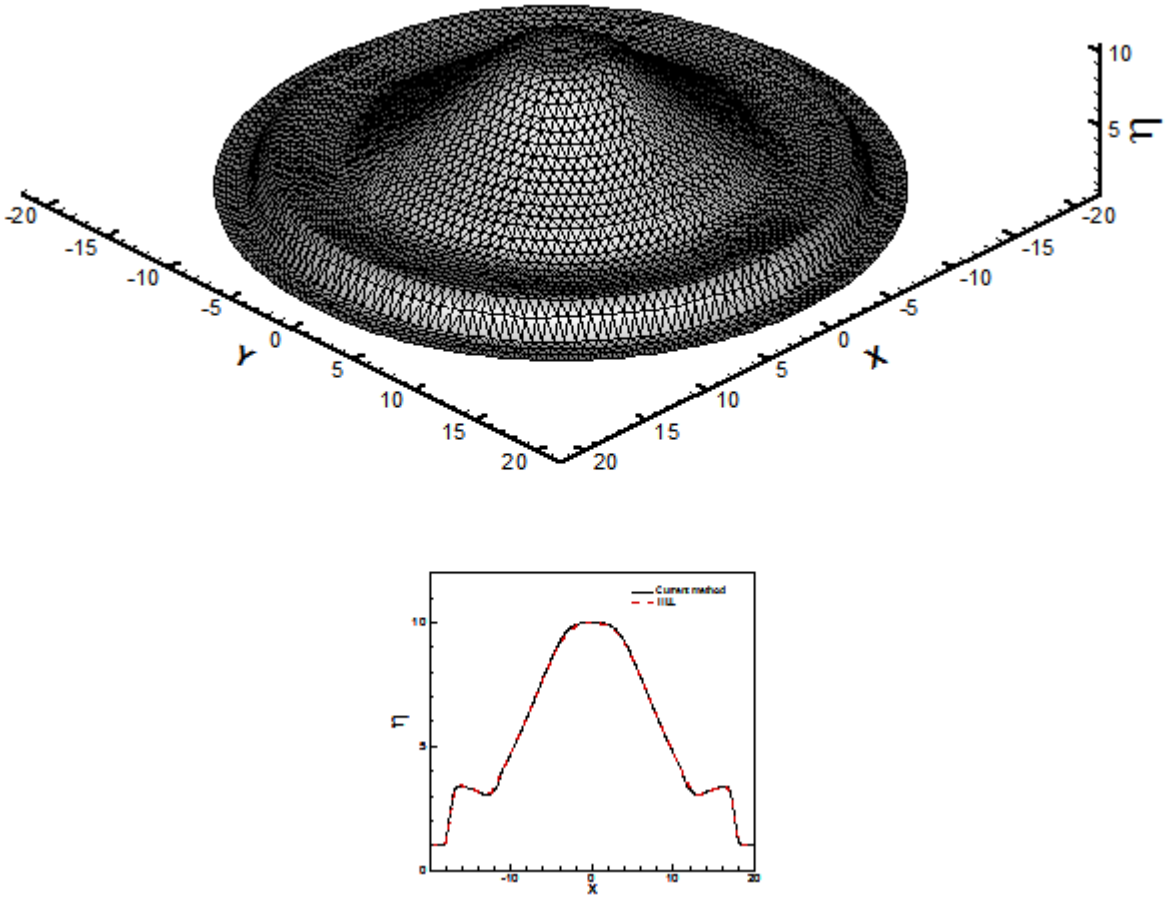

Fig. 4-6. Computed water surface level at t = 0.69s for the circular dam break problem; a 3D view (top) and a comparison with the HLL scheme (bottom).

4-7- Recirculating flow after a sudden expansion

The 2-D laminar flow past a sudden expansion in a side wall (horizontally analogous to the backward facing step) provides a well documented benchmark test for evaluating the level of numerical diffusion in conservation law schemes. Many researchers (Denham and Patrick, 1974), have provided experimental and numerical data on the flow pattern immediately after a backward facing step, where a steady vortex appears with its length depending on the Reynolds number, defined as $\mathrm{Re} = bU_1/\nu$, where U_1 is the mean inlet flow velocity, b is the dimension of the wall expansion and ν is the fluid kinematic viscosity coefficient. In Denham and Patrick (1974), $U_1 = q_x / D$ where q_x is the inlet x-direction inlet momentum flux and D is the flow depth. The channel width is $2b$ before, and $3b$ after the expansion, where $b = 1m$. At the expansion, the mean flow velocity is U_1=0.5 m/s, the flow depth at the downstream is 1 m and the eddy viscosity is 0.00685 m^2/s, also considered by Denham and Patrick, corresponding to $\mathrm{Re} = bU_1/\nu = 73$. No bottom friction is applied. All numerical experiments are performed using the first order scheme, and a structured 300×100 grid is employed. Figure 4-7-1 presents the predicted velocity vectors in the x direction and the experimental data. The predicted steady-state velocity profiles at different positions along the channel past the expansion are in very close agreement with Denham and Patrick's experimental results, as shown in figure 4-7-1. The streamtraces predicted by using the proposed scheme are shown in figure 4-7-2. The length of the recirculation region is approximately 3.89b which is near the value 3.95b given by Denham and Patrick (1974) from experimental data. This recirculation zone is correctly modeled, thus demonstrating the ability of the proposed scheme to simulate circulating flows with a low level of numerical diffusion.

The results of the Nujic method are also shown in figure 4-7-2. As it can be seen the length of the recirculating zone is roughly half of the expected value, which shows a high level of numerical diffusion for the circulating flows. The HLL flux (used by Mingham et. al., 1998), and the Kurganov's central upwind scheme (2002) have even more numerical diffusion, and the recirculating zone is roughly 1.2b as shown in figure 4-7-2

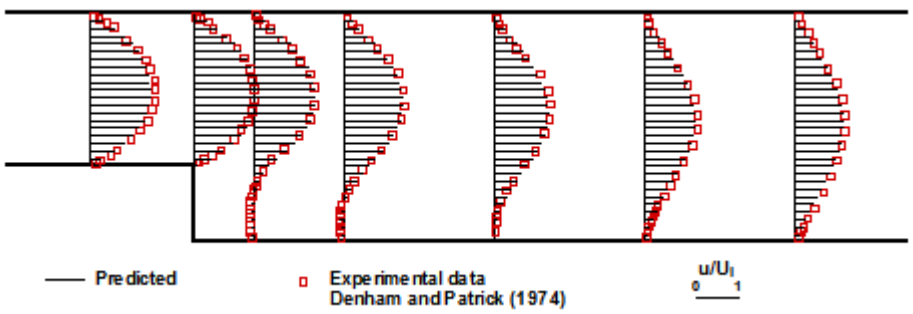

Fig. 4-7-1. Predicted velocities with the proposed method in the x-direction compared with the experimental data.

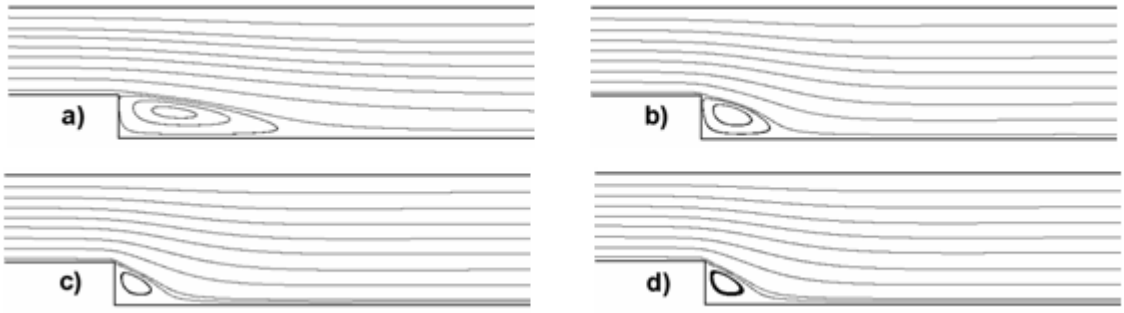

Fig. 4-7-2. Streamtraces calculated with: a) the proposed method, b) the Nujic scheme, c)the central upwind scheme, and d) the HLL flux (all first order)

4-8- Partially closed channel

A partially closed channel of length 3 km and width 1 km is considered under the steady state flow conditions. Although this is an academic case, a number of different models have been applied to it as reported in the literature (Kolahdoozan, 1999, van Rijn, 1987 and Wang, 1989). A headland of length 0.4 km is located in the middle of the channel, as shown in figure 4-8-1. The bed roughness height is assumed to be 0.25 m and the horizontal mixing coefficient is 0.5 m^2/s. The upstream hydrodynamic boundary condition is assumed to be a discharge of 4000 m^3/s and the downstream boundary is h = 6 m (Kolahdoozan 1999). Figure 4-8-2 shows the mesh and the streamlines predicted by the

proposed model.

The results of the depth-averaged velocities along the streamline B obtained with the present model are compared in figure 4-8-3 with three other models. Those are GEO-DIVAST model (Kolahdoozan 1999), which is a modified version of DIVAST (Falconer 1980) and uses a finite volume method; the finite element model SUTRENCH, developed by Delft Hydraulics (van Rijn 1987); and the ESMOR two dimensional depth averaged model, also developed by Delft Hydraulics (Wang, 1989). Based on a comparison of the results in figure 4-8-3, the results of the proposed model are in a close agreement with other models. However, the proposed model has a wider applicability and is able to simulate super critical and trans-critical flows on unstructured grids. Further, it should be mentioned that in this test case, the bed is movable and the current model successfully simulated the morphological processes around a groyne (Mohammadian et. al., 2003).

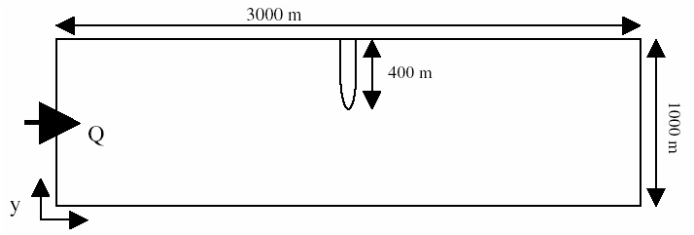

Figure 4-8-1. Schematic view of the channel

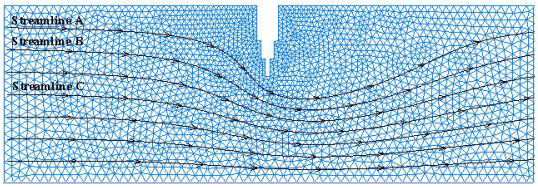

Figure 4-8-2. Streamline predicted by the proposed model.

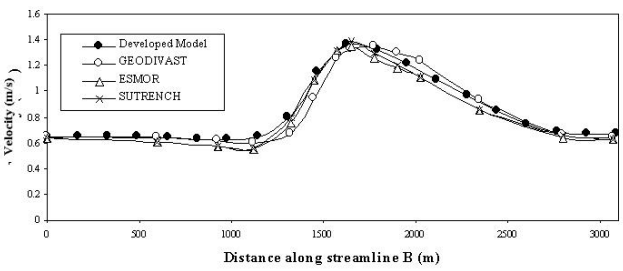

Figure 4-8-3. Depth averaged velocities along the streamline B obtained by using different models.

4-9- Small perturbation of a steady-state solution

4-9-1- One dimensional, small perturbation of a steady-state solution

This test case is concerned with wave propagation and it has been proposed by Leveque (1998). The channel has a length of 1.0 m and the topography is defined as

$$z(x,y)=\begin{cases}-0.8\exp\left(-5(x-0.9)^2-50(y-0.5)^2\right), & for\ |x-0.5|\le 0.1,\\ 0.0, & otherwise.\end{cases} \tag{4.10}$$

The flow velocity is zero and the surface profile is

$$\eta(x,y)=\begin{cases}1.0+\varepsilon & for\ 0.1<x<0.2,\\ 1.0, & otherwise.\end{cases} \tag{4.11}$$

Two cases have been considered: $\varepsilon=0.2$ m and .01 m. The solutions obtained on a grid of 100 nodes and $g=1\,\mathrm{m}^2/\mathrm{s}$ are shown in figure 4-9-1. When $\varepsilon=0.01$ the experiment is more difficult to conduct. A CFL number of 0.85 and 0.99 is used for the cases of $\varepsilon=0.2$ m and .01 m, respectively. Contrary to most existing schemes, which have used much more grid points than here (600 in Hubbard and Navarro, 2000), the present method can capture the quasi steady solutions quite well, with a very low level of numerical diffusion and without numerical oscillations.

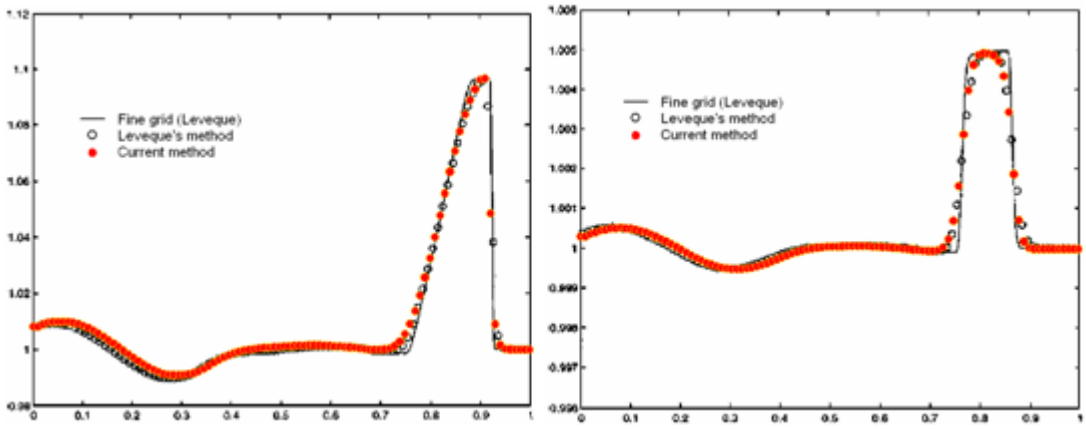

Fig. 4-9-1. Computed water surface level at t=0.7 with $\varepsilon = 0.2$ (left) and $\varepsilon = 0.01$ (right).

4-9-2- Two dimensional, small perturbation of a steady-state solution

In the test case presented by Leveque (1998), the SW equations are solved in the domain $[0,2]\times[0,1]$, and the bottom surface is an elliptical shaped hump

$$z(x,y) = -0.8\exp\left(-5(x-0.9)^2 - 50(y-0.5)^2\right). \qquad (4.12)$$

The surface is initially flat with $h(x,y) = 1$ except for $0.05 < x < 0.15$, where $h(x,y) = 1.01$m. Figure 4-9-2 displays the right-going disturbance as it propagates past the hump, using coarse (11653 control volumes) and fine (29877 control volumes) unstructured grids. The current method is clearly able to simulate this problem without facing spurious oscillations due to variable bed topography.

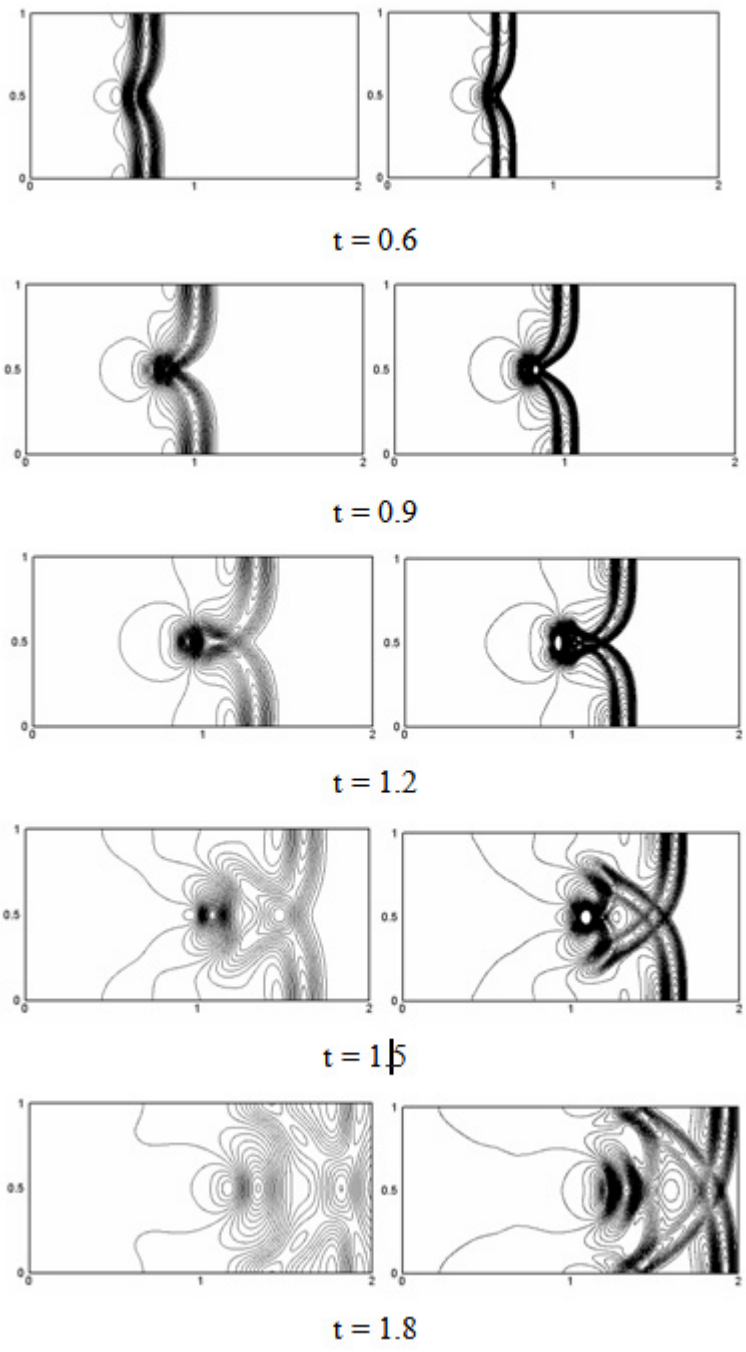

Fig. 4-9-2. Computed water surface level with a coarse grid (left) and a fine grid (right) for t=0.6, 0.9, 1.2, 1.5 and 1.8s.

7- Conclusion

A mass conservative approach has been proposed to solve the shallow-water equations. It is able to accurately simulate mild flows such as recirculating and tidal flows with low numerical diffusion.

Numerical results indicated that the proposed method can also accurately compute sub, super and trans-critical flows with discontinuity over complicated topographies.

In the proposed scheme, it is not necessary to perform an extra upwinding or Riemann solution for the source terms, which makes our method computationally efficient. Many test cases show that the proposed method can be efficiently used for a wide range of SW problems. Contrary to many available schemes, our approach can be easily implemented on unstructured grids and has the advantage of being flexible for irregular boundaries and local mesh refinement.

References

Abbot M. B. (1979), 'Computational Hydraulics: Elements of the Theory of Free Surface Flows', Longman, London.

Bermudez A. and Vazquez M. E. (1994), 'Upwind Methods for Hyperbolic Conservation Laws with Source Terms', Computers and Fluids, 23, 1049

Alcrudo F. and Benkhaldoun F. (2001), 'Exact Solutions to the Riemann Problem of the Shallow-water Equations with a Bottom Step', Computers and fluids 30, pp. 643-671

Alcrudo F. and Garcia-Navarro P. (1993), 'A High Resolution Godunov-Type Scheme in Finite Volumes for the 2D Shallow-water Equations', Int. J. Numer. Methods in Fluids, 16, pp. 489

Batina J. (1990), 'Implicit Flux-Split Euler Schemes for Unsteady Aerodynamics Analysis Involving Unstructured Dynamic Meshes', AIAA, Vol. 29, No.11, pp.1836

Bradford S. F. and Sandres B. F. (2002), 'Finite-Volume Model for Shallow-Water Flooding of Arbitrary Topography', J. Hyd. Eng. ASCE, 128, 289

Causon D. M., Mingham C. G. and Ingram D. M. (1999), 'Advances in Calculation Methods for Supercritical Flow in Spillway Channels', J. Hyd. Eng. ASCE, 125, 1039

Denham, M. K. and Patrick, M. A. (1974), 'Laminar flow over a downstream-facing step in a two-dimensional flow channel', Trans. Inst. Chemical Engineers, 52, 361-367

Falconer R. A. (1980), 'Numerical Modeling of Tidal Circulation in Harbors', J. Hyd. Eng. ASCE, 106(1), pp. 31-48.

Fenemma R. and Chaudhry M. (1987), 'Simulation of One-Dimensional Dam-Break Flows', J. Hyd. Res., vol. 25, No.1, pp. 41

P. Glaister (1988), 'Approximate Riemann Solutions of the Shallow-Water Equations'. J. Hyd. Res., 26, No. 3, 293-306

Goutal N. and Maurel F., eds. (1997), 'Proceedings of the 2nd Workshop on Dam-Break Wave Simulation', HE-43/97/016/B, France

Harten A. and Hyman P. (1983), 'Self adjusting grid methods for one-dimensional hyperbolic conservation laws', J. of Comput. Phys., 50, 235-269

Hubbard M. E. and Garcia-Navarro P. (2000), 'Flux Difference Splitting and the Balancing of Source Terms and Flux Gradients', J. Comput. Phys. 165, 89-125

Hubbard M. E. and Garcia-Navarro P. (2001), 'Balancing Source Terms and Flux Gradients in Finite Volume Schemes', Godunov Methods: Theory and Applications, edited by E. F. Toro, Kluwer Academic Publishers, New York, pp. 447-483

Jha A. K., Akiyama J., Ura M. (1995), 'First and Second-Order Flux Difference Splitting Schemes for Dam-Break Problem', J. Hyd. Eng. ASCE 121, 12, pp. 877

Kolahdoozan M. (1999), 'Numerical Modeling of Geo-Morphological processes Estuarine Waters', University of Bradford, UK, PhD Thesis.

Kurganov A., Levy D. (2002), 'Central-Upwind Schemes for the Saint-Venant System' Mathematical Modeling and Numerical Analysis, 36 , 397-425

LeVeque R. J. (2002), 'Finite Volume Methods for Hyperbolic Problems', Cambridge university press, UK.

LeVeque R. J. (1998), 'Balancing Source Terms and Flux gradients in High-Resolution Godunov Methods', J. Comput. Phys., 146, pp. 346

Mingham C.G. and Causon D. M. (1998), 'High Resolution Finite-Volume Method for Shallow-water Equation Flows', J. Hyd. Eng. ASCE 124, 605

Mohammadian A., Azad F. L., Tajrishi M. (2003), 'Two Dimensional Numerical Simulation of Flow and Geo-Morphological Processes Near Headlands by Using Unstructured Grid', XXX IAHR Congress, Greece

Garcia Navarro P. and Alcrudo F. (1992) , '1D open channel flow simulation using TVD McCormac scheme', J. Hyd. Eng. ASCE 118, 1359-1373

Nujic M. (1995), 'Efficient Implementation of Non-Oscillatory Schemes of Free Surface Flows', J. Hyd. Res., Vol. 33, No. 1, pp. 101

Russo G. (2002), 'Central Schemes for Balance Laws', Proceedings of HYP2000, Magdeburg

Shu C. W. and Osher S. (1988), 'Efficient Implementation of Non-Oscillatory Shock-Capturing Schemes', J. Comp. Phys., Vol. 77, pp. 439-471

Toro E. F. (2000), 'Shock Capturing Methods for Free Surface Shallow Flows', John Wiley and sons

van Leer B. (1979) 'Toward the Ultimate Conservative Difference Scheme V. A Second Order Sequel to Godunov's Method', J. Comp. Phys. 32, 101

van Leer B., Lee W. T. and Powell K. G. (1989), 'Sonic Point Capturing', 9th CFD Conference, American Institute of Aeronautics and Astronautics, Buffalo, N.Y.

van Rijn L. C. (1993), 'Principles of Sediment Transport in Rivers, Estuaries and Coastal Seas', Aqua Publications, The Netherlands

Vazquez-Cendon M. E. (1999), 'Improved Treatment of Source Terms in Upwind Schemes for the Shallow-water Equations in Channels with Irregular Geometry', J. Comp. Phys., 43(2), pp. 357-372

Vukovic S. and Sopta L. (2002), 'ENO and WENO Schemes with the Exact Conservation Property for One-Dimensional Shallow-Water Equations', J. Comp. Phys. 179, 593-621

Wang J. S. (2000), 'Finite Difference TVD Scheme for Computation of Dam-Break Flows', J. Hyd. Eng. ASCE, No.4, pp. 253

Wang Z. B., (1989), 'Mathematical Modeling of Morphological Processes in Estuaries', Delft Uni. of Tech., The Netherlands

Xu K. (2002), 'A Well-balanced Gas-Kinetic Scheme for the Shallow-water Equations with Source Terms'.

Zhao D., Shen H. W., Tabios G. Q. III, Lai J. S. and Tan W. Y. (1994), 'Finite-Volume two-Dimensional Unsteady-Flow Model for River Basins'. J. Hyd. Eng. ASCE 120 (7), 863-883

Zhao D., Shen H., Tabios G., Lai J. and Tan W. (1996), 'Approximate Riemann Solver in FVM for 2d Hydraulic Shock Wave Modeling', J. Hyd. Eng. ASCE, No.12, pp. 692

Zhou J. G., Causon D. M., Mingham C. G. and Ingram D. M. (2001), 'The Surface Gradient Method for the Treatment of Source Terms in the Shallow-water Equations', J. Comp. Phys. 168, 1-25

CHAPTER 5

Simulation of shallow flows over variable topographies using unstructured grids

In chapter 4, a well balanced scheme was developed for the numerical simulation of 2-D shallow water problems using a characteristics-based finite volume method. However, it is not fully conservative and may give rise to problems in presence of strong shocks. In this chapter, two new fully conservative schemes are introduced to overcome this problem while preserving the balance between flux and source terms. Further, they directly deal with the source terms without changing the flux terms. This makes it possible to combine them with most existing Riemann solvers.

Simulation d'écoulements peu profonds en présence de topographies variables et des maillages non structurés.

Résumé

La simulation d'écoulements peu profonds en présence de topographies variables est un cas difficile pour la plupart des schémas disponibles. Le problème vient du fait que les termes source et les gradients de flux ne sont pas équilibrés dans les calculs numériques. Les améliorations apportées à cette difficulté fonctionnent généralement bien sur des maillages structurées, mais ils sont habituellement trop coûteux et non directement applicables aux maillages non structurés. Dans cet article nous proposons deux méthodes efficaces pour traiter les termes source sans utiliser la méthode dite d'upwinding et pour satisfaire la condition de compatibilité sur des maillages non structurés. Dans la première méthode, le calcul des termes source, à cause de pente au fond, est déterminé en utilisant une approximation compatible de profondeur de l'eau aux interfaces des cellules. Dans la seconde, différentes composantes du terme de pente au fond sont considérées séparément et une discrétisation compatible des composantes est proposée. Les améliorations introduites ici sont applicables pour la plupart des schémas, incluant la méthode de Roe, sans modifier la performance du schéma original pour des topographies régulières.

SIMULATION OF SHALLOW FLOWS OVER VARIABLE TOPOGRAPHIES USING UNSTRUCTURED GRIDS

A. MOHAMMADIAN, D. Y. LE ROUX

Abstract. *Simulation of shallow flows over variable topographies is a challenging case for most available shock-capturing schemes. This problem arises because the source terms and flux gradients are not balanced in the numerical computations. Treatments for this problem generally work well on structured grids, but they are usually too expensive, and most of them are not directly applicable to unstructured grids. In this paper we propose two efficient methods to treat the source terms without upwinding and to satisfy the compatibility condition on unstructured grids. In the first method, the calculation of the bed slope source term is performed by employing a compatible approximation of water depth at the cell interfaces. In the second one, different components of the bed slope term are considered separately and a compatible discretization of the components is proposed. The present treatments are applicable for most schemes including the Roe method without changing the performance of the original scheme for smooth topographies.*

Key Words: Shallow-water, variable topography, unstructured grid, finite volume method

1- Introduction

The shallow-water (SW) equations govern many practical applications like river and tidal flows in estuary and coastal water regions where variable topographies are usually present. The simulation of these flows is of great interest for hydraulic engineers, particularly on unstructured grids. Unstructured grids are attractive because of their flexibility for representing irregular boundaries and for local mesh refinement. On the other hand, for many fluvial flows, the flow regime changes from subcritical to supercritical and the employed numerical method should be able to solve sub, super and trans-critical flows.

The discretization of the shallow-water equations has received considerable attention in the past two decades and many upwind schemes have successfully solved channel flows (Glaister, 1988, Fenemma and Chaudry, 1987, Zhao et. al., 1994 and Mingham and Causon, 1998). However, their use in the presence of irregular topographies is usually problematic, due to *the imbalance between the source terms and the flux gradients* (Bermudez and Vazquez-Cendon, 1994). In fact, most shock capturing finite volume schemes for the shallow water equations, are obtained by using approximate Riemann solvers which have been originally designed for hyperbolic systems without considering the source terms (such as bed topography in the case of shallow water equations). Therefore, in the presence of source terms, those schemes may lead to oscillations. Numerically, this problem is due to an imbalance between discretized source and flux terms.

Some modifications have been brought to the above mentioned methods in the case of variable topographies and structured grids. For example, the van Leer's Q-scheme was extended by Bermudez and Vazquez-Cendon (1994) for the SW equations, and an *upwind discretization of the source terms* for variable topographies has been formulated. The C property, which states that the scheme should preserve the stagnant conditions was also introduced. In the stagnant conditions, water is initially at rest inside of some closed area with variable bottom topography. Hence, without influence from outside, the water should stay at rest. This work has been improved in the case of a general 1-D channel with breath variation by Vasquez-Cendon (1999). The Vasquez-Cendon approach was then extended to flux difference splitting schemes by Hubbard and Navarro (2001). However, upwinding the source terms is computationally expensive for practical applications because those terms have to be projected on a basis of eigenvectors. LeVeque (1998), introduced *a Riemann problem inside a cell* for balancing the source terms and the flux gradients, and the resulting method was found to preserve both *stagnant* and *quasi steady state* conditions. However, the LeVeque's scheme is not directly transportable to unstructured grids. On the other side, Kurganov and Levy (2002) extended the *Central-Upwind* (CU) scheme to the shallow-water equations and by using the water surface elevation instead of the depth, they proposed an adaptive algorithm for variable topographies. They also proved that their scheme preserves the steady state condition with a positive depth, without resorting to any artificial drying and wetting strategies. Unfortunately, their scheme poorly performs in the

case of circulating flows, as shown in Mohammadian et. al. (2005). In a different approach, Alcrudo and Benkhaldon (2001) defined the bed level such that a sudden change in the topography occurs at the interface of two cells. They also developed a Riemann solver at the interface with a sudden change in the bed elevation. However, their approach leads to several cases of shock and rarefaction wave patterns and it is numerically too expensive. The ENO and Weighted ENO (WENO) schemes were extended by Vukovic and Sopta (2002) to the shallow-water equations including the source terms, but they are restricted to 1-D channels. Jin (2002) developed the *interface method*, which preserves the steady state condition up to second order accuracy on structured grids, but his approach is not directly usable on unstructured grids. A second order gas kinetic scheme for shallow-water flows over variable topographies was also proposed by Xu (2002). However, the gas kinetic schemes are basically different from characteristics based schemes and they should be tested for challenging test cases such as recirculating flows. Rogers et. al. (2003), proposed a numerical scheme where the balance is achieved by the incorporation of extra physical information, but, only structured grids are employed. Nujic (1995) used the water level variable instead of the depth and he extracted the gravitational terms from the flux functions in the Shu and Osher (SO) scheme (1988) to solve for variable topographies. Unfortunately, the SO scheme (1988) generates a high level of numerical diffusion in the case of recirculating flows, as shown in Mohammadian et. al. (2005).

Zhou et. al. (2001) introduced the *surface gradient method* where the depth is interpolated at the cell interface considering the bed variations. They showed that by combining their approach with the HLL flux function (Harten et. al., 1983) the C property is satisfied, and the resulting scheme performs well for variable topographies without any extra efforts for balancing the source terms and the flux gradients. However, the C property does not hold on unstructured grids and moreover, the HLL flux induces a high level of numerical viscosity in recirculating flows, as shown in Mohammadian et. al. (2005).

Mohammadian et. al. (2005) showed that the Roe method produces much less numerical diffusion than the SO, HLL and CU schemes in the case of circulating flows and they developed a numerical scheme using the Roe method which satisfies the C property. However, although their scheme is mass conservative, it is not fully conservative since the gravity terms are not discretized in a conservative manner.

In this paper we present two efficient numerical methods for flows over variable topographies on unstructured grids. The proposed two methods are shown to satisfy the C property when combined with the Roe scheme and the surface gradient method (Zhou et. al., 2001) for calculating the water depth at the interface. Several numerical tests are presented to show the performance of the two schemes over variable topographies.

The main feature of the methods presented here is that, since they are working directly on the discretization of the source terms, they are not restricted to the Roe method and they can be used with a large range of existing shock capturing schemes such as the Roe, the HLL, the HLLC, the central upwind methods etc…

This paper is organized as follows. The model equations are introduced in section 2. The numerical scheme, the treatment of the source term and the proof of the C property are presented in section 3. In section 4, some numerical test cases show the performance of the proposed schemes. Some concluding remarks complete the study.

2- Governing equations

The 2-D SW equations in a conservative form are written as

$$\frac{\partial \vec{U}}{\partial t} + \nabla \cdot \vec{F} = \vec{S} + \nabla \cdot \vec{F}^{d}, \tag{2.1}$$

with $\vec{U}^{t} = (h, uh, vh)$, $\vec{F} = (\vec{E}, \vec{G})$ and

$$\vec{E} = \begin{pmatrix} uh \\ u^2 h + 0.5gh^2 \\ uvh \end{pmatrix}, \quad \vec{G} = \begin{pmatrix} vh \\ uvh \\ v^2 h + 0.5gh^2 \end{pmatrix}, \tag{2.2}$$

where h is the water depth, u and v are the velocity components (Figure 2-1) and g is the gravitational acceleration.

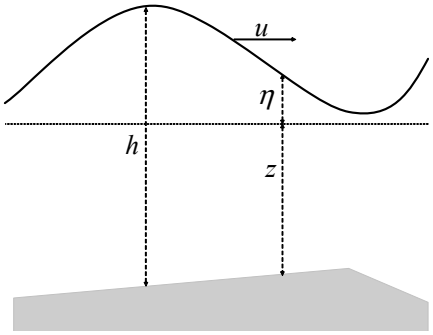

Fig. 2-1. Schematic diagram of an unsteady flow over an irregular bottom and the corresponding notation.

The superscript ^{d} refers to the diffusion and the diffusive flux has the following form

$$\vec{F}^d = (\vec{E}^d, \vec{G}^d), \tag{2.3}$$

where

$$\vec{E}^d = \begin{pmatrix} 0 \\ (\nu + \nu_t) h \partial u / \partial x \\ (\nu + \nu_t) h \partial v / \partial x \end{pmatrix} \quad , \quad \vec{G}^d = \begin{pmatrix} 0 \\ (\nu + \nu_t) h \partial u / \partial y \\ (\nu + \nu_t) h \partial v / \partial y \end{pmatrix} \tag{2.4}$$

and ν and ν_t are water and eddy viscosity coefficients respectively.

The source term $\vec{S}$ is written as

$$\vec{S} = \begin{pmatrix} 0 \\ c_f u \sqrt{u^2 + v^2} + gh\partial z \ / \partial x \\ c_f v \sqrt{u^2 + v^2} + gh\partial z \ / \partial y \end{pmatrix}, \tag{2.5}$$

where z is the distance between the bed surface and the reference level (Figure 2-1; z is zero in the reference level and increases downward) and c_f is the friction coefficient.

The SW equations may also be written in a non-conservative form

$$\frac{\partial \vec{U}}{\partial t} + A \frac{\partial \vec{U}}{\partial x} + B \frac{\partial \vec{U}}{\partial y} = \vec{S} + \nabla \cdot \vec{F}^d, \tag{2.6}$$

where A and B are the Jacobian matrices

$$A = \frac{\partial \vec{E}}{\partial \vec{U}} = \begin{pmatrix} 0 & 1 & 0 \\ -u^2 + c^2 & 2u & 0 \\ -uv & v & u \end{pmatrix} \quad , \quad B = \frac{\partial \vec{G}}{\partial \vec{U}} = \begin{pmatrix} 0 & 0 & 1 \\ -uv & v & u \\ -v^2 + c^2 & 0 & 2v \end{pmatrix}, \tag{2.7}$$

and $c = \sqrt{gh}$ is the wave velocity.

The eigenvalues of A and B are

$a^1 = u + c, a^2 = u, a^3 = u - c$ and $b^1 = v + c, \quad b^2 = v, \quad b^3 = v - c$, respectively.

3- Numerical scheme

3-1-Finite volume methods on unstructured grids

A finite volume method using triangular grids is used in this paper. The variables are located herein at the geometric centers of the cells, and each triangle represents a control volume. Let $\mathcal{A}$ be the area of a triangle with boundary *s*. The SW equations are integrated over every control volume

$$\int_t \int_{\mathcal{A}} \left(\frac{\partial \vec{U}}{\partial t} + \nabla \cdot \vec{F} - \vec{S} - \nabla \cdot \vec{F}^d \right) d\mathcal{A} dt = 0. \tag{3.1}$$

A high order time stepping scheme may be employed to integrate (3.1) in time. However, for the sake of simplicity and because the discretization of the source term is the main issue, we use here the first order forward (explicit) Euler time-stepping scheme. This leads to

$$\int_t \int_{\mathcal{A}} \left(\frac{\partial \vec{U}}{\partial t} + \nabla \cdot \vec{F} - \vec{S} - \nabla \cdot \vec{F}^d \right) d\mathcal{A} dt = 0. \tag{3.2}$$

where superscript ^{n} and $^{n+1}$ refer to the variables at time t_n and t_n+1, respectively. The application of Gauss theorem to the diffusive and convective flux integrals gives

$$\int_{\mathcal{A}} \left(\nabla \cdot \vec{F} - \nabla \cdot \vec{F} \right) d\mathcal{A} = \oint_s \left(\vec{F} \cdot \vec{n} - \vec{F}^d \cdot \vec{n} \right) ds \,, \tag{3.3}$$

and the boundary integral is approximated by a summation over the triangle edges

$$\oint_s \left(\vec{F} \cdot \vec{n} - \vec{F}^d \cdot \vec{n} \right) ds - = \sum_{k=1}^{3} \left(\vec{F}_k \cdot \vec{n}_k - \vec{F}_k^d \cdot \vec{n}_k \right) ds_k \,. \tag{3.4}$$

The diffusive fluxes are approximated by a centered scheme

$$\vec{F}^d = 0.5 \left(\vec{F}_R^d + \vec{F}_L^d \right) \tag{3.5}$$

A centered scheme for the diffusion term is employed because this scheme is (i) second order accurate, (ii) economically justified and (iii) easily incorporated in the whole

numerical procedure, which is in a flux-based format. Mohammadian et. al (2005), have shown that the scheme (3.5) for the diffusive fluxes, leads to correct simulation of circulating zones.

The convective fluxes $\vec{F}$ are calculated here by a Godunov type scheme

$$\vec{F} = 0.5\left(\vec{F}_R + \vec{F}_L - \Delta\vec{F}^*\right), \tag{3.6}$$

where $\vec{F}_L = \vec{F}\left(\vec{U}_L\right)$ and $\vec{F}_R = \vec{F}\left(\vec{U}_R\right)$ are the left and right flux vectors. The subscripts $\cdot_R$ and $\cdot_L$ represent the evaluation of the right and left sides of the interface, respectively, and $\Delta\vec{F}^*$ is the flux difference based on the Roe linearization

$$\Delta\vec{F}^* = \sum_{k=1}^{3} \tilde{\alpha}^k \left|\tilde{a}^k\right| \tilde{\vec{e}}^k \ , \tag{3.7}$$

where $\tilde{a}^k$ and $\tilde{\vec{e}}^k$, k=1,2,3, are the eigenvalues and the eigenvectors of $\tilde{A}$, respectively. The matrix $\tilde{A}$ represents the Roe average Jacobian matrix, and it satisfies $\Delta\vec{F} = \tilde{A}\Delta\vec{U}$ with

$$\tilde{A} = \frac{\partial\left(\vec{F}.\vec{n}\right)}{\partial\vec{u}} = \begin{pmatrix} 0 & n_x & n_y \\ \left(\tilde{c}^2 - \tilde{u}^2\right)n_x - \tilde{u}\tilde{v}n_y & 2\tilde{u}n_x + \tilde{v}n_y & \tilde{u}n_y \\ -\tilde{u}\tilde{v}n_x + \left(\tilde{c}^2 - \tilde{v}^2\right)n_y & \tilde{v}n_x & \tilde{u}n_x + 2\tilde{v}n_y \end{pmatrix}, \tag{3.8}$$

where

$$\tilde{u} = \frac{u_R\sqrt{h_R} + u_L\sqrt{h_L}}{\sqrt{h_R} + \sqrt{h_L}} \quad , \quad \tilde{v} = \frac{v_R\sqrt{h_R} + v_L\sqrt{h_L}}{\sqrt{h_R} + \sqrt{h_L}} \quad , \quad \tilde{c} = \sqrt{g(h_R + h_L)/2}\,. \tag{3.9}$$

In the case of a dry bed problem, $\tilde{c}$ is calculated in the same manner as in (3.9), and the average velocities are

$$\tilde{u} = \frac{u_L + u_R}{2},\ \tilde{v} = \frac{u_L + u_R}{2}$$

The eigenvalues of $\tilde{A}$ are simply

$$\tilde{a}^1 = \tilde{u}n_x + \tilde{v}n_y + \tilde{c} \quad , \quad \tilde{a}^2 = \tilde{u}n_x + \tilde{v}n_y \quad , \quad \tilde{a}^3 = \tilde{u}n_x + \tilde{v}n_y - \tilde{c}\,, \tag{3.10}$$

with the corresponding eigenvectors

$$\tilde{\vec{e}}^1 = \begin{pmatrix} 1 \\ \tilde{u} + \tilde{c}n_x \\ \tilde{v} + \tilde{c}n_y \end{pmatrix} \ , \ \tilde{\vec{e}}^2 = \begin{pmatrix} 0 \\ -\tilde{c}n_y \\ \tilde{c}n_x \end{pmatrix} \ , \ \tilde{\vec{e}}^3 = \begin{pmatrix} 1 \\ \tilde{u} - \tilde{c}n_x \\ \tilde{v} - \tilde{c}n_y \end{pmatrix}, \tag{3.11}$$

respectively. The coefficients $\tilde{\alpha}^k$, k=1,2,3, are computed as

$$\tilde{\alpha}^1 = \frac{\Delta h}{2} + \frac{1}{2\tilde{c}}\left[\Delta(hu)n_x + \Delta(hv)n_y - (\tilde{u}n_x + \tilde{v}n_y)\Delta h\right], \tag{3.12}$$

$$\tilde{\alpha}^2 = \frac{1}{\tilde{c}}\left(\left[\Delta(hv) - \tilde{v}\Delta h \right] n_x - \left[\Delta(hu) - \tilde{u}\Delta h \right] n_y \right), \tag{3.13}$$

$$\tilde{\alpha}^3 = \frac{\Delta h}{2} - \frac{1}{2\tilde{c}}\left[\Delta(hu)n_x + \Delta(hv)n_y - (\tilde{u}n_x + \tilde{v}n_y)\Delta h\right]. \tag{3.14}$$

where $\Delta(.) = (.)_R - (.)_L$.

The Roe method violates the entropy condition in the case of sonic rarefactions (transcritical flows) and it predicts an unphysical jump at the sonic point inside the rarefaction waves, which is physically incorrect. This is because hyperbolic conservation laws admit, for example, rarefaction shocks and compressive shocks. In the shallow water equations, only the compressive shocks are physically acceptable. The entropy condition is a criterion for selecting the physically meaningful solution, in such cases.

Many methods have been proposed to improve the Roe method for these flows such as Harten and Hyman (1983). Here, we employ an approach proposed by van Leer et. al. 1989, and already used by Bradford and Sanders (2002). It consists of modifying the values $\left|\tilde{a}^k\right|$, k=1,2,3, in (3.7) when

$$-\frac{\Delta a^k}{2} < \tilde{a}^k < \frac{\Delta a^k}{2}, \tag{3.15}$$

and replacing them by $\left|\hat{a}^k\right|$ defined as

$$\left|\hat{a}^k\right| = \frac{(\tilde{a}^k)^2}{\Delta a^k} + \frac{\Delta a^k}{4}, \tag{3.16}$$

where

$$\Delta a^k = 4\left(a_R^k - a_L^k\right). \tag{3.17}$$

where, a_R^k and a_L^k are calculated as in (3.10), but using u_L, v_L, c_L and u_R, v_R, c_R, respectively. Such a simple modification enables the scheme to simulate the transcritical flows correctly.

3-2- Calculation of derivatives

The divergence theorem is employed to obtain the derivatives of a scalar variable *c* on a triangular cell *i* (shown in figure 3-1) as

$$\left(\frac{\partial c}{\partial x}\right)_i = \frac{1}{\mathcal{A}_i}\int_{\mathcal{A}} \frac{\partial c}{\partial x} d\mathcal{A} \approx \frac{c_1 \Delta y_1 + c_2 \Delta y_2 + c_3 \Delta y_3}{\mathcal{A}_i}, \tag{3.15}$$

$$\left(\frac{\partial c}{\partial y}\right)_i = \frac{1}{\mathcal{A}_i}\int_{\mathcal{A}} \frac{\partial c}{\partial y} d\mathcal{A} \approx -\frac{c_1 \Delta x_1 + c_2 \Delta x_2 + c_3 \Delta x_3}{\mathcal{A}_i}, \tag{3.16}$$

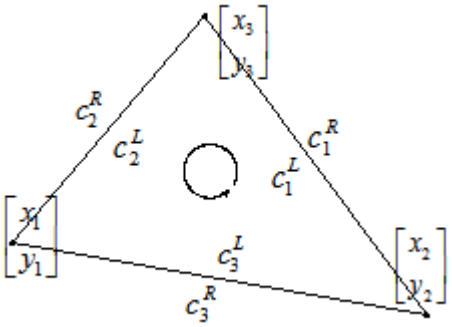

Fig. 3-1. The triangular cell i with the quantities c_j^R and c_j^L computed at the right (R) and left (L) sides respectively at a given face j, j=1,2,3. The coordinates (x_j, y_j), j=1,2,3, are located at the three vertices of cell i.

where

$$\Delta y_1 = y_3 - y_2 \quad , \quad \Delta x_1 = x_3 - x_2 \quad , \quad c_1 = (c_1^L + c_1^R)/2 , \tag{3.17}$$

$$\Delta y_2 = y_1 - y_3 \quad , \quad \Delta x_2 = x_1 - x_3 \quad , \quad c_2 = (c_2^L + c_2^R)/2 , \tag{3.18}$$

$$\Delta y_3 = y_2 - y_1 \quad , \quad \Delta x_3 = x_2 - x_1 \quad , \quad c_3 = (c_3^L + c_3^R)/2 . \tag{3.19}$$

The viscous terms are then calculated as

$$\left(\nu h \frac{\partial u}{\partial x}\right)_i \approx \nu h_i \frac{u_1 \Delta y_1 + u_2 \Delta y_2 + u_3 \Delta y_3}{\mathcal{A}_i} . \tag{3.20}$$

3-3- Interpolation Scheme

The values of the variables at the left and right sides of the interface are needed to compute the numerical fluxes in (3.5) and (3.6). Those values may be calculated using a piecewise constant or a piecewise linear interpolation scheme. Because this paper focuses on the discretization of the source terms, for the sake of simplicity, a piecewise constant approach has been employed in all the computations (except where mentioned otherwise). However, the methods presented in the next section to calculate the source terms, also preserve the C property when high accurate interpolation schemes are employed (e.g. Appendix I). This is because the C property proofs given in section 3-4 are independent of the method for calculating the variables at the left and right sides of the interface, provided $\Delta h = 0$ at the cell interfaces (which is the case when the surface gradient method employed) in stagnant conditions.

In the surface gradient method (Zhou et. al. 2001) the water surface elevation η is interpolated at the cell faces instead of the water depth. Once η_L is calculated, the water depth can be obtained as

$$h_L = \eta_L + z_e , \tag{3.24}$$

where z_e is the distance between the bed surface and the reference level at triangle edge midpoints and is known from topography data.. In the case of the stagnant conditions $\eta_L = \eta_R = \eta_0$, where η_0 is the constant water level and using (3.24) we obtain $h_L = h_R = \eta_0 + z_0$, which leads to $\Delta h = 0$ at the cell faces. This is crucial to guarantee the C property proofs given in the next section.

An interpolation procedure (Appendix I) is also needed to calculate the depth integrated discharges uh and vh at the cell interfaces, and we obtain

$$u_L = \frac{(uh)_L}{h_L} . \tag{3.25}$$

3-4- Computation of Bed Slope Term in Variable Topographies

As mentioned before, the bed slope term is considered separately in the source term (2.5). This usually leads to an incompatible discretization of the water surface gradient term

($0.5gh^2$) and the bed slope term and consequently produces an artificial source term in the numerical solution. For example, in complicated topographies with the stagnant initial condition, the water will not remain stagnant (Bermudez and Vazquez-Cendon, 1994).

In the following we introduce two methods to overcome this problem.

3-4-1-Method I- Compatible discretization of the bed slope term using a modified water depth

We first explain a simplified version of the method in one dimension. For a cell *i*, with edges *i*+1/2 and i-*1*/2, and length Δx ,the bed slope term is usually approximated as

$$\left(gh\frac{\partial z}{\partial x}\right)_i \approx gh_i\frac{\left(z_{i+1/2}-z_{i-1/2}\right)}{\Delta x_i}, \tag{3.26}$$

where h_i is the water depth in the cells. Recall z is the distance between the bed surface and the reference level (Figure 2-1). However, (3.26) does not satisfy the C property. In order to balance the source terms and the flux gradients, h_i is approximated by $\hat{h}_i$ as

$$\hat{h}_i = \frac{h^R_{i+1/2}+h^L_{i+1/2}+h^R_{i-1/2}+h^L_{i-1/2}}{4}. \tag{3.27}$$

In the case of the stagnant water conditions we have

$$h^R_{i+1/2} = h^L_{i+1/2} = h_{i+1/2}\ , \tag{3.28}$$

$$h^R_{i-1/2} = h^L_{i-1/2} = h_{i-1/2}, \tag{3.29}$$

$$\eta^R_{i-1/2} = \eta^L_{i-1/2} = \eta_0, \tag{3.30}$$

where η_0 is the constant water surface elevation over the domain and hence, $(\Delta h)_k = h^R_k - h^L_k = 0$, with *k*= *i*-1/2 and *i*+1/2 . Further, because all velocities are zero (due to the stagnant conditions), we obtain $\Delta\vec{F}^* = 0$ and the flux vector is then

$$\vec{F} = \begin{pmatrix} 0 \\ 0.5gh^2 \end{pmatrix}, \tag{3.31}$$

In 1-D, (3.2) reduces to (see 3.3 and 3.4)

$$\frac{\vec{U}_i^{n+1}-\vec{U}_i^{n}}{\Delta t}\Delta x + \left(\vec{F}_{i+1/2}-\vec{F}_{i-1/2}\right) - \vec{S}_i\Delta x = 0,$$

or

$$\vec{U}_i^{n+1}\Delta x = \vec{U}_i^{n}\Delta x - \Delta t\left(\vec{F}_{i+1/2} - \vec{F}_{i-1/2}\right) - \Delta t\vec{S}_i\Delta x = 0.$$

Therefore, the discretized momentum equation corresponding to cell *i* (for stagnant conditions) is (see 3.31)

$$\begin{aligned}(uh)_i^{n+1}\Delta x_i &= (uh)_i^{n}\Delta x_i - 0.5g\Delta t(h_{i+1/2}^2 - h_{i-1/2}^2) + g\Delta t\frac{h_{i+1/2}+h_{i-1/2}}{2}(z_{i+1/2}-z_{i-1/2})\\ &= (uh)_i^{n}\Delta x_i - 0.5g\Delta t(h_{i+1/2}+h_{i-1/2})(\eta_{i+1/2}-\eta_{i-1/2})\\ &= (uh)_i^{n}\Delta x_i .\end{aligned} \tag{3.32}$$

Hence, the C property holds.

This approach can be extended to arbitrary control volumes. Indeed, following (3.15), the bed slope term in a cell *i* (figure 3-3) is discretized as

$$\left(gh\frac{\partial z}{\partial x}\right)_i \approx gh_i\left(\frac{\partial z}{\partial x}\right)_i \approx gh_i\left(\frac{z_1\Delta y_1 + z_2\Delta y_2 + z_3\Delta y_3}{\mathcal{A}_i}\right), \tag{3.33}$$

where Δy_3 is replaced by $\Delta y_3 = -(\Delta y_1 + \Delta y_2)$ and this leads to

$$\left(gh\frac{\partial z}{\partial x}\right)_i = \frac{g}{\mathcal{A}_i}\left(\underbrace{h_i\Delta y_1(z_1 - z_3)}_{part\,1} + \underbrace{h_i\Delta y_2(z_2 - z_3)}_{part\,2}\right). \tag{3.34}$$

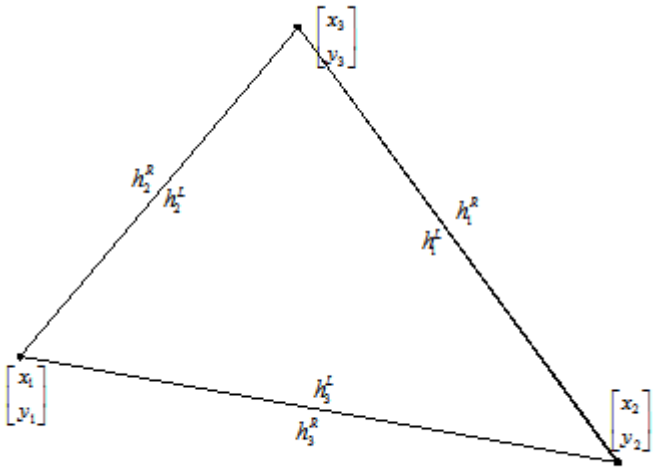

Fig. 3-3. The triangular cell i with the quantities h_j^R and h_j^L computed at the right (R) and left (L) sides respectively at a given face j, j=1,2,3. The coordinates (x_j, y_j), j=1,2,3, are located at the three vertices of cell i.

Again, (3.34) does not satisfy the C property because there is still an imbalance between the bed slope and the flux terms. In order to reach the balance, the right hand side of (3.34) is expressed in two parts (part 1 and part 2). Following the same procedure than in (3.26) and (3.27), we replace h_i by

$$\hat{h}_{1-3} = \frac{h_1^R + h_1^L + h_3^R + h_3^L}{4} \tag{3.35}$$

and

$$\hat{h}_{2-3} = \frac{h_2^R + h_2^L + h_3^R + h_3^L}{4}, \tag{3.36}$$

in parts 1 and 2 of (3.34), respectively (Fig. 3-3), and this leads to

$$\left(gh\frac{\partial z}{\partial x} \right)_i = \frac{g}{\mathcal{A}_i}\left(\frac{h_1^R + h_1^L + h_3^R + h_3^L}{4}\Delta y_1 (z_1 - z_3) + \frac{h_2^R + h_2^L + h_3^R + h_3^L}{4}\Delta y_2 (z_2 - z_3) \right) \tag{3.37}$$

Proposition I. *The numerical scheme presented in sections 3-1 to 3-3, satisfies the C property with (3.37).*

Proof: In the case of stagnant water conditions we have

$$h_1^R = h_1^L = h_1 \,, \tag{3.38}$$

$$h_2^R = h_2^L = h_2 \,, \tag{3.39}$$

$$h_3^R = h_3^L = h_3 \,, \tag{3.40}$$

$$\eta_1 = \eta_2 = \eta_3 = \eta_0 \,, \tag{3.41}$$

and the corresponding term of $\int_{\mathcal{A}} \nabla \cdot \vec{F} d\mathcal{A}$ in (3.2) for the x-momentum equation, reduces to $\int_{\mathcal{A}} \frac{\partial (0.5gh^2)}{\partial x} d\mathcal{A}$. By using the divergence theorem as in (3.3), it is numerically approximated as (see 3.4) $0.5g\left(h_1^2 \Delta y_1 + h_2^2 \Delta y_2 + h_3^2 \Delta y_3\right)$. Therefore the discretized momentum equation corresponding to cell *i* is

$$\begin{aligned}
(uh)_i^{n+1} \mathcal{A}_i &= (uh)_i^n \mathcal{A}_i - 0.5g\Delta t\left(h_1^2 \Delta y_1 + h_2^2 \Delta y_2 + h_3^2 \Delta y_3\right) \\
&\quad + g\Delta t\left(\frac{h_1 + h_3}{2} \Delta y_1 (z_1 - z_3) + \frac{h_2 + h_3}{2} \Delta y_2 (z_2 - z_3)\right) \\
&= (uh)_i^n \mathcal{A}_i - \frac{g\Delta t}{4}\left((h_3 + h_1)(h_3 - z_3 - h_1 + z_1)\Delta y_1 + (h_3 + h_2)(h_3 - z_3 - h_2 + z_2)\Delta y_2\right) \\
&= (uh)_i^n \mathcal{A}_i - \frac{g\Delta t}{4}\left((h_3 + h_1)(\eta_3 - \eta_1)\Delta y_1 + (h_3 + h_2)(\eta_3 - \eta_2)\Delta y_2\right) \\
&= (uh)_i^n \mathcal{A}_i \,.
\end{aligned} \tag{3.42}$$

The C property thus holds. The extension of the present method for an arbitrary control volume with *m* edges is straightforward by considering

$$\sum_{k=1}^{m} \Delta y_k = 0 \,. \tag{3.43}$$

Therefore, (3.33) and (3.34) could be generalized as

$$\left(gh\frac{\partial z}{\partial x}\right)_i \approx gh_i\left(\frac{\partial z}{\partial x}\right)_i \approx gh_i\left(\frac{\sum_{k=1}^{m} z_k \Delta y_k}{\mathcal{A}_i}\right),$$

with $\Delta y_m = -\sum_{k=1}^{m-1} \Delta y_k$ is deduced from (3.43) and this leads to

$$\left(gh\frac{\partial z}{\partial x}\right)_i = \frac{g}{\mathcal{A}_i}\left(\sum_{k=1}^{m-1} \hat{h}_k \Delta y_k (z_k - z_m)\right)$$

with

$$\hat{h}_k = \frac{h_k^R + h_k^L + h_m^R + h_m^L}{4}.$$

The proof of proposition I is then generalized in a similar manner.

3-4-2- Method II- Considering different components of the bed slope term separately

In method I, two different approximations (3.35 and 3.36) have been used to approximate the depth inside a given triangular cell in order to balance the source and the flux gradient terms. For general control volumes having more than three edges (such as quadrilaterals) the accuracy of method I may be decreased in the case of stretched cells. This problem motivates the introduction of method II in which the source and the flux gradient terms are inherently balanced by considering different components of the bed slope term separately.

Here, the bed slope term is written as

$$\begin{aligned} gh\frac{\partial z}{\partial x} &= g\frac{\partial (hz)}{\partial x} - gz\frac{\partial h}{\partial x} \\ &= 0.5g\frac{\partial (hz)}{\partial x} + 0.5g\frac{\partial (hz)}{\partial x} - gz\frac{\partial h}{\partial x} \\ &= \underbrace{0.5g\frac{\partial (hz)}{\partial x}}_{B_1} + \underbrace{0.5gh\frac{\partial z}{\partial x}}_{B_2} - \underbrace{0.5gz\frac{\partial h}{\partial x}}_{B_3}, \end{aligned} \tag{3.44}$$

where

$$B_1 = \frac{0.5g}{\mathcal{A}_i}\left(\frac{h_1^L + h_1^R}{2} z_1 \Delta y_1 + \frac{h_2^L + h_2^R}{2} z_2 \Delta y_2 + \frac{h_3^L + h_3^R}{2} z_3 \Delta y_3\right), \tag{3.45}$$

$$B_2 = \frac{0.5gh_i}{\mathcal{A}_i}\left(z_1 \Delta y_1 + z_2 \Delta y_2 + z_3 \Delta y_3\right), \tag{3.46}$$

$$B_3 = \frac{0.5gz_i}{\mathcal{A}_i}\left(\frac{h_1^L + h_1^R}{2} \Delta y_1 + \frac{h_2^L + h_2^R}{2} \Delta y_2 + \frac{h_3^L + h_3^R}{2} \Delta y_3\right). \tag{3.47}$$

In the case of a horizontal bed, B_1 and B_3 cancel each other and B_2 is equal to zero.

Proposition II. *The numerical scheme presented in sections 3-1 to 3-3, satisfies the C property with (3.44) to (3.47).*

Proof: The stagnant condition leads to

$$
\begin{aligned}
(uh)_i^{n+1}\mathcal{A}_i &= (uh)_i^n\mathcal{A}_i - 0.5g\Delta t\left(h_1^2\Delta y_1 + h_2^2\Delta y_2 + h_3^2\Delta y_3\right) + \Delta t\mathcal{A}_i\left(B_1 + B_2 + B_3\right)\\
&= (uh)_i^n\mathcal{A}_i - 0.5g\Delta t\left(h_1(h_1 - z_1)\Delta y_1 + h_2(h_2 - z_2)\Delta y_2 + h_3(h_3 - z_3)\Delta y_3\right) + \Delta t\mathcal{A}_i\left(B_2 - B_3\right)\\
&= (uh)_i^n\mathcal{A}_i - 0.5g\eta_0\Delta t\left(h_1\Delta y_1 + h_2\Delta y_2 + h_3\Delta y_3\right) + \Delta t\mathcal{A}_i\left(B_2 - B_3\right) \qquad (3.48)
\end{aligned}
$$

and

$$
\begin{aligned}
\left(B_2 - B_3\right)\mathcal{A}_i &= 0.5gh_i\left((h_1 - \eta_1)\Delta y_1 + (h_2 - \eta_2)\Delta y_2 + (h_3 - \eta_3)\Delta y_3\right) - 0.5gz_i\left(h_1\Delta y_1 + h_2\Delta y_2 + h_3\Delta y_3\right)\\
&= 0.5g\left(h_i - z_i\right)\left(h_1\Delta y_1 + h_2\Delta y_2 + h_3\Delta y_3\right) + 0.5g\eta_0 h_i\left(\Delta y_1 + \Delta y_2 + \Delta y_3\right)\\
&= 0.5g\eta_0\left(h_1\Delta y_1 + h_2\Delta y_2 + h_3\Delta y_3\right)\\
&= 0.5g\eta_0\left(h_1\mathcal{A}_1 + h_2\mathcal{A}_2 + h_3\mathcal{A}_3\right). \qquad (3.49)
\end{aligned}
$$

Substituting (3.49) in (3.48) we obtain

$$(uh)_i^{n+1}\mathcal{A}_i = (uh)_i^n\mathcal{A}_i. \qquad (3.50)$$

Hence, the C property holds. This proof is directly generalized in the case of an arbitrary control volume having more than three edges, by adding the corresponding terms to (3.45) to (3.47).

3-5- Computational modeling of wetting and drying fronts

It is generally accepted that the wetting-drying simulation is very hard (Toro 2000). This is particularly the case in real applications with complicated topographies using unstructured grids. Therefore an algorithm to treat wetting and drying fronts is generally needed.

In this paper, if the water depth in a cell is less than a specified value h_{min} , then this cell is considered as a dry cell. In such a cell all *outward* fluxes and also the bed slope and friction source terms are set to zero. Inward fluxes are always active, as a mechanism for wetting the dry cells. There are other strategies for handling moving fronts such as level set methods and also volume of fluid methods, but they are usually too expensive for unstructured grids.

3-6- Boundary conditions

In order to treat the boundary conditions, the variables at boundary faces are imposed as following:

Subcritical flow:

inflow: two external conditions

outflow: one external condition

Supercritical flow

inflow: three external conditions

outflow: none

Solid walls:

Velocity components are set zero

All remaining conditions may be calculated based on the characteristics theory, i.e. by using the information carried out by the outgoing bicharachteristics (the Riemann invariants). However, in most practical cases those may be simply set to the corresponding values of the adjacent inner cells.

4- Numerical results

In order to study the performance of the numerical scheme, some tests have been performed herein for variable topographies. In all figures and tables, the SI system has been used, i.e. the water depth and the water surface elevation are in meters (m) and the water discharge is in m^3/s. Note that methods I and II present the same results in the following tests and no visible difference is observed.

4-1-Tidal wave flow over an irregular topography

The topography for this case is defined in table 1 (Goutal and Maurel, 1997) and graphically represented in figure 4-1-1.

Table 1. Topography for an irregular bed.

X(m)	0	50	100	150	250	300	350	400	425	435	450	475	500	505
Z(m)	0	20	2.5	5	5	3	5	5	7.5	8	9	9	9.1	9
X(m)	530	550	565	575	600	650	700	750	800	820	900	950	1000	1500
Z(m)	9	6	5.5	5.5	5	4	3	3	2.3	2	1.2	0.4	0	0

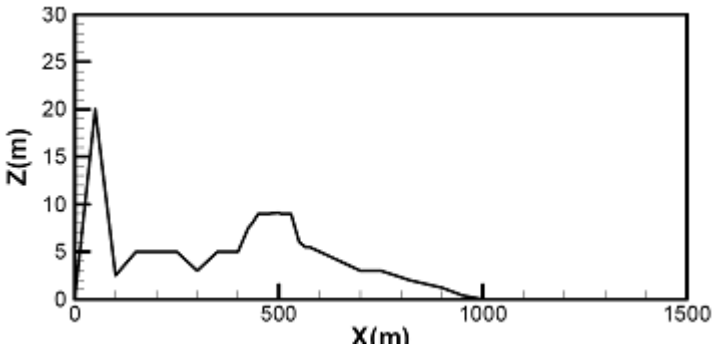

Figure 4-1-1. Topography for an irregular bed

The initial conditions write

$$h(x,0) = H(x), \tag{4.1}$$

$$u(x,0) = 0, \tag{4.2}$$

with

L=1500 m, $H(x)= H(0)-z(x)$, $H(0)=16m$.

The boundary conditions are

$$h(0,t) = H(0) + 4 - 4\sin\left[\pi\left(\frac{4t}{86400} + \frac{1}{2}\right)\right], \tag{4.3}$$

$$u(L,t) = 0. \tag{4.4}$$

For this test, Bermudez and Vazquez (1994) derived the following "asymptotic" unsteady solution by writing the equations in dimensionless form and asymptotic expansions in terms of the Froude number.

$$h(x,t) = H(x) + 4 - 4\sin\left[\pi\left(\frac{4t}{86400} + \frac{1}{2}\right)\right], \tag{4.5}$$

$$u(x,t) = \frac{(x-L)\pi}{5400h(x,t)}\cos\left[\pi\left(\frac{4t}{86400} + \frac{1}{2}\right)\right]. \tag{4.6}$$

At time t = 10800, the numerical results using a CFL number of 0.63 and 100 grid points are shown in figure 4-1-2 (left) . The results of the original scheme i.e. using (3.33), (instead of the proposed methods I or II i.e. (3.27) or (3.44), respectively), are also presented in figure 4-1-2 (right). In this test case, the original scheme shows a high level of oscillations due to the irregular topography which can not be handled because of the imbalance between the source and flux terms, while a considerable improvement is observed with method I or II. The numerical results for water surface are shown in figure 4-1-3, which again show the performance of the proposed methods. Finally, in order to verify the *C* property, the numerical result of velocity and water surface elevation obtained by the proposed method and the original scheme for a stagnant initial condition are presented for t = 40 in figures 4-1-4 and 4-1-5 respectively. As, shown, contrary to the original scheme, the proposed method can preserve the stagnant conditions.

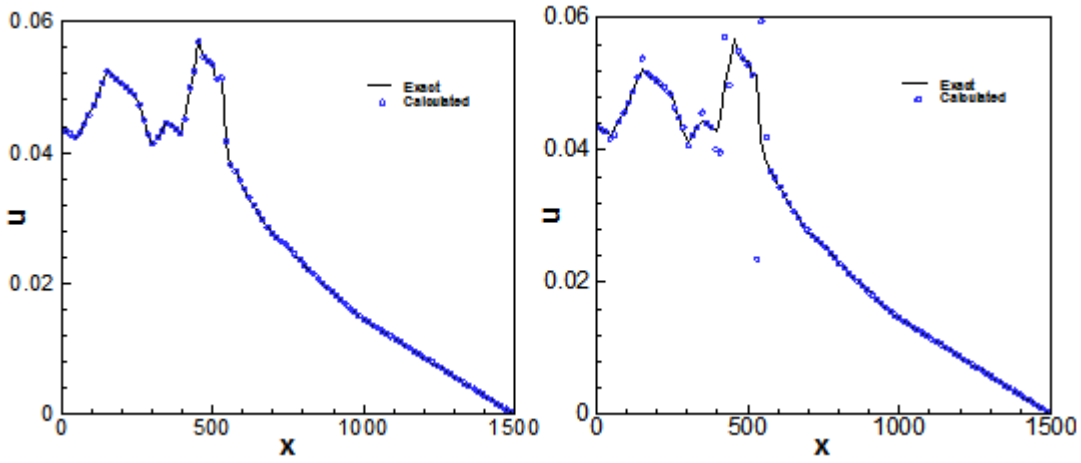

Figure 4-1-2. Tidal wave flow over an irregular bed, velocity: Present method (left) and the original scheme (right).

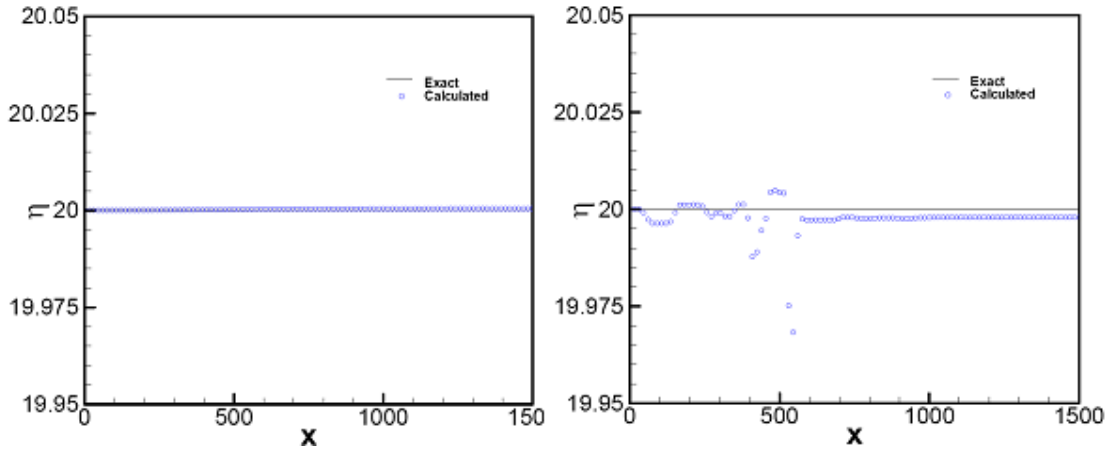

Figure 4-1-3. Tidal wave flow over an irregular bed, water surface elevation: Present method (left) and the original scheme (right).

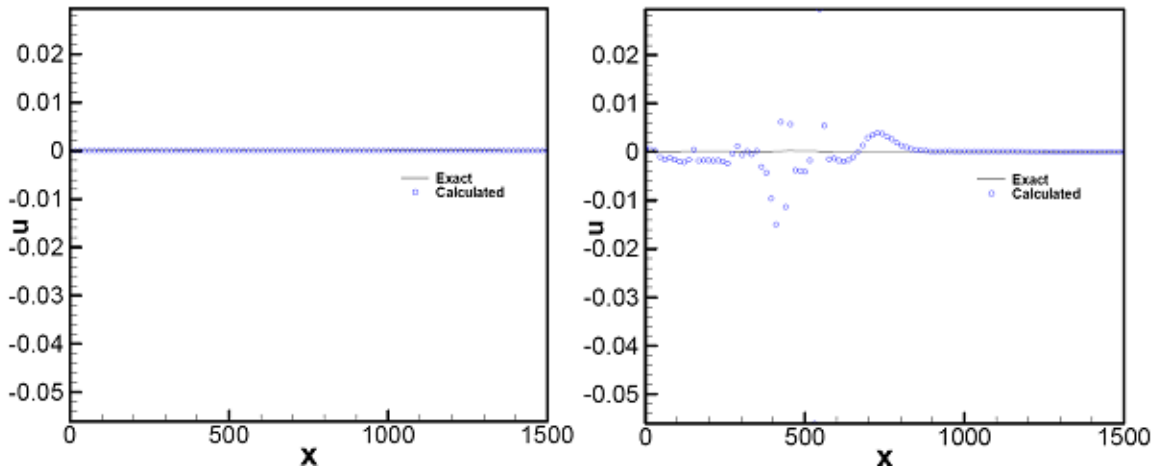

Figure 4-1-4. Stagnant condition over an irregular bed, velocity: Present method (left) and the original scheme (right).

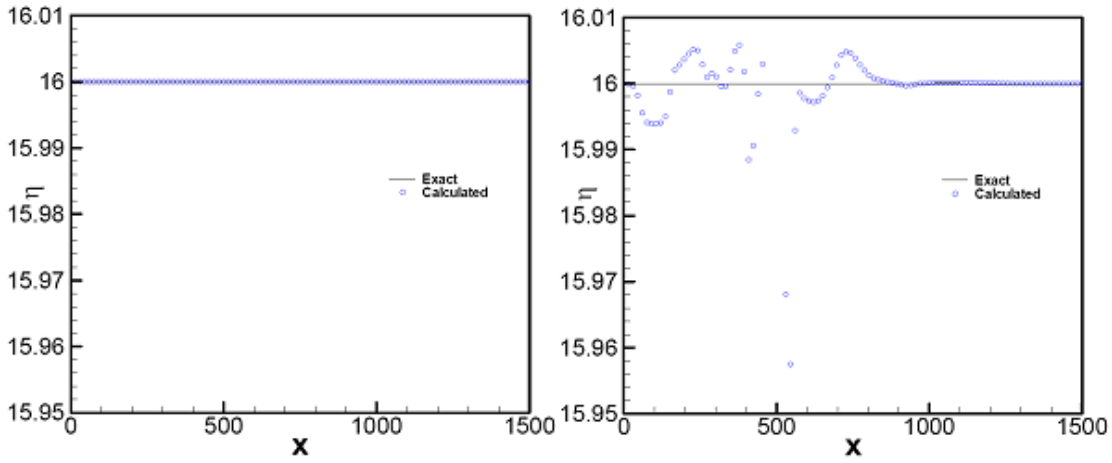

Figure 4-1-5. Stagnant condition over an irregular bed, water Surface: Present method (left) and the original scheme (right).

4-2- A surge crossing a step

Here we consider a surge crossing a step. A channel of length 10000m is used with a step of height 2 m, located at the middle of the channel (Figure 4-2). This test case has been previously studied by Hu et. al. (2000) who replaced the step by a steep bed slope. A grid of 400 uniform cells is used here.

The initial water surface is 5 m in the channel, the water depth at the upstream end is 10m, and the velocity of the surge at the entrance is defined as (Hu et. al., 2000)

$$u(0,t) = (\eta_u - \eta_d)\sqrt{\frac{g(\eta_u + \eta_d)}{2\eta_u \eta_d}} \qquad (4.7)$$

where η_u =10 m and η_d =5m.

In figure 4-2, the numerical results obtained using method I or II are compared with the analytical solution (Hu et. al., 2000). They show the ability of the model in simulating surges over discontinuous bed profiles.

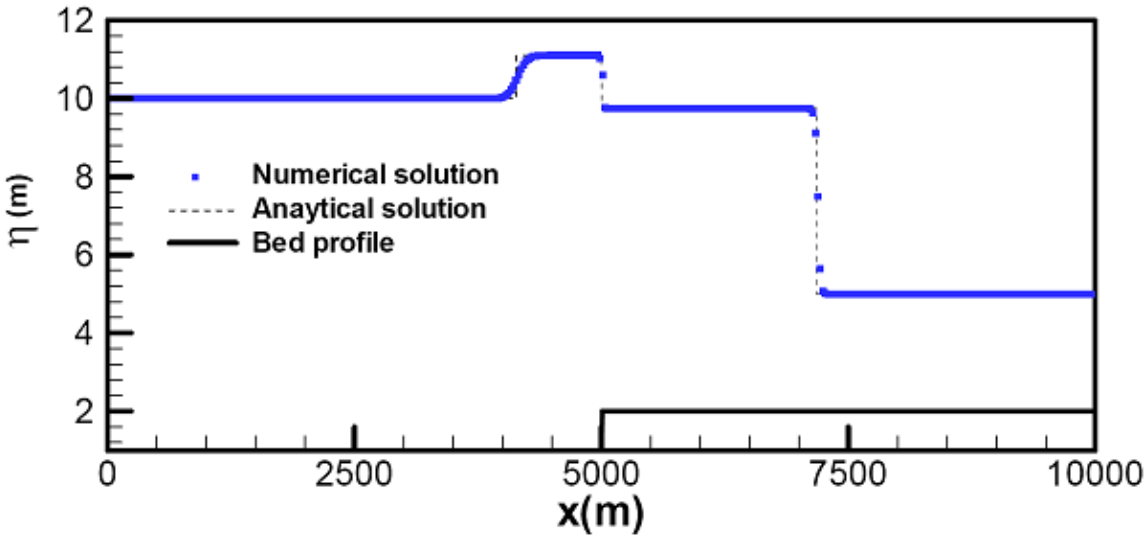

Fig. 4-2. Surge crossing a step: computed water surface at t =600 s.

4-2- One dimensional, small perturbation of a steady-state solution

A small perturbation of a steady-state solution, proposed by Leveque (1998), is a challenging test for evaluating the performance of numerical schemes over variable topographies. A channel of length 1.0 *m* is considered with the following topography

$$z(x,y)=\begin{cases}-0.8\exp\left(-5(x-0.9)^2-50(y-0.5)^2\right), & for\ |x-0.5|\le 0.1,\\ 0.0, & otherwise,\end{cases} \tag{4.7}$$

with a zero initial flow velocity and a surface profile defined as

$$\eta(x,y)=\begin{cases}1.0+\varepsilon & for\ 0.1<x<0.2,\\ 1.0, & otherwise.\end{cases} \tag{4.8}$$

Following Leveque (1998), $\varepsilon = 0.01\,\mathrm{m}$ and the reduced gravitational acceleration is $g = 1\,\mathrm{m}^2/\mathrm{s}$. Here, a CFL number of 0.99 is used. The numerical results obtained on a very fine grid (1500 nodes), using method I or II, are used as reference solutions in the absence of an analytical one. On a grid of 100 nodes, the results obtained with method I or II and the original scheme are compared with the reference solution in figure 4-2. This case is a challenging one, and most existing schemes have used considerably more grid points than here (such as 600 in Hubbard and Navarro, 2000). As shown in figures 4-2, method I or II

can capture the quasi steady solutions quite well, and a considerable improvement is observed compared to the original scheme.

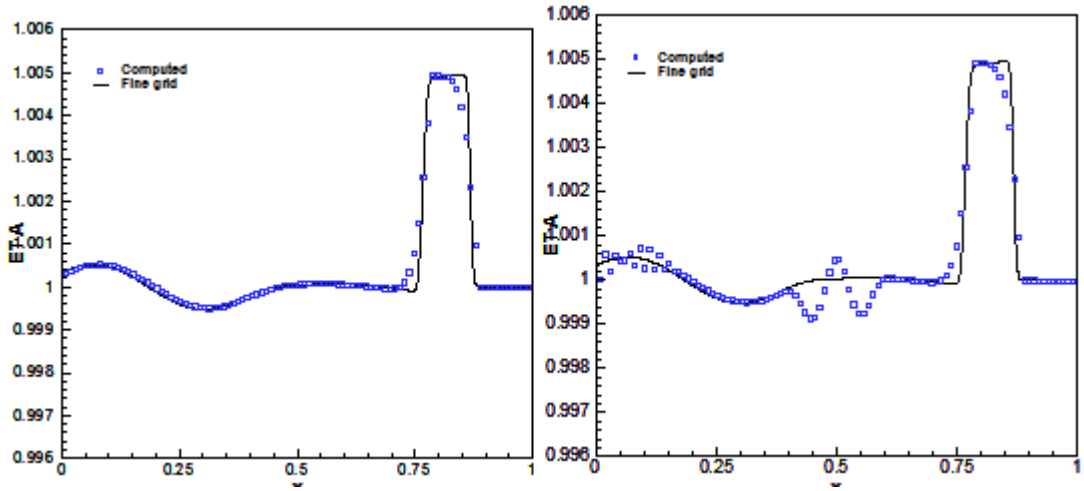

Fig. 4-2. Computed water surface level at t=0.7 with $\varepsilon = 0.01$: Present method (left) and the original scheme (right).

4-4- Two dimensional, small perturbation of a steady-state solution

In this test case (Leveque, 1998), the SW equations are solved in a domain $[0,2]\times[0,1]$, and the bottom surface is an elliptical shaped hump

The water surface is initially flat with $h(x,y)=1$ except for $0.05 < x < 0.15$, where $h(x,y)=1.01$ m. An unstructured grid with 12344 triangular cells and a CFL number of 0.6 is used for this test. Figure 4-3 displays the right-going disturbance at t=1.8s as it propagates past the hump. This shows the ability of the model in simulating 2-D problems with variable topographies without producing numerical oscillations.

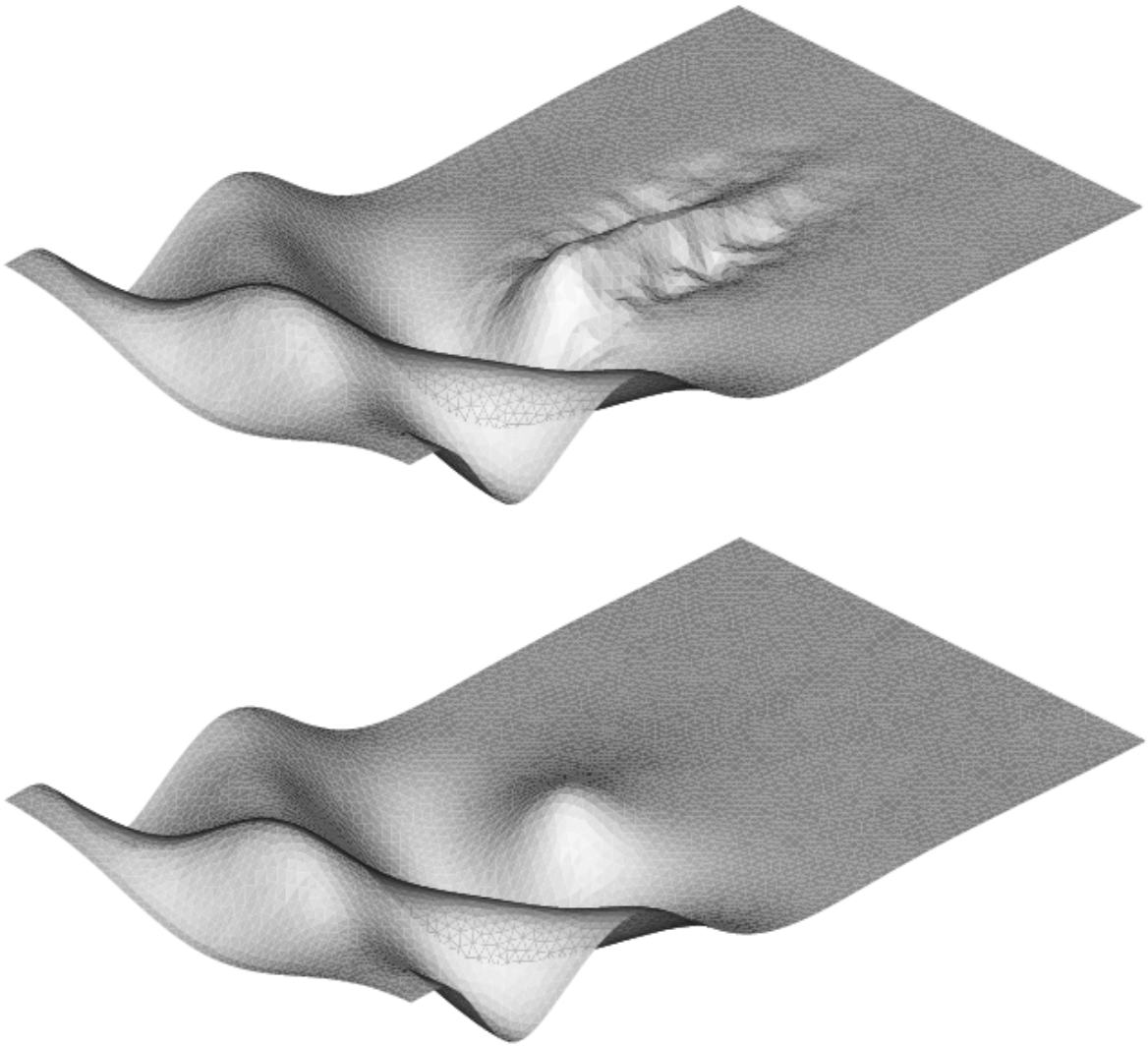

Fig. 4-3. Computed water surface level at t=1.8 with $\varepsilon = 0.01$: Present method (bottom) and the original scheme (top).

4-5- Steady flow over a bump

The topography is now defined (Goutal and Maurel, 1997) as

$$z(x) = \begin{cases} 0.2 - 0.05(x-10)^2 & if\ 8 < x < 12, \\ 0 & otherwise. \end{cases} \tag{4.8}$$

Depending on the initial and boundary conditions, the flow may be subcritical, transcritical (with or without a steady shock), or supercritical. The analytical solution of

this problem is given in Goutal (1997). An unstructured grid of average triangle edges equal to 0.075 m was used in all computations. A high order accurate interpolation scheme (Appendix I) was employed in this test case.

Three different cases are considered below by imposing downstream and upstream boundary conditions for the water level (h) and the discharge (uh), respectively:

(i)*Transcritical flow without a shock:* h=0.66m only when the flow is subcritical and uh=1.53 m^3/h.

(ii) *Transcritical flow with a shock:* h=0.33m and uh=0.18 m^3/h.

(iii) *Subcritical flow:* =2.m and uh=4.42 m^3/h.

The surface profiles are plotted in figures 4-5-1-a,b,c for method I or II, and they show good agreements with the analytical solutions. The computed discharges are also compared in figures 4-5-2-a,b,c with the analytical ones, which show a low level of numerical oscillations. It should be mentioned that such a level of numerical oscillations is also present in most existing schemes. This is because the C property, although widely accepted in the literature as a good measure to test the ability of numerical schemes in the presence of real topographies, does not guarantee that the steady state conditions with non-zero discharge is well captured.

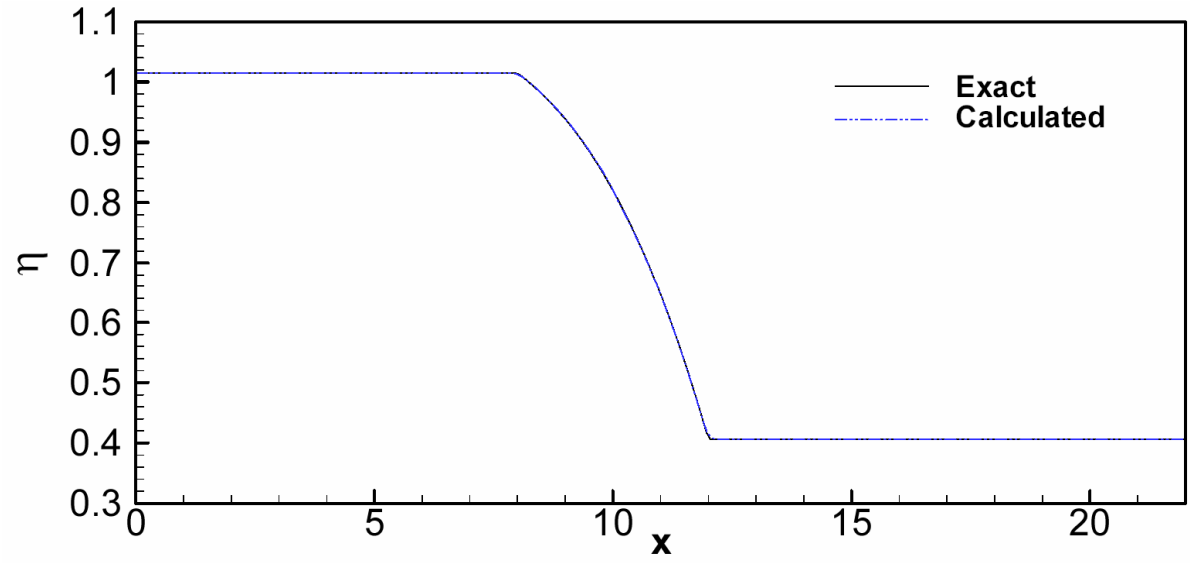

Figure 4-5-1-a. Steady transcritical flow over a bump without a shock: Water surface elevation.

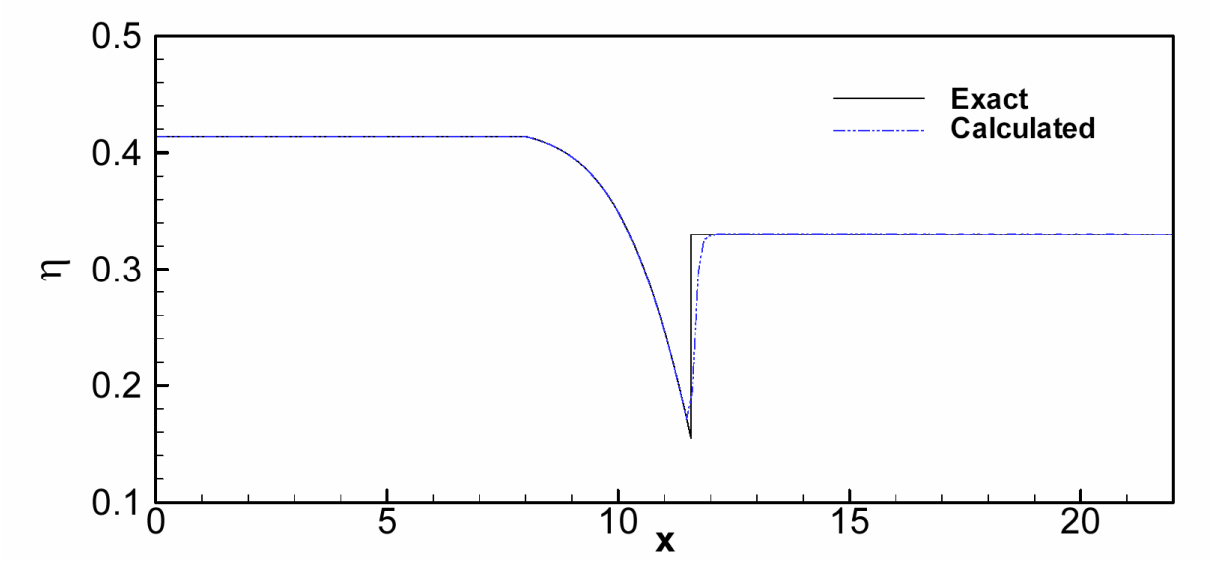

Figure 4-5-1-b. Steady transcritical flow over a bump with a shock: Water surface elevation.

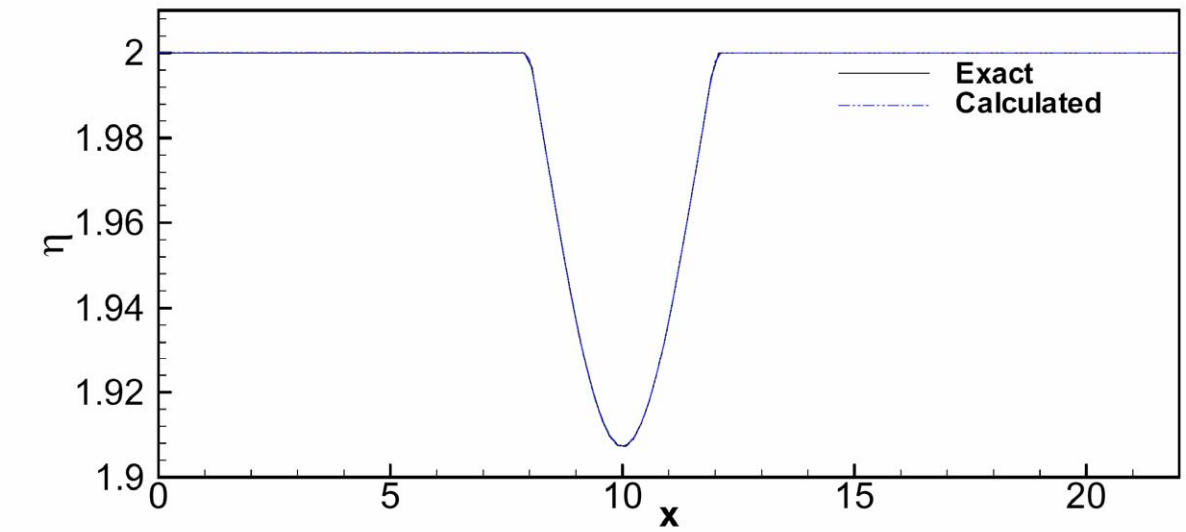

Figure 4-5-1-c. Steady subcritical flow over a bump: Water surface elevation.

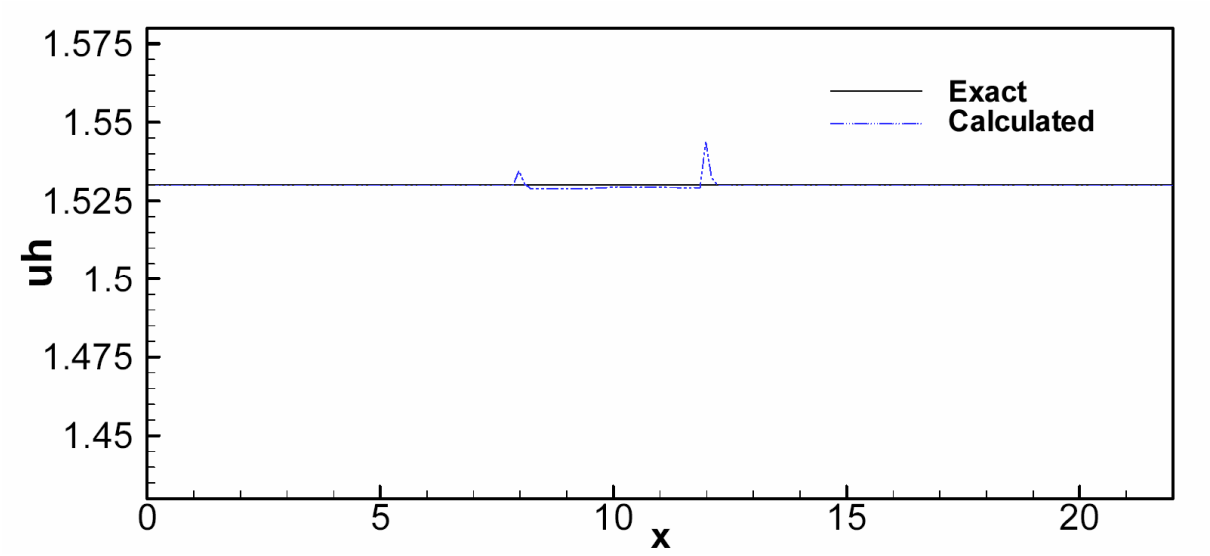

Figure 4-5-2-a. Water discharge in steady transcritical flow over a bump without a shock

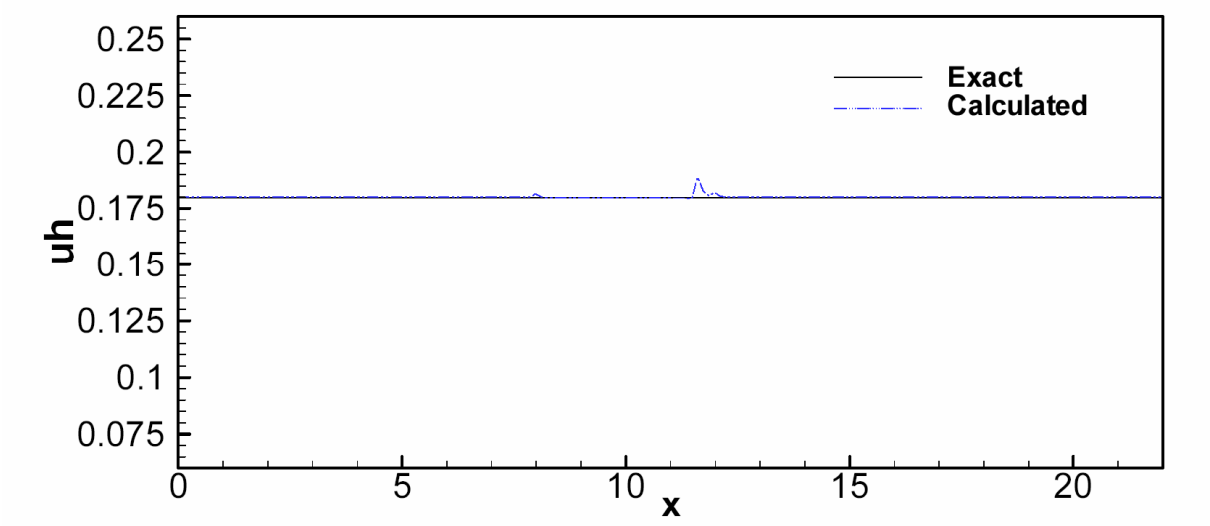

Figure 4-5-2-b. Water discharge in steady transcritical flow over a bump with a shock

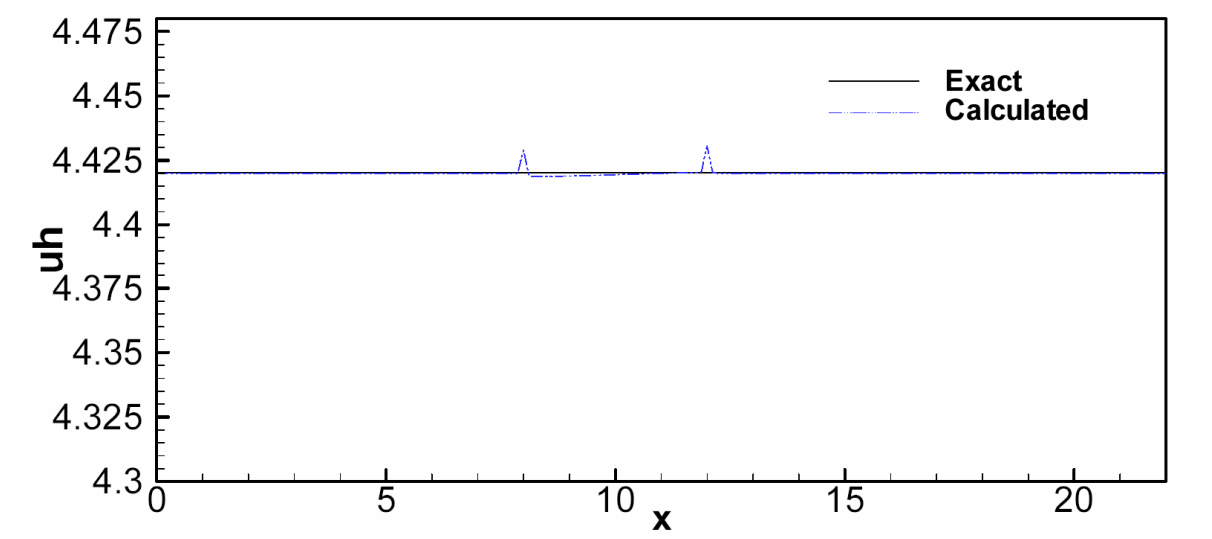

Figure 4-5-2-c. Water discharge in steady subcritical flow over a bump without a shock

4-6- Dam break and advance over a triangular obstacle

In this test case, evolution of a dam-break wave over a triangular obstacle is examined. The channel geometry is presented in Figure 4-6-1. The physical model combines a reservoir connected to a rectangular channel. The length of the entire model is 22.5m. The dam is situated at x=15.5m. A triangular obstacle (6m long, 0.4m high) is situated 13m downstream the dam over the bed of the channel. The slopes of the obstacle are symmetric. The initial conditions considered are 0.75m of water depth in the reservoir and dry bed in the rest of the channel. The fixed boundaries are solid walls except for the free outlet. The Manning roughness coefficient is 0.0125 for the bed and 0.011 for the vertical walls of the rectangular channel, values supplied by the experimentalists from a steady flow test case. Gauging points are located: G4 at 4m, G10 at 10m, G11 at 11m, G13 at 13m and G20 at 20m as shown in Fgure 4-6-2. Experimental data are reported in Brufau et. al. 2002 which are obtained from the Recherches Hydrauliques Lab. Chatelet together with the University of Bruxelles (Belgium) under the supervision of J.M. Hiver.

A minimum wet depth of h_{min}=0.004 m was considered in the numerical calculations. Sensitivity computation with the 1D model showed that reducing the h_{min} has minor effects on the numerical results. The predicted and measured water depth time evolutions during 40 s at the gauging points are presented in Figure 4-6-3 which shows a satisfactory

concordance. The water depth and the arrival time of the wave are predicted well at G4, G10 and G11 which are located before the obstacle. Moreover, the transition from wet to dry is correctly predicted at point G13 which is a critical point since it is located at the vertex of. At the last point (G20) a little disagreement between measures and numerical results is observed but the amount of water is insignificant. The same feature is also observed in Brufau et. al. 2002 and may be related to vertical non-hydrostatic motions that are ignored in shallow water equations.

Finally, figure 4-6-4 compares the numerical results obtained for the water depth at different times from the 1D and 2D numerical schemes. As it can be seen in Figure 4-6-4, results of two models coincide, which is expected due to the nearly one-dimensional feature of the flow (i.e. lateral changes are negligible) and this shows the coherence of both models.

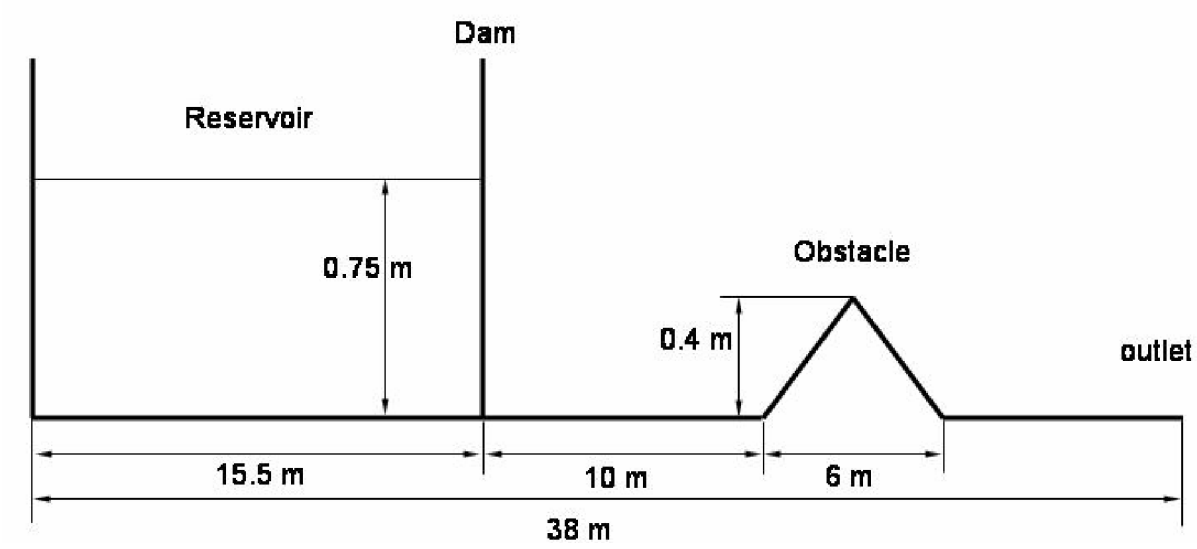

Figure 4-6-1. Geometry of the experimental model in the simulation of a dam break and advance over a triangular obstacle.

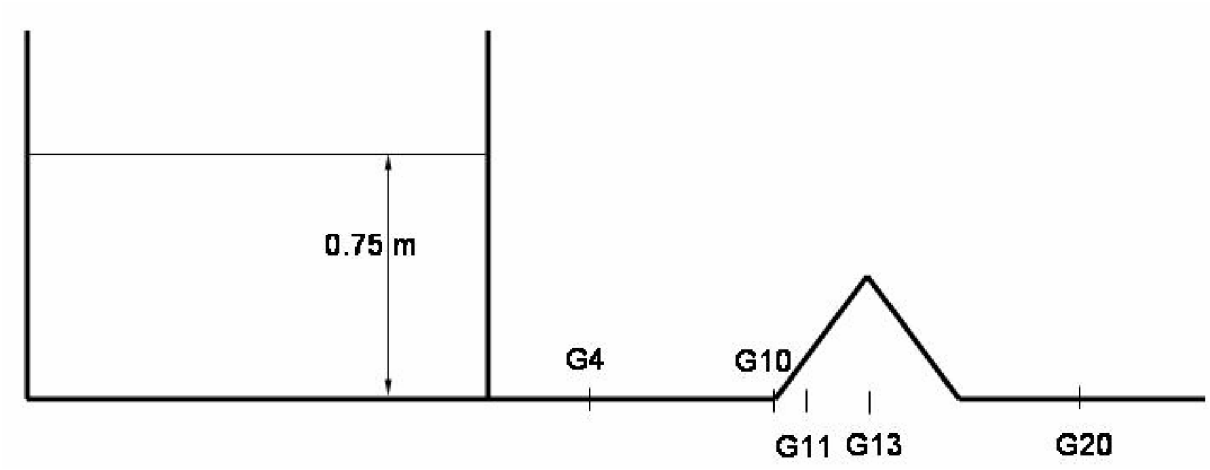

Figure 4-6-2. Location of the gauging points in the experimental model for the simulation of a dam break and advance over a triangular obstacle.

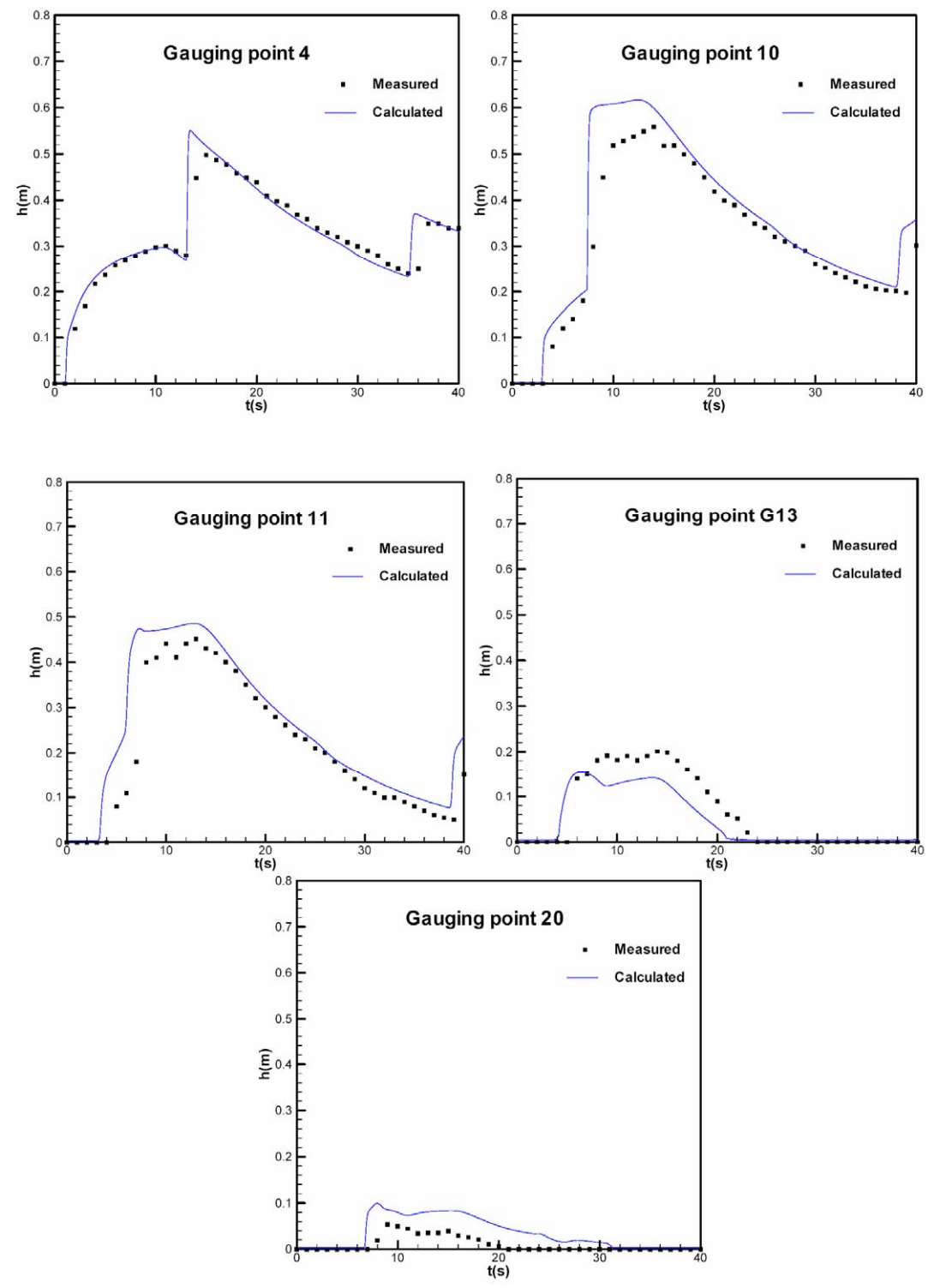

Figure 4-6-3. Time evolution during 40 s of the water depth measured and computed at gauging points: G4, G10, G11, G13 and G20 in the simulation of a dam break and advance over a triangular obstacle. Points stand for experimental measures and solid line for numerical results.

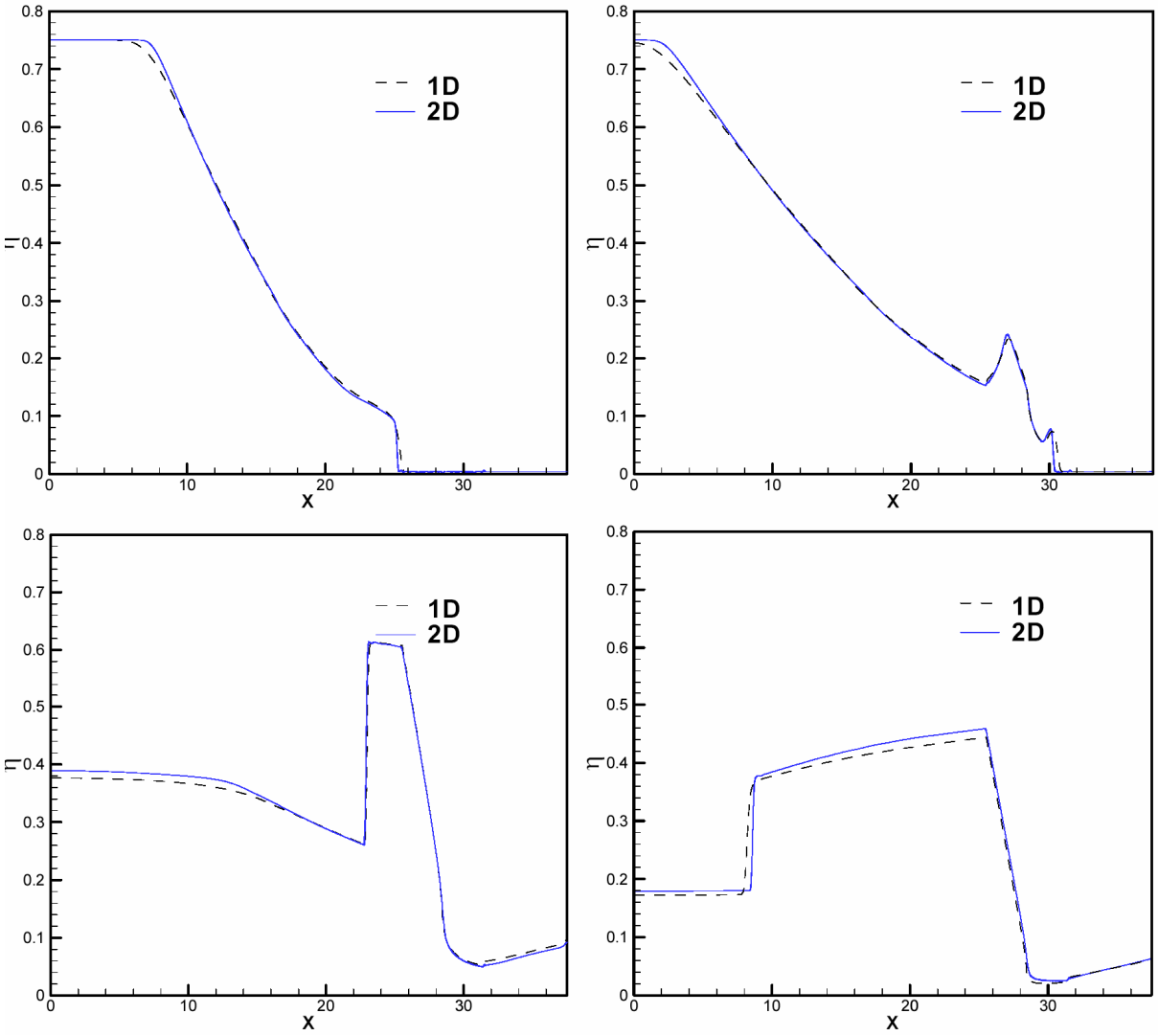

Figure 4-6-4. Numerical results obtained with a 1D and a 2D scheme on the water depth profiles along the channel at times: T =3; 5; 10 and 20 s in the simulation of a dam break and advance over a triangular obstacle.

5- Conclusion

Two efficient methods have been proposed to treat the source terms and to satisfy the compatibility property on unstructured grids. In the proposed methods, it is not necessary to perform extra upwinding or Riemann solution for the source terms. Contrary to many

available schemes, our approach can be easily implemented on unstructured grids and it takes advantage of being flexible for irregular boundaries and local mesh refinement. Numerical results indicated that the proposed methods accurately simulate sub, super and trans-critical flows in complicated topographies and also the circulating flows.

Appendix I- Interpolation scheme

In the present cell-centered scheme, the variables are located at the triangle barycenters and the values of the variables at the left and right sides of the interface are needed to compute the numerical fluxes and source terms. Consider two adjacent triangles as shown in figure I-1.

A first order approximation of η, uh, vh at left and right hand side of the cell interfaces is simply equal to their values in the corresponding cell. For example

$\eta_L = \eta_{b_L}$,

$(uh)_L = (uh)_{b_L}$,

$(vh)_L = (vh)_{b_L}$.

Various methods have been proposed for developing higher order accurate interpolation schemes. Here, some details of a high order monotonic interpolation method, is described.

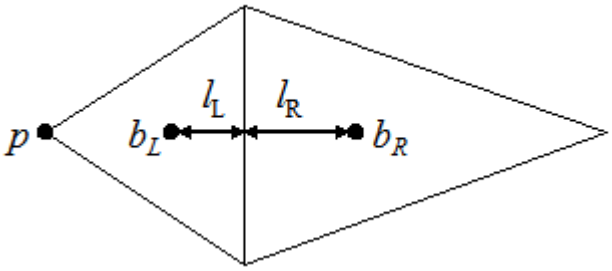

Fig. I-1. Two adjacent triangles with barycenters b_L and b_R, where l_L and l_R are the lengths between the mid-side node of the common face and b_L and b_R, respectively.

For a scalar variable *such as* η, the interface values η_L and η_R (on the left and right sides of a given face respectively) are calculated by the κ scheme (Battina 1990). For example, η_L is calculated as

$$\eta_L = \eta_{b_L} + \frac{s}{4}\left[(1-\kappa s)\Delta_- + (1+\kappa s)\Delta_+\right], \tag{3.24}$$

$$\Delta_- = \left(\eta_{b_L} - \eta_p\right) \quad , \quad \Delta_+ = \left[2l_L \Big/ \left(l_L + l_R\right)\right]\left(\eta_{b_R} - \eta_{b_L}\right), \tag{3.25}$$

where κ = -1 leads to an upwind scheme, κ = 0 to the Fromm scheme, κ = 1 to a central scheme and κ=1/3 to a third order scheme (in 1-D).

The slope limiter *s*, is chosen according to Battina (1990)

$$s = \frac{2\Delta_-\Delta_+ + \varepsilon}{\Delta_-^2 + \Delta_+^2 + \varepsilon}, \tag{3.26}$$

where ε is a very small number for avoiding division by zero in the regions of mild slope. The interface values of *uh* and *vh* are calculated similarly.

References

Bermudez A. and Vazquez M. E. (1994), '*Upwind Methods for Hyperbolic Conservation Laws with Source Terms*', Computers and Fluids, 23, 1049

Brufau P, Vazquez-Cendon ME and Garcia-Navarro P (2002). *numerical model for the flooding and drying of irregular domains*. int. J. for Numer. Mcth. Fluids, 39: 247—275.

Alcrudo F. and Benkhaldoun F. (2001), '*Exact Solutions to the Riemann Problem of the Shallow-water Equations with a Bottom Step*', Computers and fluids 30, pp. 643-671

Bradford S. F. and Sandres B. F. (2002), '*Finite-Volume Model for Shallow-Water Flooding of Arbitrary Topography*', J. Hyd. Eng. ASCE, 128, 289

Denham, M. K. and Patrick, M. A. (1974), '*Laminar flow over a downstream-facing step in a two-dimensional flow channel*', Trans. Inst. Chemical Engineers, 52, 361-367

Fenemma R. and Chaudhry M. (1987), '*Simulation of One-Dimensional Dam-Break Flows*', J. Hyd. Res., vol. 25, No.1, pp. 41

P. Glaister (1988), '*Approximate Riemann Solutions of the Shallow-Water Equations*'. J. Hyd. Res., 26, No. 3, 293-306

Goutal N. and Maurel F., eds. (1997), '*Proceedings of the 2nd Workshop on Dam-Break Wave Simulation*', HE-43/97/016/B, France

Harten A. and Hyman P. (1983), '*Self adjusting grid methods for one-dimensional hyperbolic conservation laws*', J. of Comput. Phys., 50, 235-269

Hubbard M. E. and Garcia-Navarro P. (2000), 'Flux Difference Splitting and the Balancing of Source Terms and Flux Gradients', J. Comput. Phys. 165, 89-125

Hubbard M. E. and Garcia-Navarro P. (2001), '*Balancing Source Terms and Flux Gradients in Finite Volume Schemes*', Godunov Methods: Theory and Applications, edited by E. F. Toro, Kluwer Academic Publishers, New York, pp. 447-483

Hu K., Mingham C.G., Causon D.M. (2000), '*Numerical simulation of wave overtopping of coastal structures using the non-linear shallow water equations*'. Coastal Engineering 2000, 41, 433– 465.

Kurganov A., Levy D. (2002), '*Central-Upwind Schemes for the Saint-Venant System*' *Mathematical Modeling and Numerical Analysis*, 36 , 397-425

LeVeque R. J. (2002), '*Finite Volume Methods for Hyperbolic Problems*', Cambridge university press, UK.

LeVeque R. J. (1998), '*Balancing Source Terms and Flux gradients in High-Resolution Godunov Methods*', J. Comput. Phys., 146, pp. 346

Mingham C.G. and Causon D. M. (1998), '*High Resolution Finite-Volume Method for Shallow-water Equation Flows*', J. Hyd. Eng. ASCE 124, 605

Mohammadian A., Le Roux D. Y., Tajrishi M., Mazaheri K. (2005), 'A Mass Conservative Scheme For Simulating Shallow Flows Over Variable Topographies Using Unstructured Grid', Advances in water resources, Vol. 28, (5), pp. 429-539

Nujic M. (1995), '*Efficient Implementation of Non-Oscillatory Schemes of Free Surface Flows*', J. Hyd. Res., Vol. 33, No. 1, pp. 101

Rogers B. D., Borthwick A. L. and Taylor P. H. (2003), '*Mathematical balancing of flux gradient and source terms prior to using Roe approximate Riemann solver Volume*', J. Comp. Phys., Vol. 192, (2) , pp. 422-451

Shu C. W. and Osher S. (1988), '*Efficient Implementation of Non-Oscillatory Shock-Capturing Schemes*', J. Comp. Phys., Vol. 77, pp. 439-471

van Leer B., Lee W. T. and Powell K. G. (1989), '*Sonic Point Capturing*', 9th CFD Conference, American Institute of Aeronautics and Astronautics, Buffalo, N.Y.

Vazquez-Cendon M. E. (1999), '*Improved Treatment of Source Terms in Upwind Schemes for the Shallow-water Equations in Channels with Irregular Geometry*', J. Comp. Phys., 43(2), pp. 357-372

Vukovic S. and Sopta L. (2002), '*ENO and WENO Schemes with the Exact Conservation Property for One-Dimensional Shallow-Water Equations*', J. Comp. Phys. 179, 593-621

Xu K. (2002), '*A Well-balanced Gas-Kinetic Scheme for the Shallow-water Equations with Source Terms*'. J. Comput. Phys. Vol. 178, pp. 533-562.

Zhao D., Shen H. W., Tabios G. Q. III, Lai J. S. and Tan W. Y. (1994), '*Finite-Volume two-Dimensional Unsteady-Flow Model for River Basins*'. J. Hyd. Eng. ASCE 120 (7), 863-883

Zhou J. G., Causon D. M., Mingham C. G. and Ingram D. M. (2001), '*The Surface Gradient Method for the Treatment of Source Terms in the Shallow-water Equations*', J. Comp. Phys. 168, 1-25

CHAPTER 6

Fourier analysis of upwind schemes in Shallow Water systems for gravity and Rossby waves

In the previous chapters, the Coriolis parameter has not been considered and the study has been restricted to the small scale flows were convection and gravity effects are dominant. The very good performance of the conservative upwind schemes for those flows motivates the following question: How well these do schemes perform for large scale flows where the Coriolis parameter plays a key role? This question is the main subject of the last chapter and we employ the Fourier analysis approach to study the behavior of upwind finite volume schemes for both gravity and Rossby waves.

Etude de méthodes de volumes finis upwind par une analyse de type Fourier pour les ondes de gravité et de Rossby

Résumé

Une analyse de type Fourier est utilisée ici pour étudier plusieurs méthodes de volumes finis upwind, et plus particulièrement la vitesse de phase, la vitesse de groupe, l'amortissement et la dispersion. Les ondes de gravité sont tout d'abord considérées. Comme celapouvait être anticipé, la plupart des schémas upwind induisent un amortissement considérable. Cependant la vitesse de phase est mieux approximéeque pour les schémas centrés. Dans une deuxième partie, les termes de Coriolis sont introduits dans les équations et les modes de Rossby sont étudiés.Dans ce cas tous les schémas upwind considérés ici induisent un amortissement important. Les résultats numériques sont aussi comparésavec ceux obtenus en utilisant une approche de type limiteur de flux. On montre que le limiteur de flux utilisé amortit encore davantage, demanière excessive, les résultats

précédants. En conclusion, avec ou sans limiteur de flux, les méthodes de volumes finis upwind ne sont pasde bons candidats pour un calcul précis des modes de Rossby.

Fourier analysis of upwind schemes in Shallow Water systems for gravity and Rossby waves

A. M. Mohammadian and D. Y. Le Roux

Abstract. *A Fourier analysis has been performed for various upwind finite volume schemes, including the study of phase speed, group velocity, damping and dispersion. In the first part, pure gravity waves are investigated. As expected, most upwind schemes lead to a considerable damping but they exhibit a better phase behavior than most centered schemes. In the second part, the Coriolis factor is considered and the Rossby modes are studied. In this case, all selected upwind schemes lead to a severe damping. The numerical results are also compared with those obtained by using a slope limiter approach. It is concluded that most upwind schemes with or without slope limiters present poor result for an accurate calculation of the Rossby modes.*

Keywords: finite volume method; upwind schemes, shallow-water equations; gravity waves; Rossby waves

1- Introduction

Finite volume schemes are well known due to their inherent conservation properties. In addition, upwind finite volume schemes have become popular for hyperbolic systems during the past two decades due to their ability to capture discontinuities with a low level of numerical diffusion and oscillations. For these methods, the critical stage is the calculation of the numerical flux and various schemes have been developed based on different approaches for estimation of numerical fluxes (see e.g. Leveque, 2002 and Toro, 2000).

Upwind finite volume schemes use the characteristic information of the hyperbolic system to calculate numerical fluxes. In the case of the scalar advection equation, this simply leads to a biased discretization of the equation in the flow direction. However, this is not the case for coupled systems, such as the shallow water equations. This is because the flow direction is not the only factor in the calculation of the numerical fluxes. In fact, for coupled systems, the flux vector must be decomposed in the basis of eigenvectors and then each component is calculated in an upwind manner based on the sign of the corresponding eigenvalue.

An extensive research has been dedicated to the study of upwind schemes for shallow water systems, especially in the convection dominated cases, i.e. for hyperbolic formulations (see e.g. Toro, 2000). Upwind finite volume schemes have been successfully employed for the simulation of some challenging problems for shallow flows such as dam break flows and supercritical flows over spillways (e.g. Mohammadian et. al., 2005 and 2006 and Lai et. al. 2005).

Fourier analysis is a useful tool to study the effect of discrete schemes on some quantities such as wave amplitude, phase speed and group velocity. The analytical form of those quantities should be preserved by an ideal numerical method. Further, the Fourier analysis may give guidelines for a proper selection of numerical parameters such as the CFL number. Note that the Fourier analysis has been applied to the discretized form of the shallow water equations using finite difference (e.g. Batteen and Han, 1981, Wajsowicz 1986, Neta and Williams,1989, Randall, 1994, Adcroft et. al., 1999, Sankaranarayanan and Spaulding, 2003), and finite element methods (Foreman, 1984, Walters and Carrey, 1983, Atkinson et. al., 2004, Le Roux et. al. , 2006a and b). The dispersion relation for the least-squares mixed formulation of the shallow-water equations has also been analyzed by Le Roux and Carey (2004) and the results are compared with those of the Galerkin scheme. They concluded that the method should be used with care particularly for long term simulations due to its inherent numerical damping.

The discretization of the shallow water system using upwind schemes has been rarely studied by the Fourier analysis. This is because slope/flux limiters are inherent to most

upwind formulations and cannot be included in a Fourier-type analysis. Gosaard and Kolar (2003) have numerically studied the phase and damping errors of some slope limiters. However, such a study can only be performed for a few sets of parameters due to the excessive amount of required numerical computations.

Gosaard and Kolar (2000) also performed Fourier and dispersion analyses of the first order upwind finite volume scheme for the shallow water equations, where slope limiters are not involved. They have concluded that this scheme exhibits a good phase behavior. In addition, due to the inherent conservation of finite volume schemes, the work of Gosaard and Kolar (2000) motivates the study of higher order upwind finite volume schemes. Moreover, such a study is also necessary because, as shown in the following, the use of slope limiters is not necessarily recommended for all types of waves. Indeed, shallow water equations permit two types of waves, fast gravity and slow Rossby modes. The later, are due to the earth rotation, and usually need to be computed quite accurately (Vreugdenhil, 1994). This is because most energy transfer in the ocean scale is due to these waves. As shown later, the amplitude of the Rossby modes is considerably damped by the use of slope limiters in upwind finite volume schemes, which has not been reported earlier in the literature, up to our knowledge. Note that the study of Gosaard and Kolar (2000) is only concerned with the propagation of gravity waves. Such waves are important for small scale flows, e. g. estuaries, but not for large scale flows such as global ocean circulation. Indeed, unless an accurate representation of the fast modes is important, gravity waves may be regarded as small amplitude noise superimposed on the slow solution and they can be justifiably retarded or damped, which is usually the case in ocean modeling.

The present paper is dedicated to dispersion and Fourier analyses of high order upwind finite volume schemes and it is organized as follows. The model equations for the pure gravity waves are introduced in Section 2. Various finite volume schemes are presented in Section 3 for these waves with the Fourier analysis results. The model equations for Rossby waves are then introduced in Section 4 and a Fourier analysis is also performed. Some numerical test cases are presented in section 5 and concluding remarks complete the study.

2-Model problem for gravity waves

The one-dimensional, inviscid, linearized form of the shallow-water equations may be expressed in Cartesian coordinates (Vreugdenhil, 1994) as :

$$\eta_t + H u_x = 0, \quad (1)$$

$$u_t + g\eta_x = 0, \quad (2)$$

where u is the velocity variable, η is the surface elevation with respect to the reference level $z = 0$, g is the gravitational acceleration and the mean depth H is assumed constant.

In the present analysis, (1)-(2) are solved on an infinite channel (i.e., with periodic boundary conditions) subject to initial conditions. The system (1)-(2) could be written in the following conservative vector form

$$\frac{\partial \vec{U}}{\partial t} + \frac{\partial \vec{F}}{\partial x} = 0,$$

where

$$\vec{U} = \begin{bmatrix} \eta \\ u \end{bmatrix},$$

and

$$\vec{F} = \begin{bmatrix} Hu \\ g\eta \end{bmatrix} \quad (1)$$

We can also write the system in the following non-conservative form

$$\frac{\partial \vec{U}}{\partial t} + A\frac{\partial \vec{U}}{\partial x} = 0, \quad (2)$$

where

$$A = \begin{bmatrix} 0 & H \\ g & 0 \end{bmatrix}, \quad (3)$$

The matrix A has two real eigenvalues given by

$$\lambda_1 = \sqrt{gH}$$

$$\lambda_2 = -\sqrt{gH}$$

and the following corresponding eigenvectors:

$$\vec{e}_1 = \begin{bmatrix} 1 \\ +\sqrt{g/H} \end{bmatrix} \tag{4}$$

and

$$\vec{e}_2 = \begin{bmatrix} 1 \\ -\sqrt{g/H} \end{bmatrix} \tag{5}$$

The matrix A is decomposed as

$$A = PDP^{-1}$$

where

$$D = \begin{bmatrix} \lambda_1 & 0 \\ 0 & \lambda_2 \end{bmatrix}, \tag{6}$$

and P is the matrix including the eigenvectors of A as

$$P = [\vec{e}_1, \vec{e}_2], \tag{7}$$

Define

$$D^+ = \begin{bmatrix} \max(\lambda_1, 0) & 0 \\ 0 & \max(\lambda_2, 0) \end{bmatrix}, \tag{8}$$

$$D^- = D - D^+, \tag{9}$$

or

$$D^+ = \begin{bmatrix} \sqrt{gH} & 0 \\ 0 & 0 \end{bmatrix}, \tag{10}$$

$$D^- = \begin{bmatrix} 0 & 0 \\ 0 & -\sqrt{gH} \end{bmatrix}, \tag{11}$$

and

$$|D| = \begin{bmatrix} |\lambda_2| & 0 \\ 0 & |\lambda_2| \end{bmatrix}. \tag{12}$$

Therefore, the matrix A is decomposed as

$$A = A^+ + A^-, \tag{13}$$

where

$$A^+ = PD^+P^{-1}, \tag{14}$$

and

$$A^{-} = PD^{-}P^{-1}. \tag{15}$$

3-Numerical algorithm

In the finite volume method, the equations are integrated in each computational cell. This leads to

$$\int_{\Omega_c}(\frac{\partial \vec{U}}{\partial t}+\frac{\partial \vec{F}}{\partial x})dx = 0, \tag{16}$$

where Ω_c represents the area of a control volume. The divergence theorem is then employed to replace the volume integral by a surface one:

$$\frac{d}{dt}\int_{\Omega_c}\vec{U}dx+\int_{\Gamma_c}\vec{F}.\vec{n}d\Gamma_c = 0, \tag{17}$$

where Γ_c represents the boundary of a control volume, and $\vec{n}$ is its unit outward normal vector. For the one dimensional case (17) is rewritten as

$$\frac{d}{dt}\vec{U}_j(t) = -\frac{\vec{F}_{j+1/2}(t)-\vec{F}_{j-1/2}(t)}{\Delta x} \tag{18}$$

where $\vec{U}_j(t)$ represents the cell averaged value of conserved variables and $\vec{F}_{j+1/2}(t)$ is the numerical flux. For the various numerical schemes employed in this study, the corresponding numerical fluxes (see e.g. Toro, 2000) are given in the following.

For the centered scheme we have,

$$\vec{F}_{j+1/2} = 0.5(\vec{F}_{j+1}+\vec{F}_j) \tag{19}$$

The first order upwind scheme (1st) gives

$$\vec{F}_{j+1/2} = A^{+}\vec{U}_{j+1}+A^{-}\vec{U}_j \tag{20}$$

or equivalently

$$\vec{F}_{j+1/2} = 0.5(\vec{F}_{j+1}+\vec{F}_j)-0.5\,|A|\left(\vec{U}_{j+1}-\vec{U}_j\right) \tag{21}$$

where

$$|A| = P\,|D|\,P^{-1}$$

In (25), the first order upwind flux is equal to the centered flux in (23) plus an artificial diffusive flux, which stabilize the numerical scheme. Higher order schemes may be

constructed by calculating the interface values more accurately, e.g. as in the κ scheme. In this method, which includes a family of schemes, the numerical flux is calculated as

$$\vec{F}_{j+1/2} = 0.5(\vec{F}^{L}_{j+1/2} + \vec{F}^{R}_{j+1/2}) - 0.5\,|A|\,(\vec{U}^{L}_{j+1/2} - \vec{U}^{R}_{j+1/2}),$$

where the superscripts $.^{R}$ and $.^{L}$ represent the evaluation of the right and left sides of the interface, respectively, with

$$\vec{F}^{L}_{j+1/2} = \vec{F}(\vec{U}^{L}_{j+1/2}),$$

$$\vec{F}^{R}_{j+1/2} = F(\vec{U}^{R}_{j+1/2}),$$

and the interface values $\vec{U}^{L}_{j+1/2}$ and $\vec{U}^{R}_{j+1/2}$ are calculated at the interface $j+\frac{1}{2}$ as

$$\vec{U}^{L}_{j+1/2} = \vec{U}_{j} + \frac{1}{4}\Big((1-\kappa)(\vec{U}_{j} - \vec{U}_{j-1}) + (1+\kappa)(\vec{U}_{j+1} - \vec{U}_{j})\Big),$$

$$\vec{U}^{R}_{j+1/2} = \vec{U}_{j+1} - \frac{1}{4}\Big((1-\kappa)(\vec{U}_{j+2} - \vec{U}_{j+1}) + (1+\kappa)(\vec{U}_{j+1} - \vec{U}_{j})\Big).$$

Depending on the value of κ, the method leads to the following schemes:

$$\kappa = \begin{cases} -1, & second\ order\ upwind, \\ 0, & simplified\ Fromm\ \ scheme, \\ 1/6, & cell-based\ third\ order\ upwind, \\ 1/3, & third\ order\ upwind, \\ 1/2, & Quick\ scheme, \\ 1, & centered\ scheme, \end{cases}$$

Among the schemes given above, the centered and second order upwind (2nd) schemes are well documented in the literature (see e.g. Leveque, 2002), the Quick scheme is a simplified version of the method presented in Leonard (1979) where the third order upwind scheme (3rd) is also introduced, and the Fromm scheme is a limiting case of the method proposed in Fromm (1968).

The cell-based (formally) third order accurate discretization (3rdCell) in a 1D problem, which is introduced here for the first time to our knowledge, is obtained by fitting a cubic curve over four consecutive computational cells such that the total mass of each cell is correctly represented by the corresponding cubic curve for each conserved variable, i.e.

$\int_{x_{i-1/2}}^{x_{i+1/2}} \vec{U}(x)dx = \vec{U}_i \Delta x$ for $i = j-2, j-1, j, j+1$. An upwind polynomial fitting is performed by using two cells at the upstream side of the interface and one cell in the downstream side. The interface value is then adjusted such that the following condition is satisfied:

$$\left.\frac{\partial \vec{U}(x)}{\partial x}\right|_{x=x_j} = \frac{\vec{U}^L_{j+1/2} - \vec{U}^L_{j-1/2}}{\Delta x}.$$

This leads to the following interface value

$$\vec{U}^L_{j+1/2} = \frac{1}{24}(7\vec{U}_{j+1} + 22\vec{U}_j - 5\vec{U}_{j-1}). \tag{24}$$

In a similar way, but for the downwind polynomial fitting, we obtain:

$$\vec{U}^R_{j+1/2} = \frac{1}{24}(-5\vec{U}_{j+2} + 22\vec{U}_{j+1} + 7\vec{U}_j). \tag{25}$$

Note that the cell-based third order accurate method may be written in the κ scheme form, for $\kappa = 1/6$.

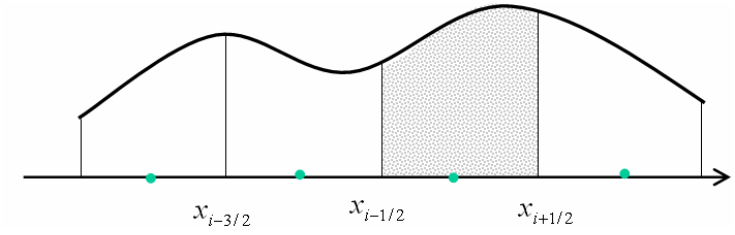

Figure 1. Polynomial fitting for the 3rdCell scheme. A cubic curve is fitted such that the mass is conserved in four consecutive cells.

4-Fourier analysis for the spatial discretization schemes

Substituting periodic solutions of the form $u = Re\left[\tilde{u}e^{i(kx+\omega t)}\right]$ and $\eta = Re\left[\tilde{\eta}e^{i(kx+\omega t)}\right]$ into (1) and (2), where $\tilde{u}$ and $\tilde{\eta}$ are amplitudes, k is the wave number in the x- direction and ω is the angular frequency, we obtain

$$\begin{pmatrix} \omega & gk \\ Hk & \omega \end{pmatrix}\begin{pmatrix} \tilde{\eta} \\ \tilde{u} \end{pmatrix} = 0 \tag{28}$$

By noting that the determinant of the matrix in the left hand side of (28) must be zero for a

nontrivial solution, an equation for the frequency or the so-called dispersion relation is obtained

$$\omega^2 - gHk^2 = 0. \tag{29}$$

The two solutions $\omega = \pm\sqrt{gH}\,k$, correspond to the free-surface gravitational modes. The gravity waves can propagate along the $-x$ axis in both directions at a speed $\omega/k = \sqrt{gH}$, independently of the wave number k, and hence there is no dispersion of the waves.

Phase (C) and group (G) velocities are then calculated using

$$C := \frac{\omega_r}{k} \tag{22}$$

$$G := \frac{\partial \omega_r}{\partial k} \tag{23}$$

where ω_r represents the real part of ω. For the analytical case, we obviously have

$$\omega_r = \omega$$

As for the continuum case, the dispersion relation for the discrete scheme is found through a Fourier expansion. The discrete solutions corresponding to $(\eta_j, u_j) = \mathrm{Re}\left[(\tilde{\eta}, \tilde{u})e^{i(kx_j + \omega t)}\right]$ are sought at node j ($j = 1,2,3\ldots$), where (η_j, u_j) are the nodal unknowns that appear in the selected discrete equations and $(\tilde{\eta}, \tilde{u})$ are amplitudes. The x_j coordinates are expressed in terms of a distance to a reference node. Substitution in the discrete equations leads to a square matrix system for the Fourier amplitudes as

$$\begin{bmatrix} i\omega + d^-\sqrt{gH}/2\Delta x & Hd^+/2\Delta x \\ gd^+/2\Delta x & i\omega + d^-\sqrt{gH}/2\Delta x \end{bmatrix} \begin{bmatrix} \tilde{\eta} \\ \tilde{u} \end{bmatrix} = \begin{bmatrix} 0 \\ 0 \end{bmatrix},$$

with

$$d^+ = 2i\sin(k\Delta x),$$

$$d^- = 2 - 2\cos(k\Delta x),$$

for the first order upwind scheme , and

$$d^+ = i\left((3-\kappa)\sin(k\Delta x) - (1/2 - \kappa)\sin(2k\Delta x)\right),$$

$$d^- = \left((3-\kappa) + (4\kappa - 4)\cos(k\Delta x) - (\kappa - 1)\cos(2k\Delta x)\right)/2,$$

for the κ scheme. The dispersion relation is then obtained by setting the determinant of the matrix system to zero, and this leads to

$$\left(i\omega + d^{-}\sqrt{gH}/2\Delta x\right)^2 = gH\left(d^{+}/(2\Delta x)\right)^2$$

The resulting equations for the frequency for the first order upwind scheme is written as (Gossard and Kolar, 2000)

$$\omega = c\sin(k\Delta x) \pm i(c(\cos(k\Delta x) - 1) + 1), \quad (24)$$

and for the κ scheme we obtain

$$\omega = \frac{\sqrt{gH}}{4}\left(\sin(k\Delta x)(-6 + 2\kappa) + \sin(2k\Delta x)(1-\kappa) \pm i(3 - 4\cos(k\Delta x) + \cos(2k\Delta x))(1-\kappa)\right),$$

(25)

An ideal numerical scheme, should present similar dispersion relation to the continuous mode in (1). A monotonic curve for $\omega(k)$ indicates that the numerical solution is free of spurious $2\Delta x$ oscillations (Platzman, 1981).

Usually, numerical models are setup (Foremann, 1982) such that the desired wavelengths are resolved at least by 20 cells (i.e. $k\Delta x/\pi \le 0.1$). Therefore, in the following, the range $k\Delta x/\pi \le 0.1$ will be referred as the region of interest. The remaining region generally is concerned with the shorter waves, which do not transfer much energy. However, phase error for these waves, particularly for the $2\Delta x$ waves, could lead to oscillatory results, unless they are effectively damped. Indeed, it is expected that the numerical scheme preserves the amplitude of the waves, i.e. zero damping error. This is the case, when all wave numbers are transferred with a correct speed. However, zero damping error is not always desirable. This is because, most schemes have phase speed errors for high frequencies and hence, it is desirable to damp them in this case. This damping does not seriously affect the whole numerical simulation because most energy is transferred via waves of intermediate and small wave numbers rather than high frequency waves.

The numerical results for $Re(\omega)$ are plotted in Figure 1a. All selected numerical methods lead to a folded dispersion plot implying potential aliasing problems since two separate

wave vectors can contribute to the same frequency (Platzman, 1981). For all schemes, the wave vector space is truncated at $k\Delta x = \pi$ due to the special discretization limitation since the maximum resolvable wavelength is $2\Delta x$. Of fundamental importance is the observation that waves of length $2\Delta x$ correspond to $\omega = 0$ and hence, those waves do not propagate because their phase speed is zero. For most numerical schemes, the cutoff frequency corresponds to zero group velocities and maximum frequencies. In Figures 1a,c, the cutoff frequency is ranging from $\pi/2$ to $\pi - \cos^{-1}\left(-\frac{1}{2}+\frac{\sqrt{3}}{2}\right)$ or approximately 0.6194π and those values correspond to the first and second order upwind schemes, respectively. The Fromm scheme gives the best approximation for the frequency before the cutoff. The second order upwind scheme overestimates the frequency while the remaining schemes underestimate it. However, it should be stressed that the temporal scheme may have a significant impact on the dispersion relation (see e.g. Beckers and Deleersnijder, 1993), this will be examined in the next section. It should be also mentioned that the cell-based third order upwind scheme gives better results than the classical (point-wise) third order upwind method for the frequency. The former, gives here intermediate results between the 3rd and Fromm schemes.

The results concerning phase and group velocities and damping are presented in Figures 1b,c,d. It is observed that the 3rdcell and Fromm schemes give very close phase and group velocities. However, the 3rdcell has better phase and group velocities than the Fromm scheme in the region of interest, as shown in Figure 2, because the former method has results closer to the analytical ones. Moreover, in Figure 1d, the 3rdcell appears less diffusive than the Fromm scheme. Hence, by considering phase and group velocities and damping, the 3rdcell may be preferred to the Fromm scheme at this stage of the argument. Finally, the Quick method leads to significant phase error with little damping, and the third order scheme, has results between the Quick and 3rdcell schemes.

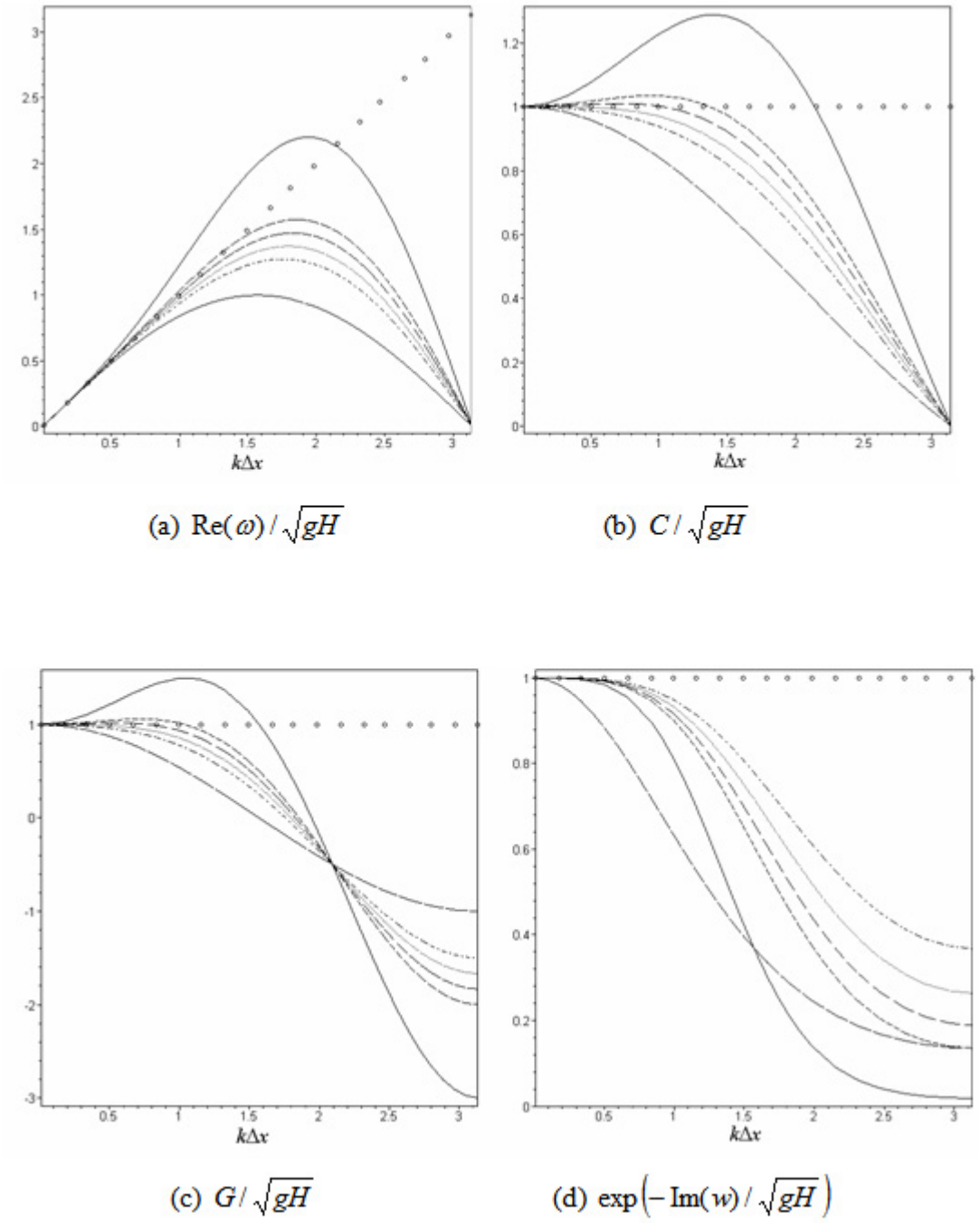

Fiugure 2. Various numerical properties of different spatial discretization schemes; (a) frequency, (b) phase speed, (c) group velocity, (d) damping.

Exact ∘, 1st——, 3rdCell——, Quick – – –, Fromm – – –, 3rd·····, 2nd——

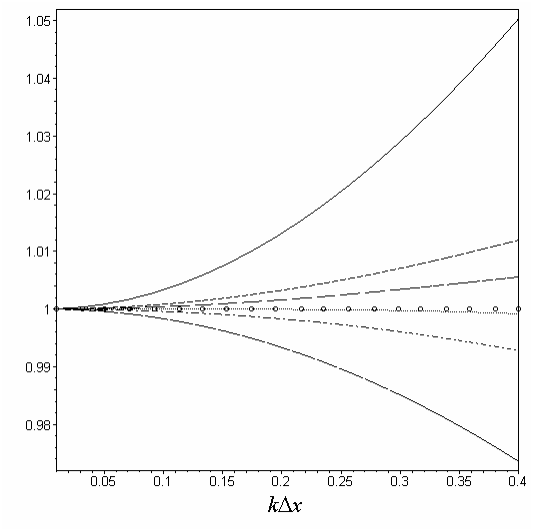

Fiugure 3. Phase velocity $C/\sqrt{gH}$ for various spatial discretization schemes in the region of interest.

Exact ∘, 1st——, 3rdCell——, Quick – – – –, Fromm – – – –, 3rd·····, 2nd——

5-Temporal discretization

At a given time step $\Delta t = t^{n+1} - t^n$ we employ a general time discretization of (2) of the form

$$u_j^{n+1} + \frac{\Delta t}{\Delta x}\sigma\left(F_{j+1/2}^{n+1} - F_{j-1/2}^{n+1}\right) = u_j^n + \frac{\Delta t}{\Delta x}(1-\sigma)\left(F_{j+1/2}^n - F_{j-1/2}^n\right) \qquad (26)$$

where σ is a real parameter such that $0 \le \sigma \le 1$. Observe that the standard choices $\sigma = 0,1/2,1$ yield the respective forward Euler, trapezoidal Crank-Nicolson and backward Euler type schemes. Other choices such as Runge Kutta schemes are possible, but they would make the present stability/dispersion analysis much less tractable.

6-Fourier analysis for the fully discretized schemes

A Fourier analysis is now conducted for both spatial and temporal schemes. By substituting periodic solutions of the form $(\eta_j^n, u_j^n) = \mathrm{Re}\left[(\tilde{\eta}, \tilde{u})e^{i(kx_j + \omega t^n)}\right]$ into (26), we obtain

$$\begin{bmatrix} E-1+ad^{-}(\sigma E+1-\sigma) & Hbd^{+}(\sigma E+1-\sigma) \\ gbd^{+}(\sigma E+1-\sigma) & E-1+ad^{-}(\sigma E+1-\sigma) \end{bmatrix} \begin{bmatrix} \tilde{\eta} \\ \tilde{u} \end{bmatrix} = \begin{bmatrix} 0 \\ 0 \end{bmatrix},$$

with $a = \sqrt{gH}\,\Delta t/(2\Delta x)$, and $b = \Delta t/(2\Delta x)$.

An equation for the propagation factor (defined by $E := e^{i\omega\Delta t}$) is then obtained by setting the determinant of the coefficients to zero for a nontrivial solution. The resulting equations for the propagation factor, for the first order and the κ schemes, lead to

$$E = \frac{1+i\omega\,(1-\sigma)}{1-i\omega\,\sigma}, \tag{27}$$

where ω denote the frequencies corresponding to the first order and the κ schemes in (26) and (25), respectively. The amplification factor ($|E|$), the group velocity, the frequency (real part) and the phase speed ratio have been plotted in Figure 2 for the schemes examined here. The phase speed ratio is defined as the ratio of the computed phase speed to the analytical one. It should be mentioned that except for the first order upwind scheme, which remains stable even for a fully explicit time-discretization scheme ($\sigma = 0$), all other schemes may lead to unstable results ($|E| > 1$) for $\sigma = 0$, as shown graphically in Figure 3.

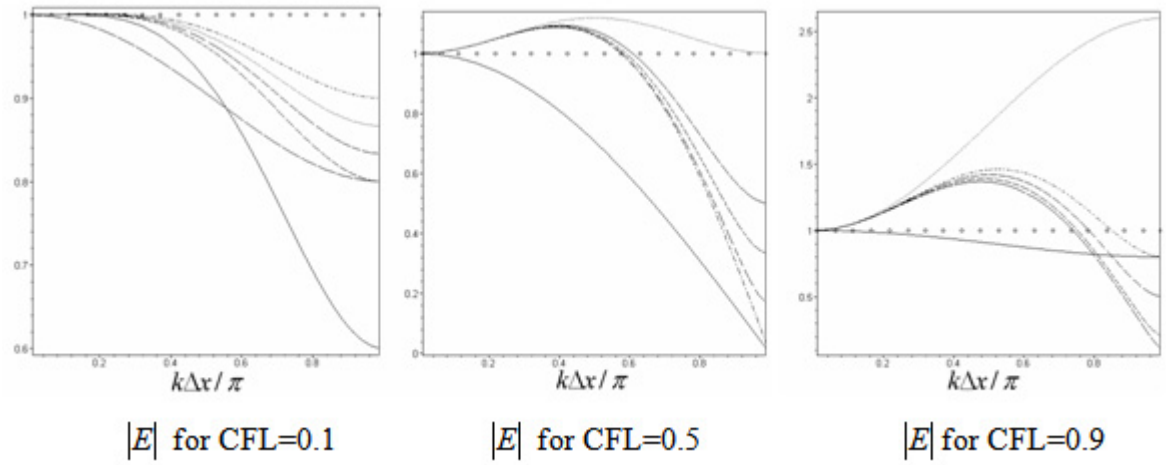

Figure 3. Amplification factor for $\sigma = 0$.

Exact ∘, 1st——, 3rdCell——, Quick – – –, Fromm – – –, 3rd……, 2nd——

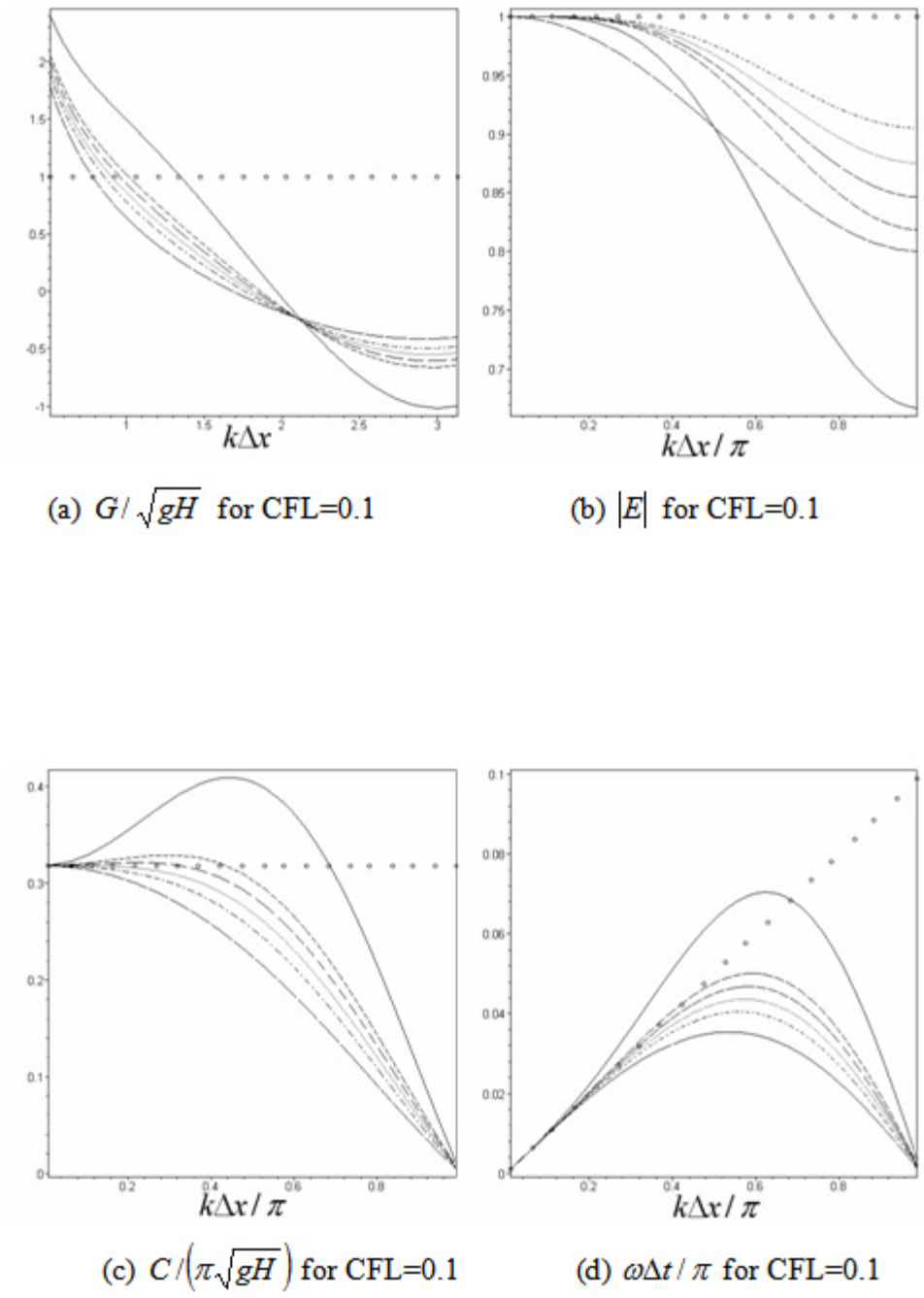

(a) $G/\sqrt{gH}$ for CFL=0.1 (b) $|E|$ for CFL=0.1

(c) $C/\left(\pi\sqrt{gH}\right)$ for CFL=0.1 (d) $\omega\Delta t/\pi$ for CFL=0.1

Figure 4- Various numerical properties of the fully discretization schemes.

Exact ∘, 1st—— ——, 3rdCell——— , Quick – – – –, Fromm ·– – – –, 3rd·····, 2nd——

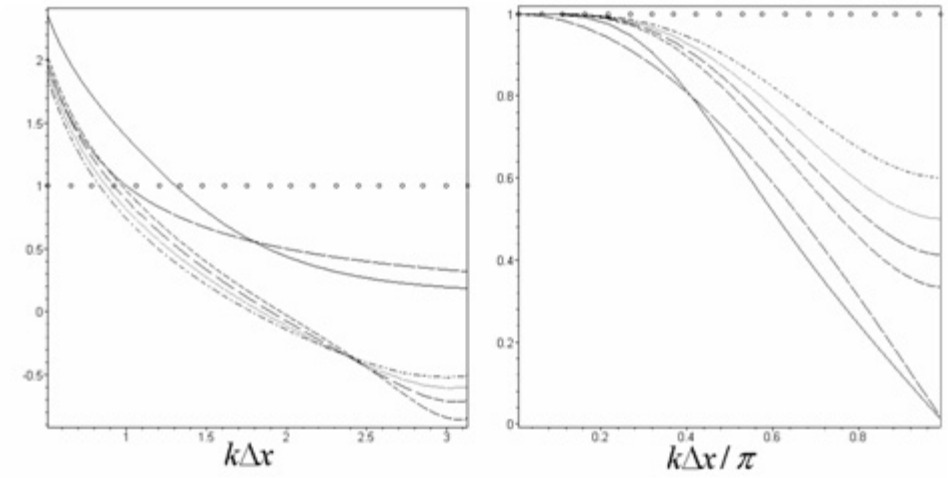

(e) $G/\sqrt{gH}$ for CFL=0.5 (f) $|E|$ for CFL=0.5

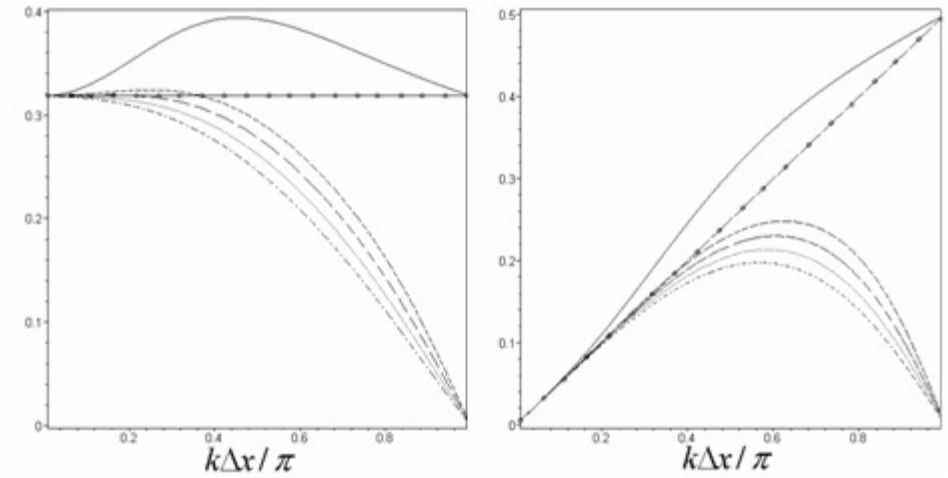

(g) $C/\left(\pi\sqrt{gH}\right)$ for CFL=0.5 (h) $\omega\Delta t/\pi$ for CFL=0.5

Figure 4- (Continue)

Exact ∘, 1st—— ——, 3rdCell———— , Quick – – - -, Fromm - - - -, 3rd……, 2nd——

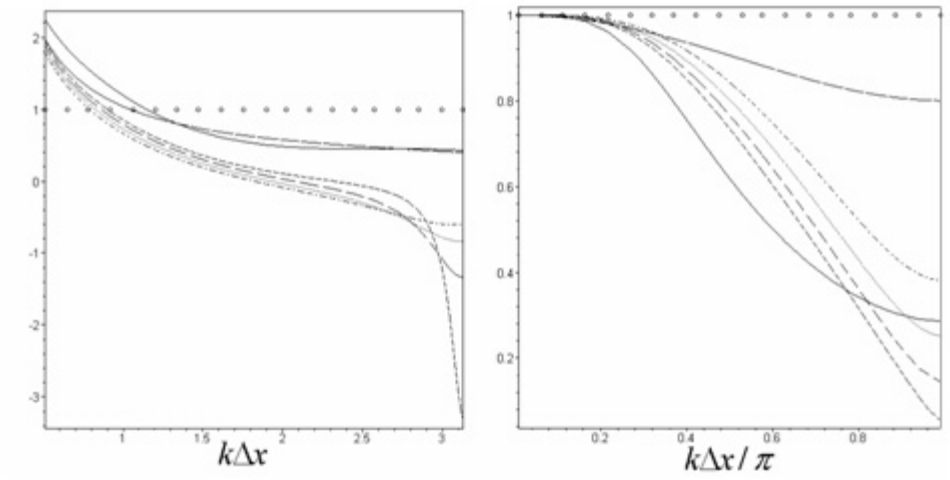

(i) $G/\sqrt{gH}$ for CFL=0.9 (j) $|E|$ for CFL=0.9

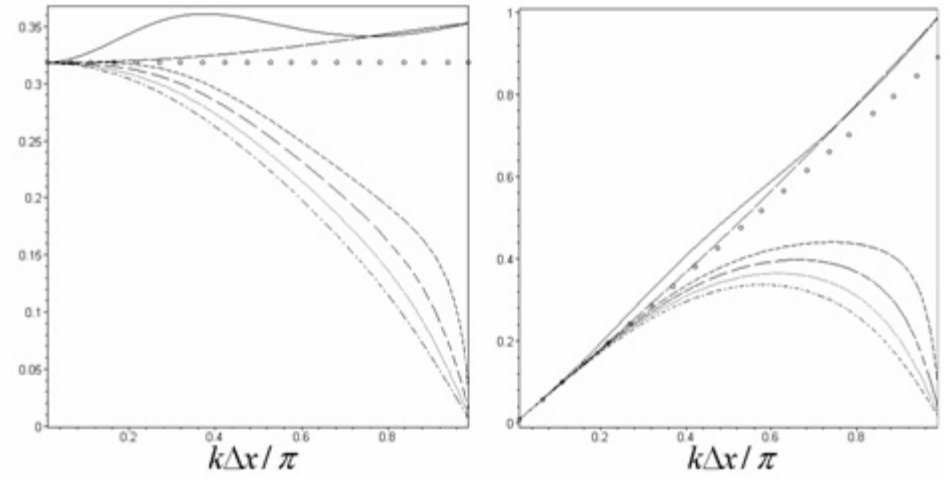

(k) $C/\left(\pi\sqrt{gH}\right)$ for CFL=0.9 (l) $\omega\Delta t/\pi$ for CFL=0.1

Figure 4- (Continue)

Exact ∘, 1st — —, 3rdCell— — — , Quick – – – –, Fromm – – – –, 3rd·····, 2nd——

Hence, for stability reasons, a Crank-Nicholson scheme is used for the κ scheme. However, for the first order upwind scheme, a fully explicit method is employed because the use of a

Crank-Nicholson scheme would bring an excessive damping. Moreover, for σ ranging from $1/2$ to 1 we also observe (results not shown) a significant damping for the κ scheme. Consequently, the graphics shown in Figure 4 have been obtained using $\sigma = 0$ for the first order upwind scheme and $\sigma = 1/2$ for the κ scheme.

Based on the Fourier analysis results, it is concluded that the numerical performance of upwind schemes highly depends on the CFL number. For CFL<0.5, e.g. in Figure 4d for CFL=0.1, all the curves are folded, and waves of wavelength $2\Delta x$ (i.e. $k\Delta x = \pi$) do not propagate and are stationary. For CFL$\geq$0.5, as shown in Figures 4h,l, the curves corresponding to the first and second order methods are no longer folded and they are closed to the monotonic continuous solution. In particular, for CFL=0.5, the first order upwind scheme exactly coincide with the analytical frequency and phase speed. However, both schemes have other serious drawbacks. Indeed, in the region of interest ($k\Delta x < \pi/10$), the first order upwind scheme leads to an excessive damping and both schemes show a significant group velocity error. Therefore, the first order and the second order upwind schemes will no longer be considered in the following.

The remaining schemes (i.e. 3rdCell, 3rd, Fromm and Quick) are now studied in more details, as the HOA (High Order Accurate) schemes. Since the performance of the HOA methods is improved as the CFL number increases regarding the phase speed and the frequency, and for all wave numbers, only high CFL numbers are considered in the following. Note the cutoff frequency is progressively increasing as the CFL number increases as shown in Figures 4d,h,l. In this respect, the Fromm scheme exhibits the best behavior and the Quick one is the worst. Similar conclusions have already been drawn for the semi discrete case.

The Fromm and the 3rdCell schemes have the most accurate phase speed, for high CFL numbers, as shown in Figure 4,k. Although they lead to zero phase speed for $2\Delta x$ waves, they also induce a significant damping for those waves. Therefore, these schemes are expected to give less oscillatory results than the others. In particular, the 3rdCell scheme gives better phase speed results in the region of interest than the Fromm one, whatever the

CFL is.

However, considering the group velocity and the damping errors, the Quick scheme exhibits the best results while the Fromm scheme has the largest errors, as shown in Figures 4i,j. In particular, the Fromm scheme shows a significant group velocity error for $2\Delta x$ waves at high CFL numbers. This is because the phase speed curve presents a sharp gradient for the $2\Delta x$ waves**.** However, this may not be an impediment since energy transfer, via the group velocity, is mostly done by long waves rather than short ones. Recall that energy is transferred at the group velocity. Again, for all HOA schemes, the group velocity accuracy is improved as the CFL increases in the region of interest.

The 3rdcell and 3rd schemes give intermediate results between those of the Quick and Fromm schemes as shown in Figure 4. The 3rdCell scheme always exhibits results closer to the Fromm ones. This was largely expected from the corresponding values of κ. The 3rdCell scheme appears to be a good choice compared to the Fromm method at this stage of the argument. Both schemes behave similarly in most cases. However, the 3rdCell method gives better group velocity results. It should be stressed that, none of the selected schemes could be considered as the "best" one since this choice largely depends on which quantity (frequency, damping, phase and group velocities) is more important regarding the physical problem at hand.

After having discussed the propagation of pure gravity waves, we now consider the Coriolis parameter. In the following we are particularly interested in the dissipative effects for Rossby waves in ocean and atmosphere modeling applications.

7-Model problem and modal behavior for Rossby modes

When the Coriolis term is taken into account, the one-dimensional, inviscid, linearized form of the shallow-water equations may be expressed in Cartesian coordinates (Vreugdenhil, 1994) as:

$$\eta_t + H u_x = 0, \tag{35}$$

$$u_t - f v + g \eta_x = 0, \tag{36}$$

$$v_t + fu = 0, \tag{37}$$

where the Coriolis parameter f is assumed constant.

Periodic solutions of the form $u = \tilde{u}e^{i(kx+\omega t)}$, $v = \tilde{v}e^{i(kx+\omega t)}$ and $\eta = \tilde{\eta}e^{i(kx+\omega t)}$ are sought again and we obtain

$$\begin{pmatrix} i\omega & iHk & 0 \\ igk & i\omega & -f \\ 0 & f & i\omega \end{pmatrix}\begin{pmatrix} \tilde{\eta} \\ \tilde{u} \\ \tilde{v} \end{pmatrix} = 0. \tag{39}$$

Letting the determinant of the matrix in the left hand side of (39) equal to zero to obtain non-trivial solution leads to

$$\omega\left(\omega^2 - f^2 - gHk^2\right) = 0 \tag{40}$$

The two first roots $\omega = \pm\sqrt{f^2 + gHk^2}$ correspond to inertia-gravity modes and the third one, $\omega = 0$, is the geostrophic mode and it would correspond to the slow Rossby mode on a β-plane.

The finite volume method and the temporal scheme (presented in Section 5), are again employed to obtain the discrete form of (35)-(37). The discretization of (35) exactly coincides with the pure gravity waves case. Equation (37) only contains a source term (fu) and it is discretized as

$$v_j^{n+1} = v_j^n - \gamma\Delta t f u_j^{n+1} - (1-\gamma)\Delta t f u_j^n, \tag{41}$$

with $0 \le \gamma \le 1$. In this study, based on numerical experiments, a fully implicit case for the Coriolis term ($\gamma = 1$) has been chosen. The case $\gamma = 1/2$ leads to similar damping while producing more oscillations. Finally, in (36) all fluxes are basically calculated as for pure gravity waves case, but now with the Coriolis term $(-fv)$ treated as the source term (fu) in (41). Again, the first order upwind and the κ schemes are used in the following.

A Fourier analysis is conducted at the discrete level, by substituting periodic solutions of the form $(\eta_j^n, u_j^n, v_j^n) = \mathrm{Re}\left[(\tilde{\eta}, \tilde{u}, \tilde{v})e^{i(kx_j+\omega t^n)}\right]$ into discretized form of (26-37). This leads to a square 3×3 matrix system for the wave amplitudes as

$$\begin{bmatrix} E-1+ad^{-}(\sigma E+1-\sigma) & Hbd^{+}(\sigma E+1-\sigma) & 0 \\ gbd^{+}(\sigma E+1-\sigma) & E-1+ad^{-}(\sigma E+1-\sigma) & -f\Delta t(\gamma E+1-\gamma) \\ & f\Delta t(\gamma E+1-\gamma) & E-1 \end{bmatrix} \begin{bmatrix} \tilde{\eta} \\ \tilde{u} \\ \tilde{v} \end{bmatrix} = \begin{bmatrix} 0 \\ 0 \\ 0 \end{bmatrix},$$

A cubic equation for the propagation factor E is then obtained by setting the determinant of the matrix system to zero. Two roots are complex conjugate and correspond to inertia-gravity modes. For these modes, $|E|$ is graphed in Figure 5,a with CFL=0.9 and $f\Delta t = 0.1$. The results are basically similar to those of the pure gravity waves case (Figure 4,f), with a shift depending on $f\Delta t$.

The third root is real and corresponds to the slow mode, the Rossby mode. $|E|$ is graphed for this mode with CFL=0.9 and $f\Delta t = 0.1$ in Figure 5,b for the first order and κ schemes. It should be mentioned that, for Rossby waves, the κ scheme is less sensitive to the CFL number than the first order upwind scheme. Therefore, only the results for CFL=0.9 are shown in Figure 5,b. The Quick scheme shows less damping than the other methods in the region of interest, while the first and second order upwind schemes, lead to the highest level of damping. However, all schemes examined in Figure 5,b exhibit a high level of damping for the Rossby mode. The observed level of damping should occur at each time-step in a numerical simulation, and would lead to an excessive damping for long term simulations. Indeed, a high order spatial accuracy is usually desirable for the treatment of the slow Rossby modes, and has proven practical and beneficial for atmospheric and oceanic prediction models.

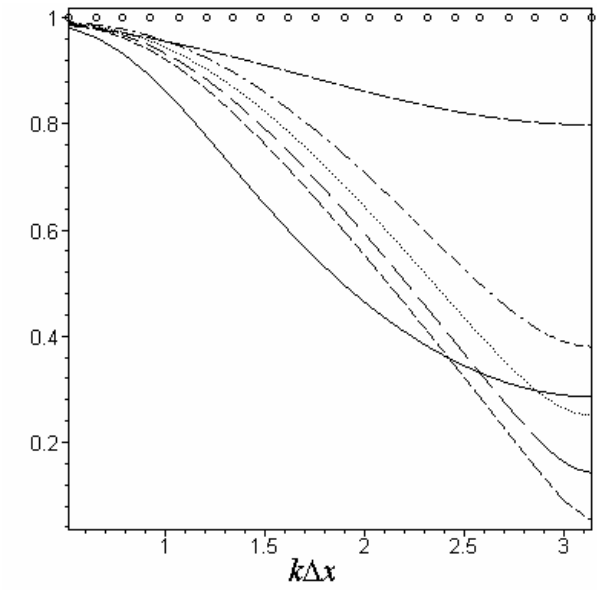

Figure 5,a. Damping error $|E|$ of inertial gravity waves for various schemes.

Exact ∘, 1st——, 3rdCell——, Quick – – – –, Fromm – – – –, 3rd……, 2nd——

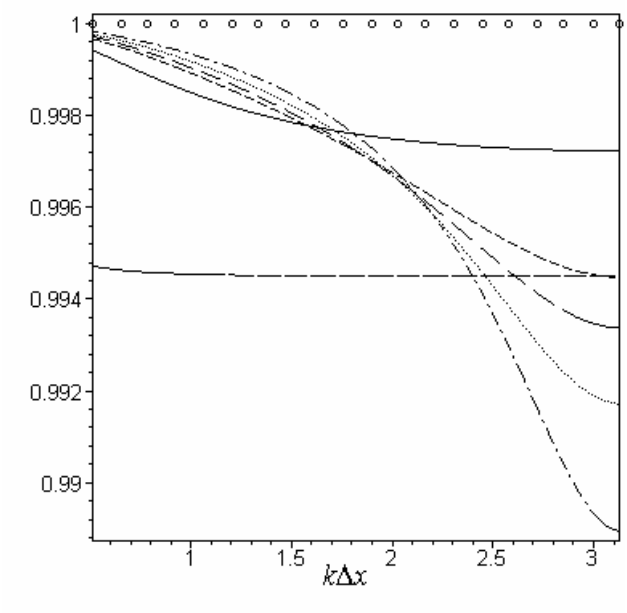

Figure 5,b- Damping error $|E|$ of fully discretization for various schemes for the Rossby waves.

Exact ∘, 1st—— ——, 3rdCell———— , Quick – – - – -, Fromm - - - -, 3rd……, 2nd——

8-Numerical results

In the following, the Fourier analysis results obtained in the previous section for the Rossby modes are computationally verified by considering two numerical tests. The first one is concerned with a single wave solution while the second test corresponds to a Gaussian initial condition. In both cases periodic boundary conditions are used and (35)-(37) are numerically solved to examine the level of damping induced by the first order and κ schemes.

8-1- Stationary wave solution

The wave solution of (35)-(37) corresponding to the geostrophic mode is

$$\eta = \tilde{\eta}\cos(kx)\,, \tag{41}$$

$$u = 0\,, \tag{42}$$

$$v = -\frac{gk}{f}\tilde{\eta}\sin(kx)\,. \tag{43}$$

Equations (41)-(43) are used here as the initial condition with $\tilde{\eta} = 0.05m$, CFL=0.9, $f\Delta t = 0.1$ and $k\Delta x/\pi = 0.1$. The latter parameter corresponds to the region of interest.

The level of damping (per time step) for the Rossby waves is examined for the Fourier analysis and the numerical test performed here. As expected, a very good matching between the damping for the velocity and surface elevation was found. In table 1, the results corresponding to the damping of both fields are presented and a close agreement between the numerical and analytical results is observed. The (explicit) first order upwind scheme leads to unstable results, although the amplification factors for both gravity and Rossby modes are less than one. Indeed, as also observed in Foreman (1983), instability may occur even if $|E|_{\max} < 1$ (where $|E|_{\max}$ is the maximum amplification actor for all modes).

Table 1. Damping (per time step) of the Rossby waves for different schemes obtained from Fourier analysis and numerical test corresponding to CFL=0.9 and $f\Delta t = 0.1$.

Scheme	Fourier analysis	Numerical test
1st	0.99509	Unstable
2nd	0.99977	0.99975
3rd	0.99992	0.99991
Fromm	0.99988	0.99987
Quick	0.99994	0.99993
3rdCell	0.99990	0.99989

8-2- A Gaussian water surface distribution

This test is performed to give a physical idea about the damping level of the Rossby waves in a realistic case. A Gaussian distribution is prescribed at initial time and the initial velocity field is taken to be in geostrophic equilibrium , a balance between the Coriolis and the pressure gradient terms, i.e.,

$\eta(x,0) = \mu e^{-\nu x^2}$

$u(x,0) = 0$

$v(x,0) = gf\eta_x(x,0)$

A computational grid with the meshlength parameter $\Delta x = 30$ km is taken and the domain is chosen sufficiently long to prevent the Gaussian from approaching the boundaries. The Coriolis parameter is evaluated at 25^o N ($f = 6.163465\text{e-}5\, s^{-1}$) with $H = 1.63$ m and the radius of deformation is thus $R_d = \sqrt{gH}/f \approx 65$ km. The parameters μ and ν are chosen such that the e-folding radius of the initial Gaussian is resolved by $3\Delta x$ and the initial maximum azimuthal velocity is 1 m/s. A simple scaling can provide more realistic atmospheric parameters without substantially modifying the results.

Numerical results corresponding to the damping of the surface-elevation are shown for

various schemes in Table 2,a and b with $\Delta t = 15$ mn ($f\Delta t \approx 0.055$) and $\Delta t = 30$ mn ($f\Delta t \approx 0.111$), respectively. It is observed that the Rossby modes are highly damped and the relative level of damping for the various schemes is in accordance with the results of the Fourier analysis in Figure 5,b. The level of dampings in Table 2,a and b are almost identical for the finite volume schemes, while the case $\Delta t = 30$ is marginally more dissipative. Although the Quick scheme has the smallest level of damping, the results are still too damped for most practical application. For the two-dimensional case, a higher level of damping is expected.

Finally, in finite volume methods, slope limiters are widely used to reduce the oscillations resulting from phase errors. In order to examine the consequence of the slope limiter approach on the accuracy of the Rossby mode approximation, the third order upwind scheme using a typical slope limiter (Batina, 1990) is employed here. The interface values e.g. for η_L, are calculated as

$$\eta_L = \eta_j + s/4\left((1-\kappa s)(\eta_j - \eta_{j-1}) + (1+\kappa s)(\eta_{j+1} - \eta_j)\right)$$

where

$$\Delta_- = \eta_j - \eta_{j-1},$$

$$\Delta_+ = \eta_{j+1} - \eta_j,$$

and the slope limiter is then written as

$$s = \frac{2\Delta_-\Delta_+ + \varepsilon}{\Delta_-^2 + \Delta_+^2 + \varepsilon}$$

where ε is a very small number to avoid division by zero in the regions of zero slope. The level of damping of the third order scheme, using the above slope limiter approach, for the Rossby modes, is shown in the last line of Table 2a and b (3rdMonotone). As observed, the level of damping of the 3rdmonotone scheme is significantly higher than the 3rd one (with $\sigma = 1/2$). This is also expected for the other upwind finite volume schemes. In Tables 2a and b the previous results are compared with those of the least-squares and the Galerkin methods, obtained with $\sigma = \gamma = 1/2$ (Le Roux and Carrey, 2003). By taking into account the dissipative nature of the least-squares scheme, the upwind finite volume schemes appear to give over damped results in Table 2a and b. For real applications, Rossby modes

are computed through non linear models. However, nonlinear finite volume methods usually require the use of slope limiters. Therefore, for real applications (for nonlinear models), upwind finite volume schemes should excessively damp the Rossby waves.

Table 2a. Damping of the Rossby waves for different schemes for Gaussian initial conditions ($\Delta t = 15\,\text{min}$)

Scheme	10 days	20 days	30 days
2nd	0.80855	0.72197	0.66763
Fromm	0.87819	0.80672	0.75708
3rdCell	0.89370	0.82711	0.77956
3rd	0.91097	0.85061	0.80605
Quick	0.93041	0.87824	0.83806
1st	0.28529	0.19982	0.16258
3rdMonotone	0.69892	0.57115	0.50429
Least-squares	0.99297	0.98625	0.97974
Galerkin	1.00000	1.00000	1.00000

Table 2b. Damping of the Rossby waves for different schemes for Gaussian initial conditions ($\Delta t = 30\,\text{min}$)

Scheme	10 days	20 days	30 days
2nd	0.80854	0.72197	0.66763
Fromm	0.87817	0.80672	0.75708
3rdCell	0.89368	0.82711	0.77956
3rd	0.91095	0.85061	0.80605
Quick	0.93039	0.87823	0.83806
1st	0.28524	0.19979	0.16256
3rdMonotone	0.69892	0.57116	0.50427
Least-squares	0.98623	0.97343	0.96142
Galerkin	1.00000	1.00000	1.00000

9-Conclusion

Different upwind finite volume schemes including first, second and third order, as well as Quick, Fromm and a cell-based third order methods have been studied here using a Fourier analysis approach. Various numerical aspects have been considered and discussed for these schemes first in the case of gravity waves. For most methods, folded frequency curves with stationary $2\Delta x$ waves have been observed in both the semi and fully-discrete cases. However, the $2\Delta x$ waves are effectively damped although they encounter high phase errors.

On the other hand, when the effect of the Coriolis terms is taken into account, all selected upwind schemes lead to a very high (and unacceptable) damping error for the Rossby waves. An academic test case was designed to accurately verify the Fourier analysis results. By performing two numerical tests, it has been numerically shown that the damping of Rossby waves is even more significant when slope limiters are used. Based on these results, it is concluded that most upwind finite volume schemes, with or without slope limiters, should be used with care (if at all) for Rossby waves and restricted to short simulations.

References

Adcroft A.J., Hill C.N. and Marshall J.C. (1999) *A New Treatment of the Coriolis Terms in C-Grid Models at Both High and Low Resolutions*. Month. Weath. Rev. 127 (8), 1928-1936.

Atkinson J. H., Westerink J. J., Luettich R. A., *'Two-dimensional dispersion analyses of finite element approximations to the shallow water equations*, *International Journal for Numerical Methods in Fluids',* 45(7), 2004, pp 715-749.

Batteen, M. L. and Han Y. J. (1981), '*On the computational noise of finite-difference schemes used in ocean models*', Tellus, 33, 387-396.

Batina J. (1990), '*Implicit Flux-Split Euler Schemes for Unsteady Aerodynamics Analysis Involving Unstructured Dynamic Meshes*', AIAA, Vol. 29, No.11, pp.1836

Beckers J.M. and Deleersnijder E. (1993), 'Stability of a FBTCS scheme applied to the propagation of shallow water inertia-gravity waves on various space grids', Journal of computational physics, 108(1), 95-104

Foreman, M.G.G. 1983. *An analysis of the "wave equation" model for finite element tidal computations*. Computational Physics 52: 290-312.

Foreman M. G. G. (1983), *An analysis of two-step time discretizations in the solution of the linearized shallow water equations*, Journal of Computational Physics, 51(3), pp.454-483.

Fromm, J. E., (1968), *A method for reducing dispersion in convective difference schemes*. J. Comput. Phys., 3, 176–189

Gossard C.M., R.L. Kolar. *Phase behavior of a finite volume shallow water algorithm.* Proceedings of CMWR XIII Volume 2: Computational Methods, Surface Water Systems and Hydrology, L.R. Bentley et al (eds.), pp. 921-928, 2000.

Lai, J.-S., Lin G.-F., Guo W.-D.,(2005) *An upstream flux-splitting finite-volume scheme for 2D shallow water equations*, International Journal for Numerical Methods in Fluids, 48(10) pp 1149-1174.

Leonard, B. P., (1979), *A stable and accurate convective modelling procedure based on quadratic upstream interpolation*. Comput. Meth. Appl. Mech. Eng., 19, 59–98.

Le Roux D. Y., Carey G. F. (2003), *Dispersion analysis of the least-squares finite-element shallow-water system*, International Journal for Numerical Methods in Fluids, 42(6), pp 607-622

Le Roux, D. Y., Rostand, V. and Pouliot B. (2006a), '*Analysis of numerically-induced oscillations in 2D finite-element shallow water models; Part I: Inertia-gravity waves*', submitted to SIAM Journal of scientific computing.

Le Roux, D. Y. and Pouliot B. (2006b), '*Analysis of numerically-induced oscillations in 2D finite-element shallow water models; Part II: Free planetary waves*', submitted to SIAM Journal of scientific computing.

Le Roux D. Y., Carey G. F. (2005), *Stability/dispersion analysis of the discontinuous Galerkin linearized shallow-water system,* International Journal for Numerical Methods in Fluids, 48(3) pp: 325-347

Le Roux, D. Y. (2005), 'Dispersion relation analysis of the $P_1^{NC} - P_1$ finite-element pair in shallow-water models', SIAM J. Sci. Comput. 27, 394-414.

R. J. LeVeque (2002), '*Finite Volume Methods for Hyperbolic Problems*', Cambridge university press, UK.

Mohamadian A., Leroux D. (2006) '*Simulation of Shallow Flows over Variable Topography Using Unstructured Grid*', International Journal for Numerical methods in Fluids (in press).

Mohamadian A., Leroux D., Tajrishi M., Mazaheri K. (2005) 'A Mass Conservative Scheme For Simulating Shallow Flows Over Variable Topography Using Unstructured Grid', Advances in water resources, (Elsevier), Vol. 28 (5), pp. 523-537.

Neta, B. and Williams, R. T. (1989), '*Rossby wave frequencies and group velocities for finite element and finite difference approximations to the vorticity-divergence and the primitive forms of the shallow water equations*', Monthly Weather Review, 117,1439-1457'

Platzman, G.W. (1981). *Some response characteristics of finite-element tidal models*. Computational Physics 40: 36-63.

Randall, D. A. (1994) '*Geostrophic adjustment and the finite-difference shallow-water equations*', Monthly Weather Review, 122, 1371-1377.

C. M. Szpilka, R. L. Kolar, "*Numerical Analogs of Fourier and Dispersion Analysis: Development, Verification, and Application to the Shallow Water Equations*," Advances in Water Resources, 26, pp. 649-662, 2003

Sankaranarayanan, S. and Malcolm L. Spaulding. *Dispersion and Stability Analyses of the Linearized Two-Dimensional Shallow Water Equations in Boundary-Fitted Co-Ordinates*. International Journal for Numerical Methods in Fluids. 42(7):741-763. July 10, 2003.

Toro E. F. (2000), '*Shock Capturing Methods for Free Surface Shallow Flows*', John Wiley and sons.

Vreugdenhil C. B., *Numerical methods for shallow-water flow*. Kluwer Academic Publishers, 1994.

Walters R. Carey G. F. (1983),'*Analysis of spurious oscillation modes for the shallow water and Navier-Stokes equations.* ', Computer and Fluids, 11, pp 51-68.

Wajsowicz R. C. (1986), '*Free planetary waves in finite-difference numerical models*', Journal of physical oceanography, 16, 773-789

CHAPTER 7

Conclusion

Different numerical schemes were studied in the 1-D and 2-D forms of the shallow water equations including the semi-Lagrangian method, the method of characteristics in the 1-D case and the finite volume method using unstructured grids in the 2-D case.

In chapter 2, the semi-Lagrangian integrated mass method (SLIM) of Laprise and Plante (1995) was extended to the conservative form of the shallow-water equations. This method was then successfully combined with a semi-implicit semi-Lagrangian one. It resulted in a fully conservative semi-Lagrangian scheme (SI-SLIM-R) where both mass and momentum are conserved while preserving stability with the use of large time steps. The full conservation property of the proposed scheme enables it to correctly simulate the shock speed in complex sub, super and trans-critical flows. The fully conservation property considerably improves the performance of common semi-Lagrangian schemes for a wide range of practical applications. Moreover, the resulting scheme is comparable to the

corrective schemes as GP, but it is free of phase problems of the corrective methods. On the other hand due to the inherently conservative approach, the highly expensive linear programming step of the corrective methods is avoided, and this makes the proposed method more efficient than the GP scheme.

A conservative MOC scheme was then introduced in chapter 3 to simulate dam break type flows. The proposed method was shown to be able to simulate sub, super and trans critical flows very accurately. By using an appropriate interpolation function, the scheme also produces high accurate low-oscillatory solutions, with a computational effort comparable to the cost of a muscle-type high resolution scheme (the Roe approximate solver with a minmod slope limiter at the reconstruction step). The conservation property of the scheme ensures a high accuracy of the shock speed and it considerably improves the performance of the original MOC scheme in complex flows, as shown in a number of challenging test cases e.g. interaction of waves and dry-bed problems.

In chapters 4 and 5, the Finite volume method over unstructured grid was considered due to its inherent conservation property and its flexibility for local mesh refinement and complex boundaries.

A mass conservative approach was proposed in chapter 4 to solve the shallow-water equations which is able to accurately simulate mild flows such as recirculating and tidal flows with low numerical diffusion, and also complex sub, super and trans-critical flows with discontinuity over complicated topographies. The proposed scheme was found to be computationally efficient because it is not necessary to perform an extra upwinding or Riemann solution for the source terms.

In chapter 5, two efficient methods were proposed to treat the source terms and to satisfy the compatibility property on unstructured grids, again, without performing any extra upwinding or Riemann solution for the source terms. Contrary to the scheme presented in chapter 4, which is not fully conservative and may give rise to problems in presence of strong shocks, these two schemes are fully conservative. Further, they directly deal with the source terms without changing the flux terms. Therefore, they could be combined with

most existing Riemann solvers and efficiently employed for a wide range of shallow water problems as shown by many challenging test cases.

Finally in Chapter 6, the performance of the upwind finite volume schemes in the case of Rossby waves was examined by a Fourier analysis approach including the study of phase speed, group velocity, damping and dispersion for the gravity waves and more importantly damping for the Rossby waves. Contrary to the usual good performance of those schemes in the case of convection dominated flows, poor results were obtained here for Rossby modes. Indeed, in this case, all selected upwind schemes lead to a severe damping. The numerical results were also compared with those obtained by using a slope limiter approach. It is concluded that most upwind schemes with or without slope limiters present poor result for an accurate calculation of the Rossby modes and therefore, they should be used with care (if at all) and restricted to short simulations.

BIBLIOGRAPHIE

Abbot M. B. (1979), 'Computational Hydraulics: Elements of the Theory of Free Surface Flows', Longman, London.

Adcroft A.J., Hill C.N. and Marshall J.C. (1999) A New Treatment of the Coriolis Terms in C-Grid Models at Both High and Low Resolutions. Month. Weath. Rev. 127 (8), 1928-1936.

Alcrudo F. and Benkhaldoun F. (2001), 'Exact Solutions to the Riemann Problem of the Shallow-water Equations with a Bottom Step', Computers and fluids 30, pp. 643-671

Alcrudo F. and Garcia-Navarro P. (1993), 'A High Resolution Godunov-Type Scheme in Finite Volumes for the 2D Shallow-water Equations', Int. J. Numer. Methods in Fluids, 16, pp. 489

Atkinson J. H., Westerink J. J., Luettich R. A., 'Two-dimensional dispersion analyses of finite element approximations to the shallow water equations, International Journal for Numerical Methods in Fluids', 45(7), 2004, pp 715-749

Aureli F., Mignosa P., Tomirotti M. (2000), 'Numerical simulation and experimental verification of dam-breack flows with shocks', Journal of hydraulic research, 38, 197.

Batteen, M. L. and Han Y. J. (1981), 'On the computational noise of finite-difference schemes used in ocean models', Tellus, 33, 387-396.

Batina J. (1990), 'Implicit Flux-Split Euler Schemes for Unsteady Aerodynamics Analysis Involving Unstructured Dynamic Meshes', AIAA, Vol. 29, No.11, pp.1836

Beckers J.M. and Deleersnijder E. (1993), 'Stability of a FBTCS scheme applied to the propagation of shallow water inertia-gravity waves on various space grids', Journal of computational physics, 108(1), 95-104

Bermudez A. and Vazquez M. E. (1994), 'Upwind Methods for Hyperbolic Conservation Laws with Source Terms', Computers and Fluids, 23, 1049

Brufau P, Vazquez-Cendon ME and Garcia-Navarro P (2002). numerical model for the flooding and drying of irregular domains. int. J. for Numer. Mcth. Fluids, 39: 247—275.

Bradford S. F. and Sandres B. F. (2002), 'Finite-Volume Model for Shallow-Water Flooding of Arbitrary Topography', J. Hyd. Eng. ASCE, 128, 289

Causon D. M., Mingham C. G. and Ingram D. M. (1999), 'Advances in Calculation Methods for Supercritical Flow in Spillway Channels', J. Hyd. Eng. ASCE, 125, 1039

Colella P. and Woodward P. (1984), 'The piecewise parabolic method (PPM) for gas-dynamical simulations', Journal of computational physics, 54, 174-201.

Denham, M. K. and Patrick, M. A. (1974), 'Laminar flow over a downstream-facing step in a two-dimensional flow channel', Trans. Inst. Chemical Engineers, 52, 361-367

Falcone M. and Ferrettiy R. (2002), 'semi-Lagrangian schemes for Hamilton–Jacobi equations, discrete representation formulae and Godunov methods', Journal of computational physics, 175, 559-575.

Fenemma R. and Chaudhry M. (1987), 'Simulation of One-Dimensional Dam-Break Flows', J. Hyd. Res., vol. 25, No.1, pp. 41

Foreman, M.G.G. 1983. An analysis of the "wave equation" model for finite element tidal computations. Computational Physics 52: 290-312.

Foreman M. G. G. (1983), An analysis of two-step time discretizations in the solution of the linearized shallow water equations, Journal of Computational Physics, 51(3), pp.454-483

Fromm, J. E., (1968), A method for reducing dispersion in convective difference schemes. J. Comput. Phys., 3, 176–189

Garcia Navarro P., Alcrudo F. and Saviron F. (1994), '1-D open channel flow simulation using TVD MacCormack Scheme', Journal of Hydraulic engineering, ASCE, 1992; 118(10), 1359-72.

Garcia Navarro P., Priestley A. (1994), 'A Conservative and Shape Preserving semi-Lagrangian Method for Solution of the Shallow-water Equations', International Journal for Numerical Methods in Fluids, 18, 2.

Glaister, P. (1988), 'Approximate Riemann Solutions of the Shallow Water Equations'. Journal of Hyd. Research, 26, No. 3, 293-306.

Goutal N. and Maurel F., eds. (1997), 'Proceedings of the 2nd Workshop on Dam-Break Wave Simulation', HE-43/97/016/B, France

Gossard C.M., R.L. Kolar. Phase behavior of a finite volume shallow water algorithm. Proceedings of CMWR XIII Volume 2: Computational Methods, Surface Water Systems and Hydrology, L.R. Bentley et al (eds.), pp. 921-928, 2000.

Gravel S., Staniforth A. (1993), 'A mass-conserving semi-Lagrangian scheme for the shallow-water equations', Monthly Weather Review, 122, 243.

Harten, A. and Osher, S. (1987), 'Uniformly high-order accurate non-oscillatory schemes, I', SIAM Journal of numerical analysis, 24, 279.

Harten A. and Hyman P. (1983), 'Self adjusting grid methods for one-dimensional hyperbolic conservation laws', J. of Comput. Phys., 50, 235-269

Henderson, F. M. (1966), 'Open channel flow', Collier MacMillan, London.

Hicks, E. F. and Steffler, P. M. (1992), 'Characteristics dissipative Galerkin scheme for open channel flow', Journal of Hydraulic Engineering, ASCE, Vol. 118, No. 2, 337-352.

Hubbard M. E. and Garcia-Navarro P. (2000), 'Flux Difference Splitting and the Balancing of Source Terms and Flux Gradients', J. Comput. Phys. 165, 89-125

Hubbard M. E. and Garcia-Navarro P. (2001), 'Balancing Source Terms and Flux Gradients in Finite Volume Schemes', Godunov Methods: Theory and Applications, edited by E. F. Toro, Kluwer Academic Publishers, New York, pp. 447-483

Hu K., Mingham C.G., Causon D.M. (2000), 'Numerical simulation of wave overtopping of coastal structures using the non-linear shallow water equations'. Coastal Engineering 2000, 41, 433– 465.

Ida M., (2002), 'A conservative semi-Lagrangian method for oscillation free computation of advection processes', Computer phys. communications 116, 121-135.

Jha A. K., Akiyama J., Ura M. (1995), 'First and Second-Order Flux Difference Splitting Schemes for Dam-Break Problem', J. Hyd. Eng. ASCE 121, 12, pp. 877

Kolahdoozan M. (1999), 'Numerical Modeling of Geo-Morphological processes Estuarine Waters', University of Bradford, UK, PhD Thesis.

Kurganov A., Levy D. (2002), 'Central-Upwind Schemes for the Saint-Venant System' Mathematical Modeling and Numerical Analysis, 36 , 397-425

Laprise J. and Plante A. (1995), 'A class of semi-Lagrangian integrated mass (SLIM)numerical transport algorithms' , Monthly Weather Review, 123, 2551-2566.

Lai, J.-S., Lin G.-F., Guo W.-D.,(2005) An upstream flux-splitting finite-volume scheme for 2D shallow water equations, International Journal for Numerical Methods in Fluids, 48(10) pp 1149-1174.

Leonard B. P. (1979), 'A stable accurate convective modeling procedure based on quadratic upstream interpolation', Comp. Methods in Appl. Mech. and Eng. 19, 59-98.

Leonard B. P. (1991), 'The ultimate conservative difference scheme applied to unsteady one-dimensional advection', Comp. Methods in Appl. Mech. and Eng. 88, 17-74.

Le Roux D. Y., Lin C. A. and Staniforth A. (2000), 'A semi-implicit semi-Lagrangian finite-element shallow-water ocean model', Monthly Weather Review, 128, 1384.

Le Roux D. Y., Carey G. F. (2003), Dispersion analysis of the least-squares finite-element shallow-water system, International Journal for Numerical Methods in Fluids, 42(6), pp 607-622

Le Roux, D. Y., Rostand, V. and Pouliot B. (2006a), 'Analysis of numerically-induced oscillations in 2D finite-element shallow water models; Part I: Inertia-gravity waves', submitted to SIAM Journal of scientific computing.

Le Roux, D. Y. and Pouliot B. (2006b), 'Analysis of numerically-induced oscillations in 2D finite-element shallow water models; Part II: Free planetary waves', submitted to SIAM Journal of scientific computing.

Le Roux D. Y., Carey G. F. (2005), Stability/dispersion analysis of the discontinuous Galerkin linearized shallow-water system, International Journal for Numerical Methods in Fluids, 48(3) pp: 325-347

Le Roux, D. Y. (2005), 'Dispersion relation analysis of the $P_1^{NC} - P_1$ finite-element pair in shallow-water models', SIAM J. Sci. Comput. 27, 394-414.

LeVeque R. J. (2002), 'Finite Volume Methods for Hyperbolic Problems', Cambridge university press, UK.

LeVeque R. J. (1998), 'Balancing Source Terms and Flux gradients in High-Resolution Godunov Methods', J. Comput. Phys., 146, pp. 346

Levy D., Puppo G. and Russo G. (2002), 'A fourth order central WENO scheme for multi-dimensional hyperbolic systems of conservation Laws', SIAM Journal on scientific computing, 24, 2002, pp. 480-506.

Lin S. J. and Rood R. B., (1997), 'An explicit flux-form semi-Lagrangian shallow-water model on the sphere', Q. J. R. Meterol. Soc. 123, 2477-2498.

Lyton A. T. and van de Panne M. (2002), 'A numerically efficient and stable algorithm for animating water wave', Visual computer, 18, 41-53.

Mingham C.G. and Causon D. M. (1998), 'High Resolution Finite-Volume Method for Shallow-water Equation Flows', J. Hyd. Eng. ASCE 124, 605

Mohammadian A., Azad F. L., Tajrishi M. (2003), 'Two Dimensional Numerical Simulation of Flow and Geo-Morphological Processes Near Headlands by Using Unstructured Grid', XXX IAHR Congress, Greece

Mohammadian A., Le Roux D. Y., Tajrishi M., Mazaheri K. (2005), 'A Mass Conservative Scheme For Simulating Shallow Flows Over Variable Topographies Using Unstructured Grid', Advances in water resources, Vol. 28, (5), pp. 429-539

Mohamadian A., Leroux D. (2006) 'Simulation of Shallow Flows over Variable Topography Using Unstructured Grid', International Journal for Numerical methods in Fluids (in press).

Nakamura T., Tanaka R., Yabe T. and Takizawa K. (2001), 'Exactly conservative semi-Lagrangian scheme for multi-dimensional hyperbolic equations with directional splitting technique', Journal of computational physics, 174, 171-207.

Neta, B. and Williams, R. T. (1989), 'Rossby wave frequencies and group velocities for finite element and finite difference approximations to the vorticity-divergence and the primitive forms of the shallow water equations', Monthly Weather Review, 117,1439-1457'

Nujic M. (1995), 'Efficient Implementation of Non-Oscillatory Schemes of Free Surface Flows', J. Hyd. Res., Vol. 33, No. 1, pp. 101

Platzman, G.W. (1981). Some response characteristics of finite-element tidal models. Computational Physics 40: 36-63.

Priestly A. (1993), 'A quasi-conservative version of the semi-Lagrangian advection scheme', Monthly Weather Review, 121, 621-629.

Randall, D. A. (1994) 'Geostrophic adjustment and the finite-difference shallow-water equations', Monthly Weather Review, 122, 1371-1377.

Roe, P. L. (1981), 'Approximate Riemann solvers, parameter vectors and difference schemes', Journal of computational physics, 43, 357-372.

Rogers B. D., Borthwick A. L. and Taylor P. H. (2003), 'Mathematical balancing of flux gradient and source terms prior to using Roe approximate Riemann solver Volume', J. Comp. Phys., Vol. 192, (2) , pp. 422-451

Russo G. (2002), 'Central Schemes for Balance Laws', Proceedings of HYP2000, Magdeburg

Sankaranarayanan, S. and Malcolm L. Spaulding (2003). Dispersion and Stability Analyses of the Linearized Two-Dimensional Shallow Water Equations in Boundary-Fitted Co-Ordinates. International Journal for Numerical Methods in Fluids. 42(7):741-763.

Savenije H. H. G. (1992), 'Lagrangian solution of St. Venant's equations for alluvial estuary', Journal of Hydraulic engineering, ASCE, Vol. 118, No. 8, 1153-1163.

C. M. Szpilka, R. L. Kolar, "Numerical Analogs of Fourier and Dispersion Analysis: Development, Verification, and Application to the Shallow Water Equations," Advances in Water Resources, 26, pp. 649-662, 2003

Shu C. W. and Osher S. (1988), 'Efficient Implementation of Non-Oscillatory Shock-Capturing Schemes', J. Comp. Phys., Vol. 77, pp. 439-471

Staniforth A. and Cote J. (1991), 'Semi-Lagrangian integration scheme for atmospheric models- a review', Monthly Weather Review, 119, 2206-2223.

Tanaka R., Nakamura T., and Yabe T. (2000), 'Constructing exactly conservative scheme in a non-conservative form', Computer physics communications, 126, 232-243.

Temperman C., Hortal M. and Simmons A. (2001), 'A two-time-level semi-Lagrangian global spectral model', Q. J. R. Meteorol. Soc, 127, 111-127.

Toro E. F. (2000), 'Shock Capturing Methods for Free Surface Shallow Flows', John Wiley and sons

Tseng M. H. and Chu C. R. (2000), 'The simulation of dam-break type flows by an improved predictor-corrector TVD scheme', Advances in water resources, 23,637-643.

Van Leer B. (1977), 'Towards the ultimate conservative difference scheme IV: A new approach to numerical convection', Journal of computational physics, 23, 276-299.

Van Leer, B. (1982), 'Flux Vector Splitting of the Euler Equations', Lecture Notes in Physics, Vol. 170, pp. 507-512.

Van Rijn L. C. (1993), 'Principles of Sediment Transport in Rivers, Estuaries and Coastal Seas', Aqua Publications, The Netherlands

Vazquez-Cendon M. E. (1999), 'Improved Treatment of Source Terms in Upwind Schemes for the Shallow-water Equations in Channels with Irregular Geometry', J. Comp. Phys., 43(2), pp. 357-372

Vreugdenhil C. B., Numerical methods for shallow-water flow. Kluwer Academic Publishers, 1994.

Vukovic S. and Sopta L. (2002), 'ENO and WENO Schemes with the Exact Conservation Property for One-Dimensional Shallow-Water Equations', J. Comp. Phys. 179, 593-621

Wajsowicz R. C. (1986), 'Free planetary waves in finite-difference numerical models', Journal of physical oceanography, 16, 773-789

Walters R. Carey G. F. (1983),'Analysis of spurious oscillation modes for the shallow water and Navier-Stokes equations. ', Computer and Fluids, 11, pp 51-68.

Wang J. S. (2000), 'Finite Difference TVD Scheme for Computation of Dam-Break Flows', J. Hyd. Eng. ASCE, No.4, pp. 253

Wang Z. B., (1989), 'Mathematical Modeling of Morphological Processes in Estuaries', Delft Uni. of Tech., The Netherlands

Xiao F., Yabe T., Ito T. (1996), 'constructing oscillation preventing scheme for advection equation by rational function', Computer physics communications, 93, 1.

Xiao F., Yabe T., Ebisuzaki T. (1999), 'An oscillation suppressing semi-Lagrangian solver for advection equation', Computer physics communications 116, 121-135.

Xiao F. and Yabe T. (2001), 'Completely conservative and oscillation-less semi-Lagrangian schemes for advection transportation', Journal of computational physics, 170, 498-522.

Xiao F. (2002), ‘Profile modifiable conservative transport schemes and a simple multi-integrated moment formulation for hydrodynamics’, "Computational Fluid Dynamics 2002”, (Proceedings of the 2nd international conference on CFD, Sydney, Australia), Springer, 2003, ISBN 3-540-00739-3.

Xiu D. and Karniadakis G. (2001),’A semi-Lagrangian High-Order Method for Navier–Stokes Equations’, Journal of computational physics, 172, 658-684.

Xu K. (2002), ‘A Well-balanced Gas-Kinetic Scheme for the Shallow-water Equations with ource Terms’. J. Comput. Phys. Vol. 178, pp. 533-562.

Yabe T., Tanaka R., Nakamura T. and Xiao F. (2001), ‘Exactly conservative semi-Lagrangian methods (CIP-CSL) in one dimension’, Monthly Weather Review, 126, 232.

Yee H. (1989), ‘A class of high-resolution explicit and implicit shock-capturing methods’, NASA TM-101088.

Zerroukat M., Wood N., and Staniforth A. (2002), ‘Slice: A semi-Lagrangian inherently conserving and efficient scheme for transport problems’, Q. J. R. Meterol. Soc. 128, 2801-2820.

Zhao D., Shen H. W., Tabios G. Q. III, Lai J. S. and Tan W. Y. (1994), ‘Finite-Volume two-Dimensional Unsteady-Flow Model for River Basins’. J. Hyd. Eng. ASCE 120 (7), 863-883

Zhao D., Shen H., Tabios G., Lai J. and Tan W. (1996), ‘Approximate Riemann Solver in FVM for 2d Hydraulic Shock Wave Modeling’, J. Hyd. Eng. ASCE, No.12, pp. 69.